Southeastern Geology: Volume 43, No. 3 February 2005

Editor in Chief: S. Duncan Heron, Jr.

Abstract

Academic journal published quarterly by the Department of Geology, Duke University.

Heron, Jr., S. (2005). Southeastern Geology, Vol. 43 No. 3, February 2005. Permission to re-print granted by Duncan Heron via Steve Hageman, Professor of Geology, Dept. of Geological & Environmental Sciences, Appalachian State University.

SOUTHEASTERN GEOLOGY

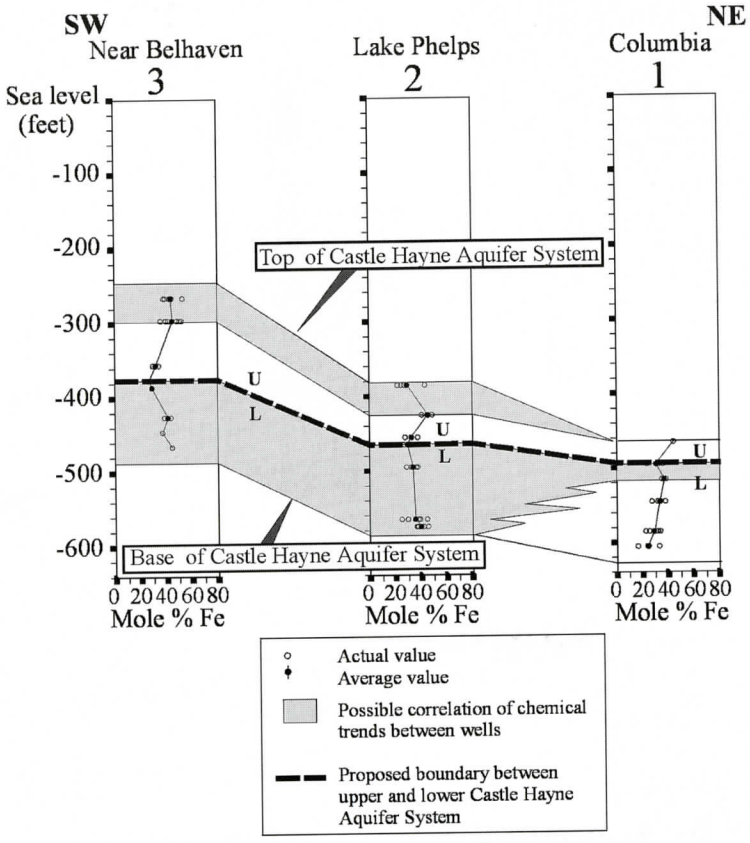

Vol. 43, No. 3 February 2005

SOUTHEASTERN GEOLOGY

PUBLISHED

at

DUKE UNIVERSITY

Editor in Chief:

Duncan Heron

This journal publishes the results of original research on all phases of geology, geophysics, geochemistry and environmental geology as related to the Southeast. Send manuscripts to **DUNCAN HERON, DUKE UNIVERSITY, DIVISION OF EARTH & OCEAN SCIENCES, BOX 90233, DURHAM, NORTH CAROLINA 27708-0233**. Phone: 919-684-5321, Fax: 919-684-5833, Email: duncan.heron@duke.edu Please observe the following:

1) Type the manuscript with double space lines and submit in duplicate, or submit as an Acrobat file attached to an email.
2) Cite references and prepare bibliographic lists in accordance with the method found within the pages of this journal. Data citations examples can be found at http://www.geoinfo.org/TFGeosciData.htm
3) Submit line drawings and complex tables reduced to final publication size (no bigger than 8 x 5 3/8 inches).
4) Make certain that all photographs are sharp, clear, and of good contrast.
5) Stratigraphic terminology should abide by the North American Stratigraphic Code (American Association Petroleum Geologists Bulletin, v. 67, p. 841-875).
6) Email Acrobat (pdf) submissions are encouraged.

Subscriptions to *Southeastern Geology* for volume 43 are: individuals - $23.00 (paid by personal check); corporations and libraries - $33.00; foreign $40. Inquires should be sent to: **SOUTHEASTERN GEOLOGY, DUKE UNIVERSITY, DIVISION OF EARTH & OCEAN SCIENCES, BOX 90233, DURHAM, NORTH CAROLINA 27708-0233**. Make checks payable to: *Southeastern Geology.*

Information about SOUTHEASTERN GEOLOGY is on the World Wide Web including a searchable author-title index 1958-2001 (Acrobat format). The URL for the Web site is: http://www.southeasterngeology.org

SOUTHEASTERN GEOLOGY is a peer review journal.

ISSN 0038-3678

SOUTHEASTERN GEOLOGY

Table of Contents

Volume 43, No. 3 February 2005

SOUTHEASTERN GEOLOGY
V. 43, No. 3, February 2005, p. 113-135

LITHOLOGY AND MINERAL CHEMISTRY OF THE CASTLE HAYNE LIMESTONE — AN IMPORTANT COASTAL PLAIN AQUIFER IN NORTH CAROLINA

D. L. T. MEHLHOP, T. L. WOODS, AND D. W. NEAL

Department of Geology
East Carolina University
Greenville, NC 27858

ABSTRACT

The Castle Hayne aquifer is one of the most extensively developed aquifers in North Carolina; however, little is known about how its lithology, mineralogy and mineral chemistry vary in the northern Coastal Plain. Seventy-seven samples from six wells penetrating the Castle Hayne were analyzed using petrography, X-ray Diffraction and Energy Dispersive X-ray to determine lithology, mineralogy, bioclast diversity and mineral chemistry.

The Castle Hayne aquifer (CHAS) is a biomicrite with quartz sand and glauconite, and contains lesser amounts of dolomite, apatite, pyrite, and aluminosilicates. Moldic porosity is high due to dissolution of bioclasts. Most samples are dominated by mollusks and echinoderm fragments, however brachiopods, bryozoans, and foraminifera are also present. Sediments were deposited on the middle to outer shelf during sea level transgressions and regressions as indicated by the bioclast assemblage. The dominant lateral trend in the study area is changing lithofacies and chemistry from the southwest to northeast. The southwest region of the study area was closer to shore with shallower, more agitated waters, indicated by the presence of more bioclasts and quartz sand and less glauconite. The northeast region in the study area was farther offshore in deeper water on the shelf, indicated by the presence of more micrite mud and glauconite and fewer bioclasts. The dominant vertical trend is changing lithofacies from sandy, glauconitic limestone in the lower CHAS to shelly lime mud in the upper CHAS. The proposed boundary between the upper and lower CHAS is noted both lithologically and geochemically.

Glauconite is the dominant clay mineral and occurs as well-rounded peloids and occasionally as infill of bryozoan skeletal grains. The amount of glauconite is greatest at the base of the aquifer, and decreases in abundance from southwest to northeast in the Upper Castle Hayne. There is a strong negative linear correlation between octahedral Al and Fe, while Mg remains reasonably constant. Average octahedral Al content of glauconite increases from southwest to northeast while average Fe content decreases. Fe concentration is much higher in peloids than in the infill material. Carbonates consist overwhelmingly of pure $CaCO_3$, but several samples contain variable amounts of $MgCO_3$ and minor dolomite was found. Phosphate minerals appear at various depths in four of the wells. They are either hydroxy-, fluor-, or carbonate-apatites, and do not contain any Cl. Four of the wells contain aluminosilicates; possibly Na-rich feldspars or zeolites. An iron sulfide is present in three wells.

The data presented in this study suggest that there are definite chemical trends in glauconite that have a strong correlation with lithofacies. The geochemical data presented, in conjunction with water chemistry, will help establish important controls on the potability of ground water from the Castle Hayne aquifer.

INTRODUCTION

The demand for potable drinking water in eastern North Carolina is increasing every year. Surface water and ground water pumped from Cretaceous aquifers and, to a lesser extent, the

Table 1. Stratigraphic Section (Modified from Gamus (1972), Lloyd and Daniel (1988), and Winner and Coble (1996).

System	Series	Stratigraphic Units	Hydrogeologic Units (aquifer and confining unit)		Description
Quaternary	Recent Pleistocene	Undifferentiated Unnamed Unit	Post-Miocene Unit		Sand, silt, shells, and some clay
Tertiary	Pliocene	Yorktown Formation	Yorktown Unit		Interbedded sand and clay with some shell beds
	Miocene	Pungo River Formation	Pungo River Unit		Phosphate and quartz sand, silt, clay, and limestone
	Oligocene	Belgrade Fm.	Castle Hayne Aquifer System	Upper Castle Hayne Unit	Permeable and porous shell limestone
		River Bend Fm.			
	Eocene	Castle Hayne Limestone		Lower Castle Hayne Unit	Shell limestone interbedded with calcareous sands
	Paleocene	Beaufort Formation	Beaufort Unit		Fine glauconitic sand, silty and clayey in part
Cretaceous	Upper Cretaceous	Peedee Formation	Peedee Unit		Sand interbedded with clay and silt
		Black Creek Formation	Black Creek Unit		Laminated clay with interbedded sand
		Cape Fear Formation	Upper Cape Fear Unit		Alternating beds of sand and clay
			Lower Cape Fear Unit		Fine sand
	Lower Cretaceous	Unnamed Formation	Lower Cretaceous Unit		Sand, shale, gravel and limestone
Basement					

upper part of the Castle Hayne Aquifer System (CHAS, Table 1, Figure 1 and 2) currently meet the needs of the central Coastal Plain (Winner and Lyke, 1989). Substantial water-level declines in the heavily pumped Cretaceous aquifers (Lyke and Brockman, 1990; Giese and others, 1997) preclude increased future exploitation of those aquifers and have encouraged increased exploitation of the CHAS. The CHAS is now extensively used as a source for public and private water supplies, irrigation, and aquaculture. It is the most productive aquifer in North Carolina with average withdrawals of 146 million gallons per day (mgd) (Winner and Coble, 1996; Lyke and Treece, 1988). The intent of this research is to provide a preliminary characterization of lithology, mineralogy, and mineral chemistry for a coastal limestone. Previous information for the study area was qualitative and mineral chemistry was virtually unknown. These new mineralogical and chemical data will improve our ability to assess how

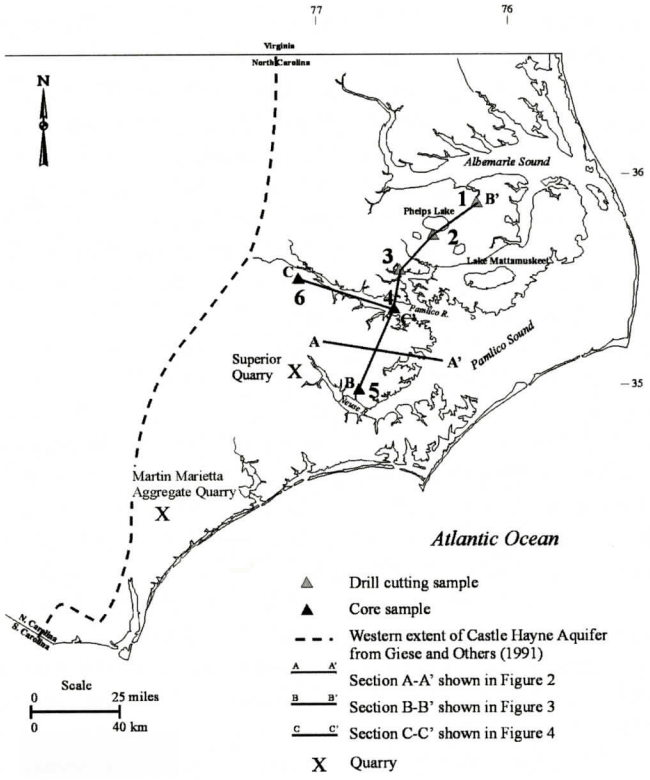

Figure 1. Study area and locations of cross-sections, drill-holes, and quarries.

reactions between ground water and coastal limestones affect water chemistry and should enhance the efficiency of exploitation of an important water source.

HYDROGEOLOGIC FRAMEWORK

The Upper Cretaceous and Cenozoic formations of the North Carolina Coastal Plain include sands, silts, clays, and limestones that dip and thicken eastward (Brown and others, 1972;

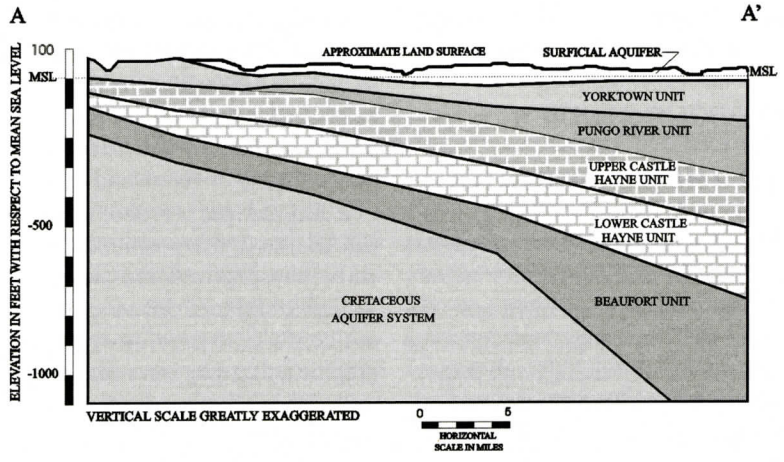

Figure 2. Generalized hydrogeologic cross-section A-A' of the Pamlico River area. (location shown on Figure 1). (Modified from Reynolds and Spruill, 1995).

Winner and Coble 1996; Figure 1 and 2; Table 1). To understand the hydrogeology of the North Carolina Coastal Plain aquifer system, Winner and Coble (1996) developed a hydrologic framework consisting of ten aquifers and nine confining beds. This framework was based on analysis and interpretation of lithologic data, geophysical logs, ground water levels, and water-quality data. Giese and others (1997) used the hydrostratigraphic framework of Winner and Coble (1996) to develop a three-dimensional model simulating ground water flow in the aquifer system. Prior to their work, Gamus (1972) had divided the CHAS into three hydrologic units based on permeability differences: the Beaufort, the Lower Castle Hayne, and the Upper Castle Hayne (Table 1). Winner and Coble (1996) and Giese and others (1997), however, considered the Beaufort Unit to be a separate aquifer based on the dominance of glauconite sand and clay. This study follows the hydrostratigraphic nomenclature of Winner and Coble (1996) and considers the Castle Hayne aquifer independently of the Beaufort hydrologic unit.

The Castle Hayne aquifer is typically overlain by either the Pungo River or Yorktown aquifers (Table 1, Figure 2). Both of these aquifers are characterized by generally low permeability and only yield minimal amounts of ground water to wells (Giese and others, 1997). In some areas, the Castle Hayne aquifer is in direct contact with the Surficial aquifer (Giese and others, 1997). Underlying the Castle Hayne aquifer are the Beaufort and Peedee aquifers.

PREVIOUS STUDIES

Castle Hayne Aquifer

The Eocene Castle Hayne Limestone has been studied since the early twentieth century (Clark, 1909; Vaughan, 1918; Brown and others, 1972). These early investigations consisted of macroscopic studies of lithology and paleontology. Textoris (1967, 1969) provided preliminary petrographic data on the CHAS, which includes the Castle Hayne Limestone and its facies, upper Oligocene beds, and carbonate-rich facies of the Cretaceous Peedee Formation. Detailed petrographic studies of the CHAS from the Superior Quarry (Figure 1) revealed a lower consolidated member and an upper friable, dolomitic member (Cunliffe, 1968; Cunliffe and Textoris, 1969). Further study at the Superior Quarry by Thayer (1972) and Thayer and Textoris (1972) related diagenetic features of the facies within the CHAS to pore-system development. Textoris and others (1972) suggested that porosity and permeability of the CHAS are extensively controlled by original skeletal mineralogy. Upchurch (1973) and Upchurch and Textoris (1973) described eight petrographic facies of the CHAS noting major diagenetic changes at the Martin Marietta Aggregates Quarry (formerly Ideal Cement Quarry, Figure 1).

Within the CHAS, Baum (1977) and Baum and others (1978 and 1979a, b) recognized three dominant lithofacies of middle and late Eocene age: a basal phosphate pebble biomicrudite overlain by a bryozoan biosparrudite, which is, in turn, overlain by a bryozoan biomicrudite. Ward (1977) and Ward and others (1978) proposed a stratigraphic framework similar to Baum (1977) and Baum and others (1978, 1979a, 1979 b) for the CHAS. Their framework included three lithofacies of middle Eocene age: a phosphatic lithocalcirudite facies (the New Hanover Member) overlain by a bryozoan and echinoid biocalcarenite facies (the Comfort Member) overlain by a siliceous, molluscan-mold biocalcirudite facies (the Spring Garden Member). Otte (1981) interpreted the CHAS to include the New Hanover and Comfort Members of Ward and others (1978) and the phosphate pebble biomicrudite, bryozoan biosparrudite of Baum and others (1978).

Zullo and Harris (1986, 1987) subdivided the CHAS into five depositional sequences separated by phosphatized and glauconitized, disconformable surfaces. Because these sequences do not conform to previously defined lithostratigraphic units, they were designated, from oldest to youngest, Sequences 0 through 4. Each sequence usually contains various proportions of biosparrudite and biomicrudite generally underlain by a basal phosphate-pebble biomicru-

dite, however, the complete section is seldom represented in a single exposure. Calcarenite, biocalcarenite, micrite, and biomicrite also occur and may dominate. Calcarenite is especially common near the base of the sequences and the concentration of quartz sand is frequently quite high throughout. As Zullo and Harris (1987, p. 197) explain, "The difficulties encountered in interpreting the stratigraphic relationships of Coastal Plain rocks are directly related to the scarcity of natural exposure, and the lack of subsurface control and modern biostratigraphic studies."

Moran (1989) separated the CHAS in southeastern North Carolina into forty-six stratigraphic units based on macroscopic, microscopic and field observations. Four lithofacies occur among the stratigraphic units: a biomicrite/ biomicrudite (indurated and unindurated), a pebble biomicrite/ conglomerate (indurated), a biosparite/ biosparrudite (indurated and unindurated), and a phosphorite (indurated).

Glauconite

In 1978, the Association Internationale Pour l'Etude des Argiles (AIPEA) Nomenclature Committee recommended the following definition of glauconite: "Glauconite is defined as an Fe-rich dioctahedral mica with tetrahedral Al (or Fe^{3+}) usually greater than 0.4 atoms per formula unit and octahedral R^{3+} correspondingly greater than 2.4 atoms (Buckley and others, 1978; Bailey, 1980). A generalized formula is:

(octahedral) (tetrahedral)

$2[K\ (R^{+3}_{1.33}\ R^{+2}_{0.67})\ (Si_{3.67}\ Al_{0.33})\ O_{10}\ (OH)_2]$

with $R^{+3} = Fe^{3+} >> Al$ and $R^{+2} = Mg >> Fe^{2+}$ ..." (Odom, 1984, p.546). Many of the green peloids and internal molds analyzed during this study appear to meet these criteria, if the tendency of the semi-quantitative EDX analyses to overestimate SiO_2 and Al_2O_3 and underestimate Fe_2O_3 is kept in mind (see discussion below). Therefore, the more specific term "glauconite" will be used to describe the green clay minerals found in the CHAS instead of the generic term "glaucony" suggested by Odin and Matter (1981).

Morton and others (1984) suggested that the chemistry of glauconite is controlled by sedimentary environment, not the host material. Glauconite is thought to grow authigenically in a restricted microenvironment that is partially reducing/ partially oxidizing at or near the sediment-water interface under marine conditions (Odin and Matter, 1981; Ireland and others, 1983; Odin and Fullagar, 1988; Weaver, 1989; O'Brien and others, 1990). Traditionally, it was thought that the reducing conditions liberated Fe from either sea water or Fe-rich pore water for glauconite formation (Burst, 1958a, 1958b). It is now clear that the reduction of Fe^{3+} oxide coatings on mineral grains in continental shelf sediments is largely mediated by microbial processes (Lovley and others, 1991). Weaver (1989) and Odin and Fullagar (1988) reported that typical depths of glauconite formation on modern continental shelves and upper slopes are between 100 and 500 meters. For instance, glauconite internal molds commonly form on the deepest part of the present continental shelf off Morocco, Norway and the southeastern United States (Boichard and others, 1985). Other constraints on the formation of glauconite are: 1) presence of an initial substrate (esp. fecal pellets, clay books, or mud lumps), 2) source of renewing ions (Fe and Al), and 3) time for substrate to evolve in an area of low sedimentation (Odin and Matter, 1981; Odin and Stephan, 1981). It is known that there is no correlation between verdissement of glauconite and the amount of Fe_2O_3; iron content is high in all stages of verdissement (Ehlmann and others, 1963; Birch and others, 1976).

METHODS

Rock samples from six wells (three cores and three sets of drill cuttings) were used to evaluate the mineralogy and geochemistry of the Castle Hayne aquifer in east-central North Carolina between Albemarle Sound and the Neuse River (Figure 1, Table 2). Samples were provided by the North Carolina Geologic Survey. When the holes were drilled, cuttings were washed to remove driller's mud so much of the fine material was washed away and, therefore, was not

available for identification and analysis. Initially, the drill cuttings from wells 1, 2, and 3 were examined under a binocular microscope and analyzed by powder X-ray diffraction (XRD) to distinguish areas within the CHAS that contained minerals other than calcite and quartz. Samples representing mineralogically distinct zones were chosen for Energy Dispersive X-ray analysis (EDX). Core samples from wells 4, 5, and 6 were analyzed petrographically and by EDX. Because they contain abundant peloids, two samples from well 6 were also analyzed by XRD.

Table 2. Drill hole locations.

Well Symbol	Well Name	Latitude	Longitude
1	TY-T1-76	35° 50' 59"	76° 15' 50"
2	WH-T2-78	35° 43' 30"	76° 26' 30"
3	BF-T5-67	35° 33' 30"	76° 37' 30"
4	BF-T6-69	35° 24' 56"	76° 48' 30"
5	PA-T2-XX	35° 05' 30"	76° 50' 30"
6	BF-T1-69	35° 26' 30"	77° 09' 30"

Petrographic Analysis

Thin sections were made from three cores (Figure 1) that were sampled at intervals correlative to lithologic changes in the CHAS. Lithologic determination for each was made by a point count of 200 points per thin section except for the slide with a small sample area from the interval 52 to 62 feet below sea level (fbsl) in well 6. Thin sections were stained with a mixture of Alizarin Red-S and potassium ferricyanide in 0.2% hydrochloric acid.

X-ray Diffraction Techniques (XRD)

Bulk rock samples from drill cuttings and one of the cores were examined by XRD to distinguish areas within the CHAS that contained minerals other than calcite and quartz. The dominant calcite and quartz peaks mask peak intensities of accessory minerals that are generally of lower intensity. Therefore, petrographic and EDX analyses often revealed minerals missed by XRD analysis.

All depth intervals were analyzed by XRD in wells 1, 2, and 3; however, in well 6 (core sample) only the intervals with high point count for peloids were selected for XRD analysis. After petrographic analysis, it was decided that samples from wells 4 and 5 would not be X-rayed because they contained mostly calcite and quartz with only minor concentrations of accessory minerals.

Sixty samples were analyzed by XRD to determine their mineralogy. Each sample was ground with a mortar and pestle and sieved (88 microns) to remove large pieces. Samples were X-rayed from 5° 2θ to either 45° 2θ or 57° 2θ. The more restricted X-ray patterns were on preliminary samples, but the majority of the samples were X-rayed over the longer range. Samples representing each mineralogically distinct zone were chosen for EDX analysis.

Energy Dispersive X-ray Analysis (EDX)

A separate set of 45 polished sections from cores and drill cuttings was made for Scanning Electron Microscope (SEM) and EDX study. Each sample was analyzed using a Phillips SEM equipped with hardware and ZAP data reduction software from HNU Systems, Inc. The ZAP program is a standardless analysis system that incorporates routine corrections based on background subtraction, peak overlap, characteristic line fluorescence, etc. and converts peak heights directly to weight percents. Each sample was analyzed at 0-10KeV for 200 seconds of Live Time. These parameters were chosen because they produced the best analyses of standards similar in structure and chemistry to the minerals to be analyzed.

The majority of grains analyzed by EDX were chosen based on their morphology. Peloidal grains of glauconite or phosphate were chosen most frequently, but carbonate matrix and cement were also analyzed. Of the approximately 500 grains evaluated, 250-300 were either pure quartz or calcite and were not analyzed further after collection of initial spectra. Analyses of standards indicate that in order

Table 3. Statistics for EDX standard analyses.

Mineral	Oxide OR Carbonate	Accepted Value[1]	Value normalized w/o H_2O[2]	Mean[3]	Standard Deviation[4]	Accuracy% [5]	Normalized Accuracy% [6]
Albite	Na_2O	11.59		8.0	1.4	-31	
	Al_2O_3	19.54		19.9	0.6	2	
	SiO_2	68.52		72.1	1.9	5	
	K_2O	0.22		0.0	0.0	-95	
	CaO	0.13		0.0	0.1	-69	
Apatite	CaO	55.81		61.1	2.1	9	
	P_2O_5	42.39		40.6	6.6	-4	
Biotite	Al_2O_3	15.13	15.78	17.6	1.4	16	12
	SiO_2	38.72	40.38	45.8	2.8	18	13
	K_2O	9.91	10.33	9.3	0.5	-7	-10
	CaO	0.10	0.10	0.2	0.3	80	80
	MgO	19.52	20.36	18.6	1.2	-5	-9
	TiO_2	1.77	1.84	1.2	0.5	-34	-37
	MnO	0.04	0.04	0.4	0.9	1000	1000
	FeO	10.72	11.18	6.9	1.3	-35	-38
	H_2O	4.11	NA[7]	NA[7]	NA[7]	NA[7]	NA[7]
Chlorite	Al_2O_3	18.08	20.98	23.3	0.6	29	11
	SiO_2	30.04	34.85	39.8	0.7	33	14
	CaO	0.03	0.03	ND[8]	ND[8]	ND[8]	ND[8]
	MgO	33.51	38.88	33.7	0.6	0	-13
	FeO	3.31	3.84	1.9	0.8	-41	-49
	NiO	0.24	ND[8]	ND[8]	ND[8]	ND[8]	ND[8]
	Cr_2O_3	0.98	1.14	1.3	0.6	31	13
	H_2O	13.76	NA[7]	NA[7]	NA[7]	NA[7]	NA[7]
	CO_2	0.07	NA[7]	NA[7]	NA[7]	NA[7]	NA[7]
	F	0.02	NA[7]	NA[7]	NA[7]	NA[7]	NA[7]
Dolomite	$CaCO_3$	54.00		51.3	0.6	-5	
	$MgCO_3$	46.00		48.8	0.6	6	
Plagioclase	Na_2O	4.35		2.7	1.1	-39	
	Al_2O_3	28.53		29.2	0.4	2	
	SiO_2	54.21		57.4	1.3	6	
	K_2O	0.41		0.2	0.2	-51	
	CaO	11.80		9.5	0.6	-20	
	MgO	0.13		0.4	0.6	192	
	TiO_2	0.07		0.0	0.0	-100	
	FeO	0.37		0.8	0.3	116	

1. Values given in weight percent oxide
2. Accepted values are normalized to dry weight by recalculating total weight% excluding H20 and other volatiles
3. Mean of 10 analyses of each standard
4. Standard deviation of 10 standard analyses
5. Accuracy = [(Mean - Accepted Value)/Accepted Value] x 100
6. Accuracy for biotite and chlorite calculated using normalized accepted value
7. Not analyzed
8. Not detected

for the EDX to detect a particular oxide, the sample must usually contain at least 0.1 weight percent of that oxide. The EDX system used cannot detect or identify elements lighter than Na.

Because of the potential importance of cation exchange reactions in controlling ground water composition, glauconite chemistry was investigated in detail. Total Fe is reported as Fe_2O_3 for glauconite, because the EDX system is unable to distinguish between Fe^{3+} and Fe^{2+}. In fact, literature values of the ratio of FeO to Fe_2O_3, range, for example, from 0.04-0.56 (averaging 0.22) in the study of Buckley and others (1978), from 0.01-0.1 (averaging 0.06) from Jarrar and others (2000), and averaging somewhat greater than 0.25 from Ireland and others (1983). The simplification adopted in this paper of reporting total Fe as Fe_2O_3 introduces some error in the determination of octahedral totals. However, because data will mainly be used to delineate regional trends, to describe differences with depth in individual cores, and to give a semi-quantitative picture of mineral chemistry, these analyses still produce much useful information.

The ZAP standardless analysis program was used for all standards and samples. Standards analyzed to determine precision and accuracy of the EDX analyses were albite, apatite, biotite, chlorite, dolomite, and plagioclase. These standards were analyzed ten times each between 0 and 10 KeV for 200 seconds of Live Time (Table 3). Precision of standard analyses, indicated by standard deviation, was within 3 wt.% for all but P_2O_5, which yielded a standard deviation of 6.6 wt.%. Because the detector employed does not analyze for H_2O, oxide weight percentages for sheet-silicate standards were normalized to 0 wt.% water to permit comparison to EDX analyses. This procedure impacts the glauconite analyses most significantly as their water content typically varies from 8–16 wt.% (Birch, 1971). Except for Na_2O and FeO accuracies of standard analyses were always within 20% (and usually within 6%), when calculated as follows for oxides detected in amounts of about 10 wt.% or greater:

$$\text{Accuracy} = \frac{(\text{Mean value} - \text{Accepted value})}{\text{Accepted value}} \times 100$$

Values are given in wt.% of the oxide. The system tends to underestimate MgO and overestimate SiO_2 and Al_2O_3. Underestimation of Fe and overestimation of Al and Si in phyllosilicates explains why so many glauconite analyses do not appear to meet the chemical criteria for glauconite (Fe^{3+}>>Al). Many oxides present in fractions of a weight percent were not detected and others present in small amounts (0.2 wt.%) yielded very large errors (>340%). The lightest element measured by the detector was sodium and fairly large errors in accuracy (around 30-40 wt.% in plagioclase and albite) were observed. Iron contents (reported as wt.% FeO) for biotite and chlorite standards were underestimated by 38% and 49%, respectively. To summarize, analyses reported here give a semi-quantitative indication of mineral chemistry, and are useful for indicating compositional variation from site to site and from top to bottom of each well. They also provide the necessary information to improve geochemical modeling of the evolution of ground water chemistry in the CHAS.

RESULTS

Petrography

Within the study area, the CHAS is a sandy, fossiliferous and occasionally dolomitic limestone. It is dominated by a micrite matrix with quartz, bioclasts and a very high percentage of secondary moldic porosity due to the dissolution of bioclasts. Glauconite, phosphate, feldspar, and iron sulfide are also present. Two morphologic types of glauconite are observed in the CHAS within the study area-- internal molds of bioclasts and granular peloids. Carbonate grains stained with a mixture of Alizarin Red-S and potassium ferricyanide in 0.2% hydrochloric acid, revealed only the presence of calcite with no dolomite or ferroan calcite in samples from wells 4, 5, and 6. The lack of dolomite or ferroan calcite in those samples is also supported by EDX data. Well 1 contains rhombohedra of dolomite, some of which have been replaced with SiO_2; and XRD and EDX data support the existence of dolomite in this sample. Based on

Table 4. Point count data for wells 4, 5, and 6. (Peloids include both glauconite and phosphate.)

Well 4					
DEPTH OF SAMPLE	135-178 feet	178-198 feet	198-203 feet	203-238 feet	238-243 feet
PERCENT OF TOTAL ROCK					
matrix	42.25	55.50	50.50	54.50	59.00
cement	7.50	6.50	15.00	1.50	5.50
quartz sand	33.50	2.50	9.50	19.50	12.50
peloids		1.50		1.00	1.50
bioclasts	13.00	18.50	16.00	12.50	8.50
pore space	3.75	15.50	9.00	11.00	13.00
TOTAL	100	100	100	100	100
% BIOCLASTS (BASED ON # PRESENT IN EACH SAMPLE)					
mollusk	86.53	64	75	52	64.71
brachiopod	9.62	8	12.5	8	
bryozoan		21.33	6.25	36	26.47
foraminifera		4	3.12		
echinoderm	3.85	2.67	3.13	4	8.82
TOTAL	100	100	100	100	100
Well 5					
DEPTH OF SAMPLE	200-220	220-231	231-240	240-270	
PERCENT OF TOTAL ROCK					
matrix	56.00	57.50	53.50	33.33	
cement		0.50	3.50	7.33	
quartz sand	13.00	18.50	14.50	30.33	
feldspar			0.50		
peloids		0.50	0.50	0.33	
lithic fragments			0.50		
biotite	0.50	0.50	0.50		
opaque	1.50				
intraclasts	7.00	4.50			
bioclasts	21.50	18.00	26.00	5.68	
pore space			0.50	23.00	
TOTAL	100	100	100	100	
% BIOCLASTS (BASED ON # PRESENT IN EACH SAMPLE)					
mollusk	79.06	77.78	53.84	63.64	
brachiopod	2.33	8.33	34.62		
bryozoan	11.63	2.78		18.18	
foraminifera	6.98	2.78	3.85	18.18	
echinoderm		8.33	7.69		
TOTAL	100	100	100	100	
Well 6					
DEPTH OF SAMPLE	24-30	30-32	23.25-32.33	32.52	52-62
PERCENT OF TOTAL ROCK					
matrix	58.50	58.00	65.50	54.50	42.96
cement			1.00	2.00	7.04
quartz sand	9.00	14.50	4.00	5.50	12.68
feldspar				0.50	2.11
peloids	3.00	10.50	2.50	2.00	18.31
lithic fragments				0.50	
bioclasts	29.50	17.00	27.00	35.00	16.90
TOTAL	100	100	100	100	100

	% BIOCLASTS (BASED ON # PRESENT IN EACH SAMPLE)				
mollusk	27.12	20.60	55.56	14.29	100
brachiopod	15.25	8.82	7.41	10.00	
bryozoan	1.70	8.82	3.70	48.57	
foraminifera		5.88	11.11		
echinoderm	55.93	55.88	22.22	27.14	
TOTAL	100	100	100	100	100

the Folk (1962) classification scheme, which emphasizes composition over texture, the CHAS is a quartz glauconitic biomicrite. Using the Dunham (1962) classification, which emphasizes texture, the CHAS is a wackestone.

Matrix and Cement

The CHAS is a matrix-supported limestone with minor amounts of calcite cement. The micrite is frequently aggraded to microsparite due to burial and diagenesis. Occasionally, the cement is dolomitic (based on EDX data) partially replacing bioclasts and glauconite grains.

Allochems

Bioclasts account for up to 35% of the volume of the CHAS. Mollusks and echinoderm fragments are dominant, but brachiopods, bryozoans, and foraminifera are present. The total number of bioclasts increases from east to west in the upper CHAS (Table 4). The percentage of echinoderms increases from east to west conversely; mollusks and bryozoans decrease in abundance from east to west. The total number of bioclasts increases slightly from north to south in the study area but decreases with depth in the limestone (Table 4). Echinoderms increase in abundance from north to south, but there is no apparent north-south trend for mollusks and bryozoans.

Accessories

Non-carbonate peloids account for a smaller percentage (0.33-18%) of the CHAS. EDX and XRD analysis revealed that the peloids are either glauconitic or phosphatic in composition. They range from 0.03 to 0.22 mm in diameter and vary in color from light olive green to dark, almost-blackish green. Peloids are present in all six of the wells at various depths and abundances. They make-up 2-18% of the limestone in well 6 (Table 4). In this well there are two zones in which peloids are locally abundant, the first from 30-32 fbsl where peloids account for 10.5% of the rock, and the second from 52 to 62 fbsl where peloids comprise over 18% of the rock sample. Well 5, the southernmost well in the study area, contains the lowest percentage of peloids (0.3% of the total rock) (Table 4). Well 4 also contains few peloids, making up 1.0-1.5%. In general, the overall percentage of peloids increases from east to west and from south to north in the study area, but they are concentrated in localized vertical intervals.

Extraclasts

The extraclasts are dominated by sand-size quartz grains (0.03 to 1.88 mm) that range from well-rounded to angular. Quartz accounts for up to 33% of the rock sample (Table 4). Other extraclasts present in minor amounts are feldspar and lithic fragments found in wells 5 and 6, and biotite flakes found only in well 5 (Table 4).

Lithology

Cross-sections B-B' and C-C' (Figure 3 and 4) were constructed from the six sampled wells penetrating the CHAS. All depths are given in feet with respect to sea level. The cross-sections indicate the occurrence of accessory minerals identified within the sample intervals. Also shown is the proposed boundary between the upper and lower CHAS determined from this research. The boundary was chosen based on significant lithologic, mineralogical and chemical changes observed during this investigation. Along section B-B' (Figure 3), samples from the three northeastern wells include continuous drill cuttings of the entire CHAS, but the two southwestern wells are samples from cored intervals containing parts of the upper and lower

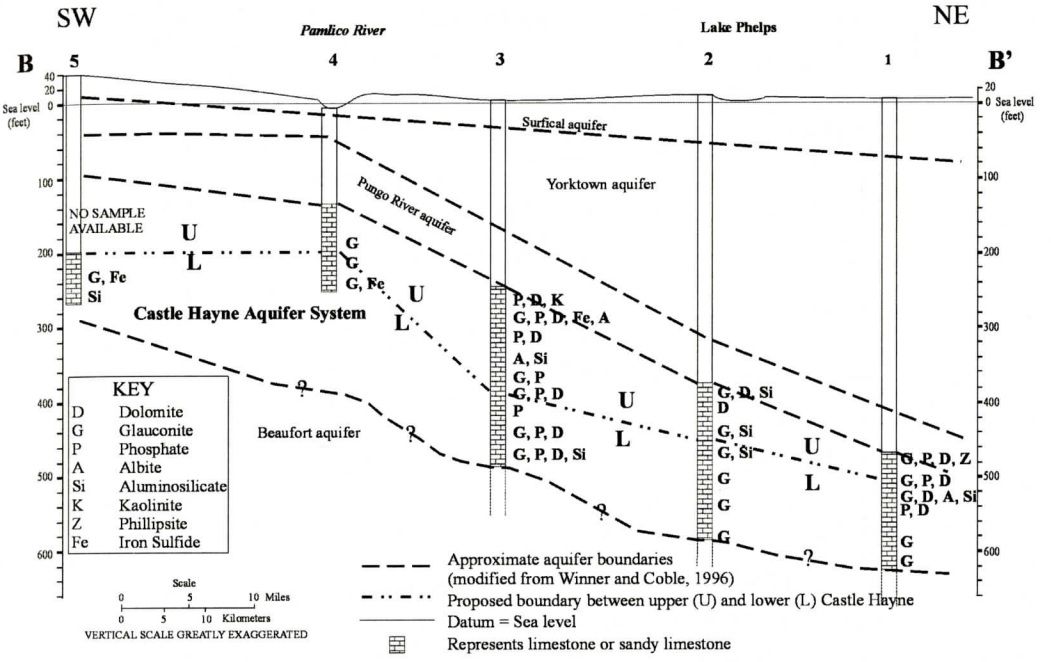

Figure 3. Cross-section B-B' (location shown on Figure 1). Mineral assemblages indicated were determined from all types of analyses. Pure calcite and quartz are abundant in all wells.

CHAS. Along section C-C' (Figure 4), the samples also represent cored intervals of parts of the upper and lower CHAS. Because the drill cuttings (wells 1, 2, and 3) were washed to remove drilling mud, most fine-grained material originally present has been lost and could not be analyzed. Therefore, the abundance of clay minerals such as kaolinite, illite, and smectite has probably been significantly underestimated. Glauconitic clays occurred mostly as peloids which were not as susceptible to removal because of coarser grain size.

The CHAS is a biomicrite with quartz sand, glauconite, dolomite, apatite, other clay minerals, and lesser amounts of iron sulfide, and aluminosilicates. The upper part of the CHAS is characterized by sandy, fossiliferous limestone containing glauconite, phosphate, dolomite and minor iron sulfide. Detailed cross sections of each core logged can be found in Tolen-Mehlhop (1998). The lower CHAS is also a fossiliferous limestone with accessory phosphate and iron sulfide, but generally contains more abundant glauconite and less dolomite than the upper CHAS. The lower part of the aquifer is also sandier than the upper part in the eastern section of the study area. Upper CHAS samples are not available for the western part of the study area.

In well 3 the aquifer becomes distinctively arenaceous between 380 - 400 fbsl, possibly representing the transition between the upper and lower units of the CHAS (Figure 3). A distinct transition to a sandier lithology is also present in well 4 at 200 fbsl (Figure 3 and 4) and in well 1, the northernmost well, the transition is at 500 fbsl (Figure 4). Wells 2 and 5 (Figure 3) are sandy, in parts, throughout the entire sampled zone. Since the entire sample section of well 5 is sandy, it is placed in the lower CHAS. The transition between the upper and lower CHAS in 2 (Figure 3) is placed at 450 fbsl based on the abundance of dolomite in the uppermost section. Samples from well 6 are placed in the lower unit based on the abundance of glauconite (Figure 4).

Dolomite is present at three localities and is most pervasive north of the Pamlico River. Well 3 (Figure 3) has zones of dolomite throughout the CHAS. Wells 1 and 2 contain dolomite in the upper part of the aquifer. Glauconite is dis-

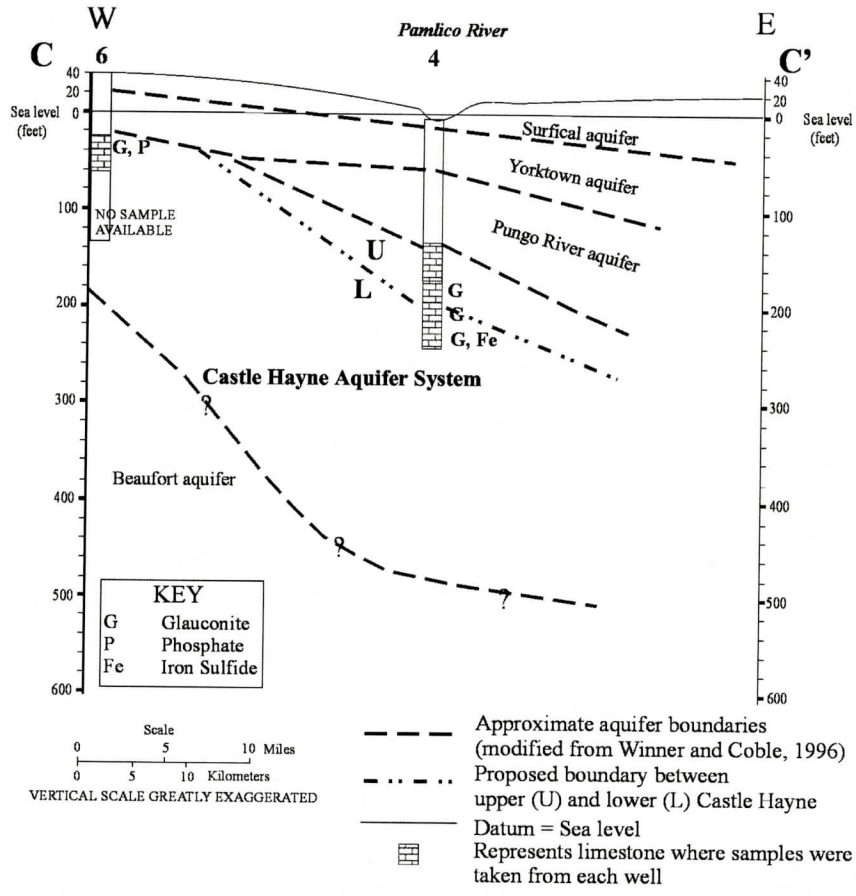

Figure 4. Cross-section C-C' (location shown on Figure 1). Mineral assemblages indicated were determined from all types of analyses. Pure calcite and quartz are abundant in all wells.

persed throughout the CHAS, but is most abundant in wells 2 (Figure 3) and 6 (Figure 4). Phosphate is also present in the CHAS and is most abundant in well 3 (Figure 3).

The two northernmost wells (1 and 2) contain the majority of the silicates (other than glauconite) observed in the upper portion of the aquifer (Figure 3). These aluminosilicate minerals are associated with glauconite, phosphate, and dolomite.

Mineralogy

The CHAS occurs between 465-625 fbsl in well 1 (Figure 3). Dolomite is pervasive in the upper half of the aquifer at this locality and all the dolomite grains analyzed by EDX were from this well or well 3. Phosphate minerals are present throughout many intervals of the aquifer, but are most abundant between 465-545 fbsl. Albite and phillipsite are present at 515-525 and 535-545 fbsl, respectively.

In well 2, the CHAS is present from 375-585 fbsl (Figure 3). Based on XRD analysis, glauconite is only detectable in the bottom 20 feet of the aquifer; however, accessory mineral absence on the XRD pattern does not mean absence from the sample because of the XRD detection limits. Dolomite is present in high relative abundance between 375-415 fbsl. In several additional intervals there may be peaks that correspond either to glauconite, dolomite, phosphate, phillipsite or albite, but due to the low intensities of additional distinguishing peaks, these minerals could not be identified with confidence.

Table 5. Summary of EDX analyses of glauconite. Accuracies of standard analyses were always within 20% and usually within 7%. Precision of standard analyses was 3% for all but P_2O_5, for which it was 7%.

Well	Ranges in Weight% Oxide					Average Weight% Oxide				
	SiO_2	Al_2O_3	Fe_2O_3	MgO	K_2O	SiO_2	Al_2O_3	Fe_2O_3	MgO	K_2O
1	44 - 60	11 - 33	8 - 20	7 - 9	4 - 8	59	17	15	9	6
2	54 - 69	6 - 18	10 - 21	3 - 9	5 - 10	65	14	17	9	8
3	45 - 61	8 - 26	2 - 24	5 - 10	5 - 8	56	13	16	8	7
4	53 - 70	6 - 17	14 - 22	0 - 9	5 - 8	58	11	18	7	7
5	64	11	9	7	9	64	11	9	7	9
6	54 - 68	7 - 23	6- 20	0 - 17	3 - 9	63	13	15	7	7

Well	# of ions on the basis of 22 O equivalents, ignoring H_2O^-						# of ions on the basis of 22 O equivalents, ignoring H_2O^-					
	Tetrahedral		Octahedral				Tetrahedral		Octahedral			
	Si	Al	Al	Fe+3	Mg	K	Si	Al	Al	Fe+3	Mg	K
1	5.6 - 7.4	0.5 - 2.4	0.8 - 2.5	0.7 - 2.0	1.3 - 1.7	0.7 - 1.3	7.1	0.9	1.5	1.4	1.6	1
2	6.9 - 8.7	0.0 - 1.1	0.9 - 1.9	1.0 - 2.1	0.7 - 1.7	0.8 - 1.3	7.4	0.6	1.3	1.4	1.5	1.1
3	5.9 - 7.8	0.4 - 1.9	0.5 - 2.1	1.0 - 2.4	1.0 - 1.7	0.9 - 1.3	7	0.7	1.2	1.6	1.5	1
4	6.8 - 8.9	0.0 - 1.0	0.6 - 1.5	1.3 - 2.4	0.0 - 1.7	0.8 - 1.3	7.6	0.5	1.1	1.7	1.3	1.1
5	8.1	0.0	1.6	0.9	1.3	1.4	8.1	0	1.6	0.9	1.3	1.4
6	7.3 - 8.5	0.0 - 0.7	1.0 - 2.8	0.5 - 2.0	0.0 - 1.7	0.5 - 1.5	7.7	0.4	1.5	1.3	1.3	1.1

In well 3, the CHAS occurs from 246-486 fbsl. Glauconite, dolomite, and phosphate are present throughout the section although glauconite is most abundant in the lower portion. Albite and kaolinite were detected in a few intervals in the upper part of the core. Well 6 contains a portion of the lower CHAS between 24-62 fbsl (Figure 4) and glauconite and phosphate were detected throughout.

Mineral Chemistry

Spectra were collected for 250 to 300 pure calcium carbonate or pure quartz samples, but no semi-quantitative analysis was performed. Semi-quantitative analysis of 147 glauconite grains, 48 phosphates, 23 Mg carbonates, 9 aluminosilicates, and 5 iron sulfide grains was conducted (Tolen-Mehlhop, 1998).

Glauconite Chemistry

Glauconite is present in all six of the wells at various depths and abundances and will be discussed in more detail below (Table 5). Complete EDX results for glauconite can be found in Tolen-Mehlhop (1998). In well 5 only one grain was found for analysis.

Carbonate Chemistry

Hundreds of spectra revealed predominately pure calcium carbonate grains with only 21 dolomites and two low-Mg calcites. In wells 1 and 3 dolomite is found with low-Mg calcite and in the northernmost well, 1, dolomite is present with glauconite. Baum and others (1985) described dolomite from the upper part of the Castle Hayne.

Chemistry of Minor Minerals

Phosphate minerals are present as peloids in three wells within the study area. EDX analyses of 47 phosphate grains yielded a range in P_2O_5 and CaO of 30.0-37.4 wt.% and 61.9-69.9 wt.%, respectively. Because the detector could not analyze elements lighter than Na, it was not possible to determine the amount of carbonate, fluoride, or hydroxyl; however, no chloride was detected. Phosphate is most abundant in well 3 where it is found with glauconite and iron sulfide (Figure 3). Well 1 has intervals containing

both phosphate and dolomite. Well 6, the westernmost and shallowest, has phosphate with glauconite (Figure 4).

An iron sulfide mineral (possibly pyrite) was analyzed at three locations and aluminosilicate minerals, most likely zeolites (phillipsite) and/or feldspar, were found in four of the wells sampled (Figure 3). Baum and others (1985) and Moran (1989) noted the presence of zeolites in the CHAS.

DISCUSSION

Glauconite Chemistry

To elucidate differences in glauconite chemistry from well to well and with depth in each well, the average mole percents of K in the interlayer, Al and Si in the tetrahedral site, and Al, Fe, and Mg in the octahedral site for each sample were calculated and plotted on various diagrams. There is a strong negative linear correlation between octahedral Al and Fe [correlation coefficient (r = -0.88)]. As observed by others, Al increases as Fe decreases, whereas, Mg shows only minor variability (Cimbalnikova, 1971; Weaver and Pollard, 1975; Jarrar and others, 2000). While the total sample population consists of peloids and internal molds of bioclasts, the high-Al outliers are all peloids (Figure 5). Octahedral Fe and Al show no obvious correlation with octahedral Mg. There is a weak positive correlation (r = 0.38) between octahedral and tetrahedral Al. Data for tetrahedral Si versus K yield a weak positive correlation (r = 0.48). There is a very weak negative correlation between octahedral Mg and K (r = -0.29). The average K concentration in glauconite increases with depth in each well. Faure (1998) states that the concentration of K is variable and increases with time depending on the availability of K in the environment.

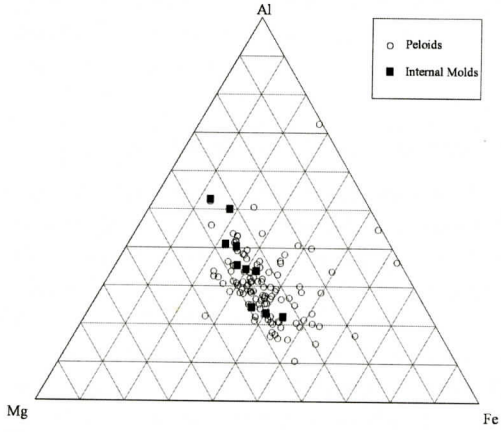

Figure 5. Ternary diagram representing mole percent of octahedral Al, Fe, and Mg for all glauconite peloids and internal molds.

Comparison of these data with more quantitative studies such as those of Jarrar and others (2000), Birch and others (1976), Buckley and others (1978), Ireland and others (1983) is difficult because of the semi-quantitative nature of our results. However, a few general comparisons can be made. As in the present study, Birch and others (1976) did not see a strong inverse relationship between wt.% Fe_2O_3 and K_2O, although Jarrar and others (2000) did report such a relationship. Based on their work and that of others, Odin and Matter (1981, p. 623) saw no correlation between interlayer cations (mainly K) and iron in octahedral positions because "... incorporation of the two cations takes place by different processes and at different times during the glauconitization process. The fixation of iron precedes the incorporation of potassium." The data of Birch and others (1976) showed a weak positive correlation between K_2O and SiO_2, as do the present results, however those researchers described a strong correlation between MgO and K_2O not revealed during this study.

The ternary diagrams in Figure 6 depict mole percents of Al, Fe, and Mg found in the octahedral site of glauconite grains from throughout the study area.Along the west/east cross section iron contents of glauconite grains are significantly higher in well 4 than in 6. Magnesium contents are very similar throughout both cores. The mole% Mg is fairly constant from southwest to northeast (wells 4, 3, 2, and 1), while the average Fe decreases as the maximum and minimum mole percents of Fe decrease. Average Al increases from the southwest to the northeast. The statistical significance of this geographic variation in iron content was verified using an

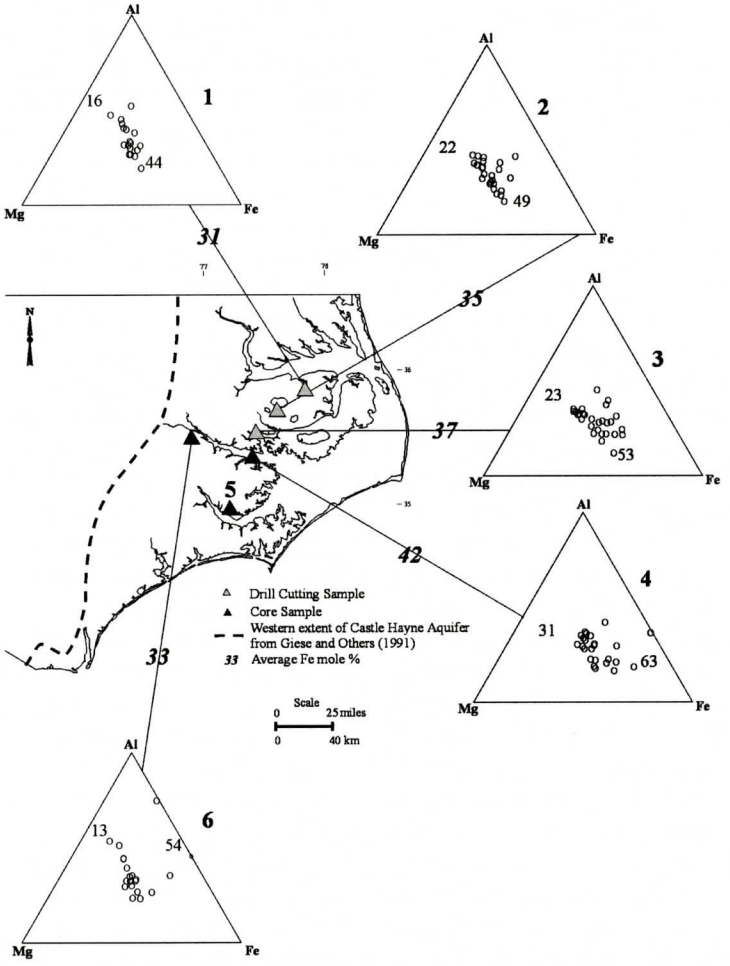

Figure 6. Ternary diagrams representing mole percent of octahedral Al (top), Fe (lower right), and Mg (lower left) for all glauconite analyses. (Numbers within triangles represent high and low mole percent values of Fe). Well 5 was only represented with a single glauconite analysis (Al = 43%, Fe = 24%, Mg = 33%), so a ternary was not drawn for this well.

Table 6. Statistical analysis of geographic variation of iron in glauconite.

Variable	Description	Mean	SD
Fe3	Mol% of Fe in octahedral site	1.52	0.35
LATITUDE	36 - latitude	0.41	0.16
DEPTH	Depth – top of formation	70.50	59.25
WELL4	1 if well 4, 0 otherwise	0.17	0.38

ordinary least squares regression (Table 6). The dependent variable is mol percent Fe in the octahedral site. The independent variables are latitude (measured as 36 – latitude), depth (measured as the top of the formation subtracted from depth), and a dummy variable for well 4.

The F statistic (Table 7) indicates that the overall model is statistically significant at the p =.0001 level. The R^2 statistic indicates that 19.5% of the total variation in the dependent variable is explained by the independent variables. Each of the independent variables is statistically significant to, at least, the p =.05 level with t-statistics (t=coefficient / standard error) greater than the critical value of 1.96.

Harris and others (1997) studied glauconites from the late Paleocene Lang Syne Formation at the Savannah River Site, in South Carolina. Their major interest was in the accuracy of Rb-

Table 7. Multiple regression Fe^3

	Coefficient	t-stat
Intercept	1.454	12.50
LATITUDE	0.576	2.56
DEPTH	-0.001	-2.28
WELL4	-0.413	-4.61
R2	0.195	
F-value	9.036	

Sr age dating on such clay minerals. In the course of their study they did microprobe analyses of glauconite grains. Quantitative comparisons of Castle Hayne glauconites with the glauconitic micas of Harris and others (1997) are not possible because of the semi-quantitative nature of our results. However, one basic difference in a major chemical trend observed during the two studies is obvious. Their results indicated that glauconitic micas originally deposited in shallower water had lower Fe contents than those deposited in deeper water. The opposite trend was observed in the present study, in which glauconite in the deeper-water part of the section (NE) had lower Fe contents. Harris and others (1997) pointed out that the Fe content of glauconites need not be a function only of water depth during original deposition. Birch and others (1976) suggested that during oxidation and maturation glaucony pellets show significant increases in Fe. The higher Fe content of our updip glauconite grains may be due to their occurring in the shallowest part of the section where they acquired their Fe content during post-depositional oxidation. Alternatively, their increased Fe content could be due to increased maturity.

Granular peloids and internal molds of bioclasts are the two morphologic types of glauconite observed in the CHAS within the study area. According to Odin and Fullagar (1988), fecal pellets are the predominate substrate on which glauconitization occurs. The samples range from 10-75 mole% Al, from 10-65 mole% Fe, and from 0-50 mole% Mg (Table 5). In general, Mg shows less variability than Al or Fe; however, the peloids have a wider variability than the internal mold glauconite. There are some outliers with zero Mg and many peloid analyses with less than 30 mole% Mg.

In the octahedral site Al and Fe contents are generally inversely related, while Mg shows less variability. As observed by Buckley and others (1978) during their study of glauconites from a wide variety of localities (i.e., land outcrops, boreholes, and submarine continental shelf deposits), glauconites analyzed from a given geological horizon generally also have a similar composition. For wells 1, 3, 4, and 6, Al increases initially with depth in the uppermost part of the upper CHAS as Fe decreases. Well 2 is the only well where Al initially decreases with depth as Fe increases. Below this interval in well 2, there is less variability of Al and Fe with depth than in the other wells. The only glauconite grain analyzed in well 5 occurred at 231 fbsl and had 24, 43, and 44 mole% Fe, Al, and Mg, respectively.

Wells 4 and 6 are along an east-west line through the study area and are approximately 20 miles (45 km) apart (Figure 1). The average Fe content in the eastern well (4) is greater than that of the western well (6). Glauconite in well 6 generally has higher Fe content when phosphate is present. In well 4, Fe is at its highest where Fe- sulfide minerals are present.

Figure 7 shows proposed correlations of changes in the concentrations of octahedral Fe in glauconite with depth (wells 1, 2, and 3). These wells represent a complete vertical sequence through the CHAS along a transect from southwest to northeast in the northern part of the study area. The shaded patterns represent zones of similar geochemical trends of Fe with depth in each zone. Similar geochemical stratigraphic relationships exist for each element (Al, Fe, Mg) in the three wells. The proposed position of the boundary between the upper and lower Castle Hayne was based mainly on lithology and mineralogy, but also appears to be marked by changes in glauconite chemistry shown here.

Chemistry of Other Minerals

Pure calcium carbonate and dolomite were identified through EDX analysis. Neither the EDX nor staining procedure detected any trace elements in the calcium carbonate. The samples may have contained traces of other elements, but in order for EDX to detect a particular ele-

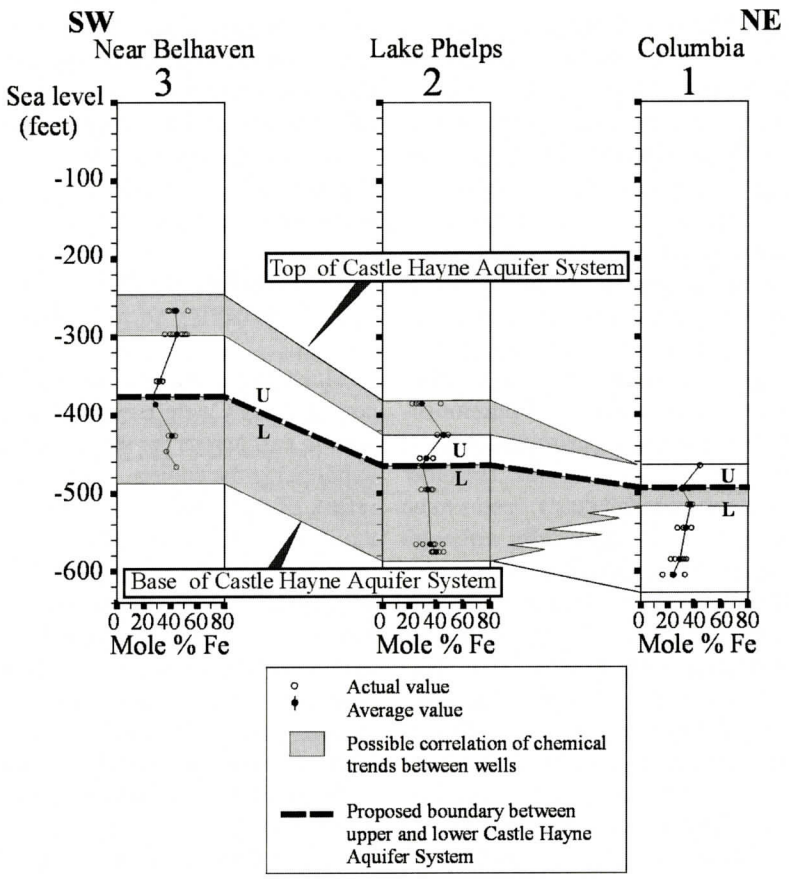

Figure 7. Proposed correlation of trends in octahedral Fe for glauconite in wells 1, 2, and 3.

ment, the sample must usually contain at least 0.1 weight percent (Table 3).

The dolomite (stoichiometric or non-stoichiometric) in this study appears to be secondary, replacing the matrix material. Stoichiometric dolomite contains 49 to 51 mole% $MgCO_3$ and non-stoichiometric dolomite contains 44 to 48 mole% $MgCO_3$ (Randazzo and Hickey, 1978). Replicate analyses of standards suggest the values for the mole% of $CaCO_3$ and $MgCO_3$ end-members determined could be as much as 3 mole% low for $CaCO_3$ and 2 mole% high for $MgCO_3$. Applying this correction still yields only one grain in well 3 that appears to be stoichiometric dolomite. Dunham (1962) observed that stoichiometric dolomite crystals are frequently found where the original texture of the rock is preserved and non-stoichiometric dolomite crystals are associated with obscured or obliterated original depositional texture (Dunham, 1962). Because of the limited accuracy of the semi-quantitative EDX analyses and the lack of dolomite in petrographic samples, it was impossible to verify these relationships in this study.

Phosphate samples are hydroxy-, fluor-, or carbonate- apatites, and do not contain any chloride (Cl^-). Based on a limited amount of reflected-light microscopy and EDX, pyrite (Fe 46.6 and S 53.4 mole%) is most likely the iron sulfide present in the CHAS. For wells 3 and 5, the formula is: $Fe_{0.9}\ S_{1.5}$. In well 4, the formula is slightly different: $Fe_{0.8}\ S_{1.8}$. If this is pyrite, its chemistry suggests S is underestimated by EDX and/or Fe is overestimated.

The aluminosilicates found in this study are most likely Na-rich feldspars, zeolites (perhaps phillipsite) or clay minerals. Feldspars and zeo-

lites are very similar in structure and chemistry. Both are built of AlO_4 and SiO_4 tetrahedral frameworks. Zeolites, however, have highly variable amounts of water in the voids of their framework (Klein and Hurlbut, 1993). Unfortunately, EDX is unable to evaluate the amount of water or other light constituents present, making it impossible to conclusively identify these minerals. The greatest variability in the aluminosilicate minerals is in the weight percent of Al_2O_3 (2-39 weight%) and SiO_2 (48-79 weight%). There is less variability in the other oxides. Well 2 contains two types of aluminosilicates. Sodium-rich feldspar occurs in veins and as replacement surrounding the veins. The other type, present as sub-rounded clasts, seems to be phillipsite (zeolite) petrographically, although the Al values are high. Data from XRD also suggest that phillipsite may be present in this well. Baum and others (1985) identified only clinoptilolite in their study. In well 1, the well-rounded clasts are possibly Na-rich feldspars with high Si and low Al values. X-ray diffraction data identified albite in this well. The analyses from wells 3 and 5 are also possibly Na-rich feldspars. Albite was identified in well 3 by XRD analysis, and petrographic analysis of well 5 revealed the presence of minor amounts of plagioclase feldspar.

Environment of Deposition

The aquifer is comprised of sediments deposited on the middle to outer shelf during sea level high- and low-stand cycles. The presence of glauconite and phosphate peloids indicates low energy and sedimentation rates in temperate latitudes during sea level high-stands. Conversely, the occurrence of abundant bioclasts (shell hash) and sand in certain intervals suggests higher sedimentation rates during sea level low-stands. This is especially evident in the lower CHAS, which is more arenaceous than the upper CHAS. The similar geochemical facies shown in Figure 7 suggest that present day rock chemistry is strongly related to lithofacies and their regional trends in the subsurface. These chemical facies trends are most likely reflecting original responses to sea level changes and the impact on the depositional environment. Furthermore, these data suggest not only changing lithofacies in response to a change in environment of deposition, but also changing geochemical facies in response to changing chemistries in the marine waters on the continental shelf during the Tertiary.

Mineral Chemistry and the Chemistry of Ground Water

Much of the change in major element concentration in Castle Hayne ground water from west to east across the study area, and from top to bottom in the aquifer, can be explained by the influx of varying proportions of seawater of various geologic ages (Sherwani, 1980; Lloyd and Daniel, 1988; Harned and others, 1989; Woods and others, 2000a, 2000b). In places, however, chemical interaction between aquifer materials and ground water is more important in determining ground water chemistry. In those cases data on the mineralogy and mineral chemistry are needed to permit geochemical modeling of ground water evolution and prediction of water quality.

Running approximately along a line passing through the eastern end of cross-section line A-A' and the western end of Albemarle Sound (Figure 1), a saltwater boundary occurs in the Upper Castle Hayne (UCH). East of this line the aquifer contains > 250 mg/L Cl^- (Woods and others, 2000a), which is the maximum allowable Cl^- concentration in drinking water in the USA. The water chemistry east of this line is dominated by seawater influx (Woods and others, 2000b). However, another water-quality standard, the concentration of total dissolved solids (TDS) in drinking water (limit=500 mg/L) is exceeded in the UCH 10-40 km west of the 250mg/L Cl^- boundary (Woods and others, 2000a). Therefore, factors other than seawater influx are having a negative impact on the quality of ground water there. These factors are related to aquifer mineralogy. Because of the high solubility of limestone, UCH ground water reaches the TDS limit many kilometers west of where it exceeds the Cl^- limit. However, also due to the dominance of limestone in the aqui-

fer, equilibrium with calcite tends to keep the TDS buffered at approximately this level (Sprinkle, 1989).

Alkalinity and the concentrations of Ca^{2+} and Mg^{2+} are very sensitive to aquifer mineralogy. Ca^{2+} dominates the cations in the calcium-rich, bicarbonate-rich waters from the UCH in the western part of the study area. As a result, much of this ground water exceeds the recommended hardness standard. On the bright side, the high alkalinity and Ca^{2+} concentration also makes this aquifer an excellent source of water for aquaculture. In some aquifers dolomite dissolution is an important Mg^{2+} source, but mineralogical data discussed above suggest the UCH contains insufficient dolomite to provide the observed Mg^{2+}. Eliminating dolomite as a significant Mg^{2+} source provides additional information about the influence of aquifer materials on water chemistry.

Fe and fluoride (F^-) in ground water are two of the most expensive water-quality issues facing suppliers, therefore, understanding the impact of aquifer mineralogy on water chemistry could guide selection of well sites. In many limestone aquifers, exchange of Ca^{2+} in ground water for Na^+ in clay minerals releases Na^+ into the water (e.g., Sprinkle, 1989). Ion-exchange that involves K^+ released into solution and Fe^{2+} adsorbed on clays is another possible process (Chapelle, 1983). Glauconite is present in most Castle Hayne core samples in amounts of 0.5-3%; but it sometimes makes up 30%. Understanding variations in regional glauconite chemistry could help elucidate causes of water-quality changes. For example, the lack of a significant correlation between K^+ and octahedral Fe in this study may be evidence that this process of K^+-Fe exchange is not occurring to a significant extent. This encourages us to consider alternatives to explain the Fe chemistry of UCH ground water. High F^- concentrations observed in the Castle Hayne cannot be explained by influx of seawater because the proportions of F^- to other ions are incompatible with this mechanism. Identification of significant apatite in the aquifer provides an alternative explanation of F^- concentrations. F^- may be released to ground water through an anion exchange mechanism involving hydroxyl ions in apatite (Zack, 1980).

Finally, computer programs such as PHREEQE and NETPATH (Parkhurst and others, 1980; Plummer and others, 1991) can be used to elucidate the geochemical processes affecting water chemistry if chemical data for minerals present are available. Such models, and more generally, basic knowledge of aquifer mineralogy, will allow us to extend our predictions about ground water chemistry beyond the few wells we can actually afford to sample.

SUMMARY AND CONCLUSIONS

Lithology

The CHAS is composed dominantly of quartz glauconitic biomicrite. Some zones also contain phosphate, dolomite, pyrite, feldspar, and minor zeolite. Mollusk and echinoderm fragments are the dominant bioclasts while brachiopods, bryozoans, and foraminifera are also present. Aragonitic fossils are frequently dissolved, leaving zones of high moldic porosity making the limestone a prolific aquifer in eastern North Carolina.

Diagenesis

The micrite matrix is commonly aggraded to microsparite due to burial and diagenesis. Dolomite is found in low abundance in both the upper and lower portions of the CHAS, but is slightly more pervasive north of the Pamlico River. In addition, some dolomite rhombohedra have been replaced by silica during diagenesis. Because of its presence in low quantities throughout the aquifer, and the lack of abundance at any specific depth or geographical location, dolomite was probably not deposited primarily, but rather is a secondary diagenetic mineral.

Lateral Trends

The dominant lateral trend in the study area is changing lithofacies and chemistry from the southwest to northeast. The total number of bio-

clasts increases from east to west and slightly from north to south in the study area. Glauconite abundance generally increases from southwest to northeast. Average octahedral Al content of glauconite increases from southwest to northeast, while average octahedral Fe content decreases from southwest to northeast in the study area. Al and Fe content are inversely related to each other while Mg content in the octahedral site is less variable.

Vertical Trends

The dominant vertical trend in the study area is changing lithofacies from sandy, glauconitic limestone in the lower CHAS to shelly lime mud in the upper CHAS. The proposed boundary between the upper and lower CHAS is noted both lithologically and geochemically. Micrite mud, bioclasts and dolomite with minor amounts of glauconite, phosphate, and iron sulfide characterize the upper CHAS. The lower CHAS is arenaceous with more glauconite and minor amounts of phosphate, dolomite and iron sulfide. The three northeastern wells contain complete sections of the aquifer. They show definite correlations in glauconite chemistry, which correspond to lithologic changes in the aquifer. In the two southwest wells, Fe content in glauconite increases downward in the upper CHAS before it decreases. In the northeastern most well (1) this upper zone of increasing Fe content with depth is missing, but the underlying zone, in which Fe content decreases with depth, is present in all three wells. The base of the latter zone coincides with the lithologic changes that mark the boundary between the upper and lower CHAS. Iron content in glauconite increases with depth in the lower CHAS in wells 2 and 3. The increasing and decreasing trends of Fe, Al, and Mg in the octahedral site of glauconite suggest similar geochemical environments with changing environments of deposition in the upper and lower CHAS.

Environment of Deposition

Sediments were deposited on the middle to outer shelf during sea level transgressions and regressions as indicated by the bioclast assemblage (mollusks, echinoderms, bryozoan, brachiopods, and foraminifera). Quartz sand is most pervasive in the lower CHAS suggesting a stronger sediment influx during early deposition of the limestone. Micrite mud is more abundant in the upper CHAS possibly due to lower energy and higher sea level. The occurrence of glauconite and phosphate in localized zones suggests low sedimentation during sea level high-stands. The southwest region of the study area was closer to shore with shallower, more agitated waters, indicated by the presence of more bioclasts and quartz sand and less glauconite. The northeast region in the study area was further offshore in deeper water on the shelf, indicated by the presence of more micrite mud and glauconite and fewer bioclasts.

The data presented in this study suggest that there are definite chemical trends in glauconite that have a strong correlation with lithofacies. These trends are most likely related to mineral and pore water chemistry within the environment of deposition. Dissolution and precipitation of aquifer minerals and ion exchange reactions affect water chemistry within coastal limestone aquifers. The results in this study may be utilized in the construction of geochemical models designed to evaluate water/ rock geochemical interactions in aquifers such as the CHAS of eastern North Carolina.

ACKNOWLEDGEMENTS

We gratefully acknowledge the help of John C. Whitehead (UNC-Wilmington) with statistical analysis of glauconite chemistry. This work was partially supported by a grant from The Water Resources Research Institute of The University of North Carolina. The manuscript was significantly improved by the comments of Richard Spruill, Paul Fullagar, and two Southeastern Geology reviewers, W. Burleigh Harris and Michael Katuna.

REFERENCES CITED

Bailey, S.W., 1980, Summary of recommendation of AIPEA Nomenclature Committee: Clay Minerals, v. 23, p. 85-93.

Baum, G.R., 1977, Stratigraphic framework of the Middle Eocene to Lower Miocene Formations of North Carolina: Unpublished Ph.D. dissertation, University of North Carolina, Chapel Hill, North Carolina, 139 pp.

Baum, G.R., Harris, W.B., and Zullo, V.A., 1978, Stratigraphic revision of the exposed Middle Eocene to Lower Miocene Formations of North Carolina: Southeastern Geology, v. 20, p. 1-19.

Baum, G.R., Collins, J.S., Jones, R.M., Madlinger, B.A., and Powell, R.J., 1979a, Tectonic history and correlation of the Eocene Strata of the Carolinas: Preliminary report, *in* Baum, G.R. and others, editors, Structural and Stratigraphic Framework for the Coastal Plain of North Carolina: Carolina Geological Society Field Trip Guidebook, American Coastal Plain Geological Association Guidebook for the Annual Field Conference, p. 87-94.

Baum, G.R., Harris, W.B., and Zullo, V.A., 1979b, Historical review of Eocene to Early Miocene stratigraphy, North Carolina, *in* Baum, G.R. and others, editors, Structural and Stratigraphic Framework for the Coastal Plain of North Carolina: Carolina Geological Society Field Trip Guidebook, American Coastal Plain Geological Association Guidebook for the Annual Field Conference, p. 2-15.

Baum, G.R., Harris, W.B., and Drez, P.E., 1985, Origin of dolomite in the Eocene Castle Hayne Limestone, North Carolina: Journal of Sedimentary Petrology: v. 55, p. 506-517.

Birch, G.F., 1971, The glauconite deposits on the Agulhas Bank, South Africa: SANCOR Marine Geology Program Bulletin No. 4, Geology Department of the University of Cape Town, Cape Town, South Africa, 134 pp.

Birch, G.F., Willis, J.P., and Rickard, R.S., 1976, An electron microscope study of glauconites from the continental margin off the west coast of South Africa: Marine Geology, v. 22, p. 271-283.

Boichard, R., Burollet, P.F., Lambert, B., and Villain, J.M., 1985, La plateforme carbonatee du Pater Noster (Indonesie): Mem. 20, Total C^{ie} Franc. Petroles Publ., 130 pp.

Brown, P.M., Miller, J.A., and Swain, F.M., 1972, Structural and stratigraphic framework and spatial distribution of the permeability of the Atlantic Coastal Plain, New York to North Carolina: U.S. Geological Survey Professional Paper 796.

Buckley, H.A., Bevan, J.C., Brown, K.M., Johnson, L.R., and Farmer, V.C., 1978, Glauconite and celadonite: two separate mineral species: Mineralogical Magazine, v. 42, p. 373-382.

Burst, J.F., 1958a, "Glauconite" pellets: their mineral nature and application to stratigraphic interpretation: American Association of Petroleum Geologists Bulletin, v. 42, p. 310-327.

Burst, J.F., 1958b, Mineral heterogeneity in "glauconite" pellets: American Mineralogist, v. 43, p. 481-497.

Chapelle, F.H., 1983, Groundwater geochemistry and calcite cementation of the Aquia Aquifer in Southern Maryland: Water Resources Research, v. 19, p. 545-558.

Cimbalnikova, A., 1971, Chemical variability and structural heterogeneity of glauconites: American Mineralogist, v. 56, p. 1385-1392.

Clark, W.B., 1909, Results of a recent investigation of the coastal plain formations in the area between Massachusetts and North Carolina: Geological Society of America Bulletin, v. 20, p. 646-654.

Cunliffe, J.E., 1968, Petrology of the Cretaceous Peedee Formation and Eocene Castle Hayne Limestone in Northern New Hanover County, North Carolina: M.S. thesis, University of North Carolina, Chapel Hill, North Carolina, 128 pp.

Cunliffe, J.E., and Textoris, D.A., 1969, Petrology of the Cretaceous Peedee Formation and Eocene Castle Hayne Limestone in Northern New Hanover County, North Carolina: Geological Society of America Special Paper No. 121, 178 pp.

Dunham, R.J., 1962, Classification of carbonate rocks according to depositional Texture, *in* Ham, W.E., editor, Classification of Carbonate Rocks: American Association of Petroleum Geologists Memoir No. 1, p. 108-121.

Ehlmann, A.J., Hulings, N.C., and Glover, E.D., 1963, Stages of glauconite formation in modern foraminiferal sediments: Journal of Sedimentary Petrology, v. 33, p. 87-96.

Faure, G.J., 1998, Principles and Application of Inorganic Geochemistry, Prentice Hall, Upper Saddle River, NJ, 600p.

Folk, R.L., 1962, Spectral subdivision of limestone types, *in* Ham, W.E., editor, Classification of Carbonate Rocks: American Association of Petroleum Geologists Memoir No. 1, p. 62-84.

Gamus, W.J., 1972, Analysis of factors controlling groundwater flow for prediction of rates of groundwater movement and changes in quality, Atlantic Coastal Plain: Unpublished Ph.D. dissertation, University of Arizona, Tucson, Arizona, 113 pp.

Giese, G.L., Eimers, J.L., and Coble, R.W., 1997, Simulation of groundwater flow in the Coastal Plain Aquifer System of North Carolina: U.S. Geological Survey Professional Paper 1404-M.

Harned, D.A., Lloyd, O.B., Jr., and Treece, M.W., Jr., 1989, Assessment of hydrologic data at Camp Lejeune Marine Corps base, North Carolina: U.S. Geological Survey Water-Resource Investigation Report 89-4096, 64 p.

Harris, W.B., Fullagar, P.D., and Tovo, L.L., 1997, Significance of young Paleocene Rb-Sr and K-Ar glauconite dates from the Lang Syne Formation, Savannah River Site, South Carolina: Southeastern Geology, v. 37, p. 55-72.

Ireland, B.J., Curtis, C.D., and Whiteman, J.A., 1983, Compositional variation within some glauconites and illites and implications for their stability and origins: Sedi-

mentology, v. 30, p. 769-786.

Jarrar, G., Amireh, B., and Zachmann, D., 2000, The major, trace and rare earth element geochemistry of glauconites from the early Cretaceous Kurnub Group of Jordan: Geochemistry Journal, v. 34, p. 207-222.

Klein, C., and Hurlbut, C.S., Jr., 1993, Manual of Mineralogy: John Wiley and Sons, Inc., New York, 681 pp.

Lloyd, O.B., Jr., and Daniel, C.C., 1988, Hydrogeologic setting, water levels, and quality of water from supply wells at the U.S. Marine Corps Air Station, Cherry Point, North Carolina., U.S. Geological Survey Water-Resources Investigations Report 88-4034, 76 p.

Lovley, D.R., Phillips, J.P., and Lonergan, D.J., 1991, Enzymatic versus nonenzymatic mechanisms for Fe(III) reduction in aquatic sediments: Environmental Science and Technology, v. 26, p. 1062-1067.

Lyke, W.L., and Brockman, A.R., 1990, Groundwater pumpage and water-level declines in the Peedee and Black Creek aquifers in Onslow and Jones Counties, North Carolina, 1900-86: U.S. Geological Survey Water-Resources Investigations Report 89-4197.

Lyke, W.L., and Treece, M.W., Jr., 1988, Hydrogeology and effects of groundwater withdrawals in the Castle Hayne Aquifer in Coastal North Carolina, *in* Lyke, W. L., and Hoban, T.G., editors, Proceedings of the Symposium on Coastal Water Resources: Wilmington, North Carolina, p. 469-478.

Moran, L.K., 1989, Petrography of unconformable surfaces and associated stratigraphic units of the Eocene Castle Hayne Formation, Southeastern North Carolina Coastal Plain: M.S. thesis, East Carolina University, Greenville, North Carolina, 337 pp.

Morton, A.C., Merriman, R.J., and Mitchell, J.G., 1984, Genesis and significance of glauconite sediments of the Southwest Rockall Plateau, *in* Roberts, D.G. and others, editors, Initial Reports of the Deep Sea Drilling Project 81, U.S. Government Printing Office, Washington, D.C., p. 645-652.

O'Brien, G.W., Milnes, A.R., Veeh, H.H., Heggie, D.T., Riggs, S.R., Cullen, D.J., Marshall, J.F., and Cook, P.J., 1990, Sedimentation dynamics and redox iron-cycling: controlling factors for the apatite-glauconite association on the East Australian Continental Margin, *in* Notholt, A.J.G., and Jarvis, I., editors, Phosphorite Research and Development: Geological Society of America Special Publication No. 52, p. 61-86.

Odin, G.S., and Fullagar, P.D., 1988, Geological significance of the glaucony facies, *in* Odin, G.S., editor, Green Marine Clays: Developments in Sedimentology No. 45, Elsevier, New York, p. 295-332.

Odin, G.S., and Matter, A., 1981, De glauconiarum origine: Sedimentology, v. 28, p. 611-641.

Odin, G.S., and Stephan, J.F., 1981, The occurrence of deep water glaucony from the Eastern Pacific: the result of *in situ* genesis or subsidence? *in* Watkins, J.S. and others, editors, Initial Reports of Deep Sea Drilling Project 66, p. 419-428.

Odom, I.E., 1984, Glauconite and celadonite minerals, *in* Bailey, S.W., editor, Reviews in Mineralogy, v. 13, p. 545-572.

Otte, L.J., 1981, Petrology of the exposed Eocene Castle Hayne Limestone of North Carolina: Unpublished Ph.D. dissertation, University of North Carolina, Chapel Hill, North Carolina, 183 pp.

Parkhurst, D.L., Thorstenson, D.C., and Plummer, L.N., 1980, PHREEQE - A computer program for geochemical calculations: U.S. Geological Survey Water-Resources Investigations Report 80-96, 195 p.

Plummer, L.N., Prestemon, E.C., and Parkhurst, D.L., 1991, An interactive code (NETPATH) for modeling NET geochemical reactions along a flow PATH: U.S. Geological Survey Water-Resources Investigations Report 91-4078, 93 p.

Randazzo, A.F., and Hickey, E.W., 1978, Dolomitization in the Floridan Aquifer: American Journal of Science, v. 278, p. 1177-1184.

Reynolds, J.W., and Spruill, R.K., 1995, Groundwater flow simulation for management of a regulated aquifer system: a case study in the North Carolina Coastal Plain: Ground Water, v. 33, p. 741-748.

Sherwani, J.K., 1980, Public policy for the management of groundwater in the Coastal Plain of North Carolina: Univ. of North Carolina Water Resources Research Institute Report No. 129, 63 p.

Sprinkle, C.L., 1989, Geochemistry of the Floridian aquifer system in Florida and in parts of Georgia, South Carolina, and Alabama: U.S. Geological Survey Professional Paper 1403-I, 105 p.

Textoris, D.A., 1967, Preliminary investigation of the petrology of the Castle Hayne Limestone: Proceedings of Symposium on Hydrology of the Coastal Waters of North Carolina, University of North Carolina Water Resources Research Institute Report No. 5, p. 3-23.

Textoris, D.A., 1969, Porosity control by original skeletal mineralogy in Mesozoic and Tertiary carbonates: Geological Society of America Special Paper 121, 295 p.

Textoris, D.A., Randazzo, A.F., and Thayer, P.A., 1972, Diagenesis of carbonate sediments as important noncavern porosity controls: Proceedings of 24th International Geological Congress, Montreal, p. 190-197.

Thayer, P.A., 1972, Petrologic controls of porosity and permeability in Tertiary aquifer carbonates, North Carolina: Geological Society of America, Abstracts with Programs, v. 4, p. 109.

Thayer, P.A., and Textoris, D.A., 1972, Petrology and diagenesis of Tertiary aquifer carbonates, North Carolina: Transactions of the Gulf Coast Association of Geological Societies, v. 22, p. 257-266.

Tolen-Mehlhop, D.L. 1998, Mineralogical and chemical analysis of the Castle Hayne Aquifer in east-central North Carolina: M.S. thesis, East Carolina University, Greenville, North Carolina, 98 pp.

Upchurch, M.L., 1973, Petrology of the Eocene Castle Hayne Limestone at Ideal Cement Quarry, New Hanover County, NC: M.S. thesis, University of North Carolina, Chapel Hill, North Carolina, 97 pp.

Upchurch, M.L., and Textoris, D.A., 1973, Effects of sponges and sub-sea diagenesis on the formation of Eocene Castle Hayne Limestone, North Carolina: Geological Society of America, Abstracts with Programs, v. 5, p. 446.

Vaughan, T.W., 1918, Correlations of the Tertiary geologic formations of the Southeastern United States, Central America, and the West Indies: Washington Academy of Sciences Journal, v. 8, p. 268-276.

Ward, L.W., 1977, Stratigraphic revision of the Middle Eocene, Oligocene, and Lower Miocene - Atlantic Coastal Plain of North America: M.S. thesis, University of South Carolina, Columbia, South Carolina, 306 pp.

Ward, L.W., Lawrence, D.R., and Blackwelder, B.W., 1978, Stratigraphic revision of the Middle Eocene, Oligocene, and Lower Miocene Atlantic Coastal Plain of North Carolina: U. S. Geological Survey Bulletin 1457F, 23p.

Weaver, C.E., 1989, Clays, Muds, and Shales: Developments in Sedimentology No. 44, Elsevier, New York, 819 pp.

Weaver, C.E., and Pollard, L.D., 1975, The Chemistry of Clay Minerals: Elsevier, New York, NY.

Winner, M.D., and Jr., Coble, R.W., 1996, Hydrogeologic framework of the North Carolina Coastal Plain Aquifer System: U. S. Geological Survey Open-File Report 1404-I, 106 pp.

Winner, M.D., Jr., and Lyke, W.L., 1989, Aquifers in Cretaceous rocks of the Central Coastal Plain of North Carolina: U. S. Geological Survey Water-Resources Investigations Report 87-4178, 71 pp.

Woods T.L., Beck, E.G., Tolen-Mehlhop, D.L., Troiano, R. and Whitley, J.K., 2000a, Geochemical tracers of groundwater movement between the Castle Hayne and associated Coastal Plain aquifers: Univ. of North Carolina Water Resources Research Institute Report No. 328, 237 p.

Woods, T.L., Fullagar, P.D., Spruill, R.K. and Sutton, L.C., 2000b, Strontium isotopes and major elements as tracers of ground water evolution: Example from the Upper Castle Hayne Aquifer of North Carolina: Ground Water, v. 38, p. 762-771.

Zack, A.L., 1980, Geochemistry of fluoride in the Black Creek aquifer system of Horry and Georgetown Counties, South Carolina -- and its physiological implications: U.S. Geological Survey Water-Supply Paper 2067, 40 p.

Zullo, V.A., and Harris, W.B., 1986, Introduction: sequence stratigraphy, lithostratigraphy, and biostratigraphy of the North Carolina Eocene Carbonates, *in* Textoris, D.A., editor, Society of Economic Paleontologists and Mineralogist Field Guidebook, Southeastern United States: Third Annual Midyear Meeting, Raleigh, North Carolina, p. 257-263.

Zullo, V.A., and Harris, W.B., 1987, Sequence stratigraphy, biostratigraphy, and correlation of Eocene through Lower Miocene strata in North Carolina, *in* Ross, C.A. and Haman, D., editors, Timing and Depositional History of Eustatic Sequences: Constraints on Seismic Stratigraphy: Cushman Foundation for Foraminiferal Research Special Publication No. 24, p.197-214.

SOUTHEASTERN GEOLOGY
V. 43, No. 3, February 2005, p. 137-155

METHANE-INDUCED CEMENTATION IN A TRANSGRESSIVE NEARSHORE SETTING, NORTHERN GULF OF MEXICO

RALPH O. HOWARD, JR.

US Environmental Protection Agency, Region 4
61 Forsyth Street
Atlanta, Georgia 30303

ALBERT W. SHULTZ

ConocoPhillips
600 North Dairy Ashford
Houston, Texas 77079

WILLIAM W. SCHROEDER

Marine Science Program, The University of Alabama
Dauphin Island, Alabama 36528

ABSTRACT

Lithified sediments are common at seafloor sites along the Alabama inner continental shelf of the northern Gulf of Mexico. These materials are variable mixtures of sand, bioclasts, carbonate mud, and carbonate cements. Intergranular carbonate material is dominated by very high-Mg calcite (VHMC), a disordered rhombic Ca-Mg carbonate in the compositional range of 24 to 44 mol% $MgCO_3$, as determined by X-ray diffractometry and electron microprobe analysis. Authigenic high-Mg calcite (HMC), aragonite, and pyrite are also present. Stable isotope ratios are consistent with a methane source for carbon and a seawater source for oxygen. Framboidal pyrite suggests formation under hypoxic conditions associated with microbial sulfate reduction, probably near the sediment-water interface around methane seeps. Sideritic sandstones and mudstones, also common in some of the sites studied, represent a distinct set of anoxic conditions and are likely related to the zone of methanogenesis.

Bottom surveys reveal broken, abraded, and encrusted slabs of rock strewn on the seafloor. These rocks host typical "hardbottom" faunal communities rather than chemosynthetic communities, and suggest that present conditions are incompatible with the processes of carbonate authigenesis that formed the rocks. Radiocarbon analysis suggests an origin during the Holocene transgression, from biogenic rather than thermogenic methane.

Occurrence of micrometer-sized particles of HMC and VHMC in both mud-supported and grain-supported textures indicates that these materials formed syndepositionally and were mixed and infiltrated into coarser sediments before lithification. Porous mud-poor sediment was cemented by larger, more distinct crystals of aragonite, HMC, and VHMC. Modified rhombic crystals with VHMC cores and HMC rims suggest that VHMC is unstable and changes to HMC rather than to dolomite.

Recognition of methane-induced seafloor lithification in ancient rocks is complicated by uncertainties over the fate of unstable minerals found in Quaternary samples. Some ancient HMC and low-Mg calcite (LMC) muds and cements may have formed originally as VHMC and aragonite.

INTRODUCTION

Indurated surficial sediments in shallow marine environments comprise a variety of forms, materials, and origins. Lithified sediments from

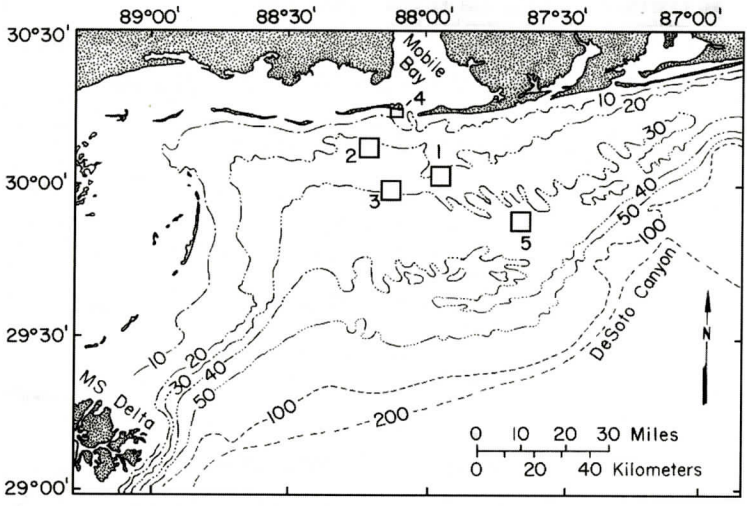

Figure 1. Study area and sample sites. Bathymetry in meters below MSL.

the sediment-water interface have been described as beachrock (Ginsburg, 1953), hardgrounds, and hardbottoms (Schroeder and others, 1988). Mechanisms proposed for cementation have included CO_2 degassing (Hanor, 1978), methane escape (Hathaway and Degens 1969, Allen and others, 1969; Ritger and others, 1987), evaporative supersaturation, and marine phreatic precipitation (Folk, 1974; Longman, 1980). Some indurated surficial materials appear to be exhumed products of subsurface cementation (Kocurko, 1986; Hovland and others, 1987).

Penecontemporaneous carbonate cementation involving many of these mechanisms has been reported previously for siliciclastic and mixed carbonate-siliciclastic sediments at several localities in the northern Gulf of Mexico, including the Chandeleur Islands (Morgan and Treadwell, 1954; Roberts and Whelan, 1975), Mississippi delta slope (Roberts and others, 1987), the southern coast of Louisiana (Kocurko, 1986), and the central Texas coast (Weiss and Wilkinson 1988).

Our field studies have revealed that lithified Quaternary sediments occur at numerous sites offshore of Mississippi, Alabama, and Florida (Schroeder and others, 1989). These materials are both similar to and different from previously described sediments, and provide a new opportunity to study penecontemporaneous cementation from a broader perspective. This article discusses the petrology of the most widespread of these materials, and its implications for paleoenvironmental interpretations in ancient rocks.

GEOLOGIC SETTING

The study area consists of five seafloor sites offshore of Alabama, in the northern Gulf of Mexico (Figure 1; Table 1). The sites are distributed across an area that extends approximately 80 km along shore and 10 to 50 km seaward from the shoreline, in water depths of 20 to 40 m. The area lies within the sandy Mississippi-Alabama-Florida (MAFLA) shelf, a province dominated by quartz sand (Doyle and Sparks, 1980). Surficial mud is locally present in significant amounts in the western part of the area (Ludwick, 1964; Shultz and others, 1990). Mixed carbonate-siliciclastic sediment occurs along the eastern and southern edges of the area (Ludwick, 1964).

Surficial sediment includes palimpsest coastal deposits of shelly sand and mud (Parker and others, 1992). Exposed Pleistocene oyster shells indicate that little or no net sediment accumulation has taken place during the Holocene (Schroeder and others, 1995). Shell and rock constitute "hardbottom," a minor seafloor type

Table 1. Hardbottom site locations and characteristics

Site	Name/ Location	Water Depth (m)	Relief (m)	Bottom characteristics
1	Southeast Banks 87° 57' W, 30° 01' N	21-26	4	Rock rubble, shell hash
2	Southwest Rock 88° 12' W, 30° 06' N	20-22	1.5	Rock outcrop and rubble
3	17 Fathom Hole 88° 03' W, 29° 56' N	30-32	1	Small rock rubble, shell hash, shelly sand
4	Dauphin Island (Casino Beach) 88° 06' W, 30° 15' N	5	< 0.5	sand, rock rubble
5	21 Fathom Area 87° 32' W, 29° 53' N	38-40	1-2	Irregular sand ridges, shell hash

Note: These locations comprise small areas rather than discrete points

in terms of areal extent but significant ecologically and geologically (Schroeder and others, 1988; Howard 1990).

SAMPLING AND ANALYSIS

Samples were obtained by dredging and SCUBA diving, and consist primarily of loose pieces of rock ranging in size from 2 cm pebbles to 1 m slabs. Samples were collected from known or suspected hardbottom areas, as part of a larger project for the characterization of hardbottoms (Howard 1990). Hardbottom materials consist of calcareous sandstones and mudstones, ferruginous sandstones and mudstones, and shells and shell fragments of oysters (*Crassostrea virginica*). Oyster shells collected from these and other sites on the MAFLA shelf provide evidence of shifting estuarine environments during the late Pleistocene and Holocene (Schroeder and others, 1995).

Samples were analyzed by thin-section petrography, x-ray diffractometry (XRD), scanning electron microscopy (SEM), energy-dispersive x-ray analysis (EDX), and electron microprobe (EMP). Analyses of stable isotopes of carbon and oxygen for most samples (23 samples shown in Table 3) were conducted at Indiana University using phosphoric acid extraction of whole-rock subsamples. Extraction of sideritic samples was performed at 75° C while the remainder were treated at 50° C. Results are reported relative to the PDB standard using the conventional delta notation in parts per thousand (‰). Accuracy for these determinations was estimated as +/- 0.1 ‰. Mineralogy of powdered subsamples was determined by XRD prior to extraction. For five samples, duplicate, relatively shell-free subsamples were drilled out using a high-speed rotary drill, to assess potential effects from skeletal carbonate material.

Radiocarbon analysis of 14 samples (Table 5) was performed by Beta Analytic, Inc. of Mi-

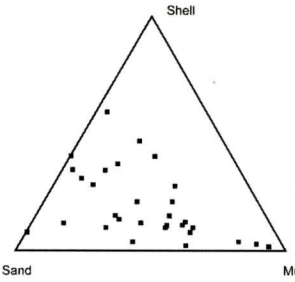

Figure 2. Texture and composition of calcareous sandstones and mudstones.

ami, Florida. Procedures included acid extraction, benzene synthesis, and beta decay counting. Results are reported as radiocarbon years before A.D. 1950, based on a ^{14}C half-life of 5568 years, without corrections for ^{13}C fractionation or secular variations in radiocarbon abundance. Samples submitted for radiocarbon analysis were also analyzed for ^{13}C and ^{18}O. Results were reported as +/- 0.01 ‰ and were rounded to the first decimal place for consistency among the sample group.

LITHOLOGY

Hardbottom rock types span a continuum from well-sorted, fine-grained quartzose sandstone to silty carbonate mudstone to sandy coquina (Figure 2). Individual samples display a great diversity of sizes, shapes, and surfaces. More or less rounded shapes are common, suggesting abrasional rounding in some cases but formation as rounded nodular masses in others. Larger specimens (>20 cm) tend to have tabular, slab-like shapes, whereas smaller cobbles and pebbles are generally equant. Complex forms are common, and include knobby, branching masses suggesting burrow-casts (Figure 3A), and tabular slabs or blocks with internal strata of differing hardness (Figure 3B). Hardbottom surfaces range from bare to completely encrusted with modern, often living, benthic biota that include barnacles, bryozoans, sponges, corals, serpulid worms, and bivalves. Borings by bivalves (*Lithophaga* sp.) are common.

Calcareous Sandstones and Mudstones

These samples contain significant shell material and mud (Figure 2; Table 2). Siliciclastic sand consists of subangular fine to medium grains. Grains are dominantly monocrystalline quartz with significant amounts of polycrystalline quartz, feldspar, mica, and rock fragments of sedimentary and plutonic-metamorphic provenance. Accessory minerals include zircon, tourmaline, staurolite, and kyanite. Peloidal glauconite grains are present in most samples.

Carbonate grains vary with grain size. Gravel-sized grains are generally molluscan shell fragments, and some samples of sandy coquina contain as much as 45% molluscan shell fragments. Mollusks, echinoderms, benthic foraminifera, bryozoans, and ostracodes are the main contributors of carbonate grains in the sandstone samples.

Siltstones and mudstones consist of variable amounts of siliciclastic silt and calcareous microfossils, especially foraminifera and ostracodes, in a micritic matrix. Fine-grained carbonaceous organic matter is disseminated in most samples; it is scarce in shelly sandstone and coquina (<1%) but conspicuous in fine sandstones, siltstones, and mudstones (up to 5%).

Rock colors range from tan and light gray to dark gray. The darker-colored rocks contain disseminated carbonaceous organic matter. Pyrite is present in most samples, as framboids and as casts of foraminifera; it is suspected as the source of iron for a faint limonitic staining on the surfaces of some samples. Lithification in all cases is due to authigenic carbonate minerals, but many samples retain high primary porosity.

Ferruginous Sandstones and Mudstones

Ferruginous sandstones and mudstones are characterized by high density and red-brown to olive-brown color. Exterior colors tend to be rusty, and interior colors tend to be drab. Visible

Table 2. Petrography of calcareous sandstones and mudstones

Sample	Site	Framework%			Cement minerals	
		Shell	Sand	Mud	Aragonite	HMC, VHMC
1	1	45	28	3	18	6
2	1	38	27	29	6	0
3	1	36	24	17	17	6
4	2	31	37	16	0	15
5	1	29	52	3	17	0
6	1	26	26	42	0	6
7	1	25	49	7	10	9
8	1	24	35	11	24	6
9	1	22	45	11	11	11
10	2	21	31	0	0	48
11	1	21	45	34	0	0
12	2	21	32	47	0	0
13	2	15	36	49	0	0
14	2	15	56	29	0	0
15	2	13	53	30	2	2
16	1	12	31	55	0	2
17	2	12	48	40	0	0
18	2	11	39	50	0	0
19	2	11	33	56	0	0
20	1	10	40	50	0	0
21	1	10	62	28	0	0
22	1	10	30	50	0	10
23	3	10	30	60	0	0
24	1	10	65	10	0	15
25	1	8	32	60	0	0
26	1	6	69	0	25	0
27	2	4	16	80	0	0
28	2	4	55	41	0	0
29	2	3	10	87	0	0
30	2	2	31	52	0	15
31	2	2	6	92	0	0

Note: Percentages of solids; porosity ignored.

porosity is generally very low. Shell content is much lower than in calcareous sandstones. Sandstones and mudstones intergrade; some rocks are heterogeneous mixtures of both. Shapes of individual specimens are equant to cylindrical, rarely flattened, but often very irregularly shaped (Figure 3A). A sideritic mudstone mold and replacement of a small crab carapace (*Callinectes sapidus*) was found at Site 1; a sandstone mold of a whole *Mercenaria* bivalve was found at Site 2.

CARBONATE MINERALS

Carbonate minerals are present in three textural modes: skeletal detritus, cryptocrystalline mud, and authigenic cements. Detrital components are dominant in some samples and were easily identified by biotic morphology. Cryptocrystalline mud occurs both as matrix in coarse-grained, grain-supported rocks and as the supporting phase in mudstones. Authigenic cements consist of discrete, often well-formed, pore-filling crystals.

Carbonate mineral varieties identified in this

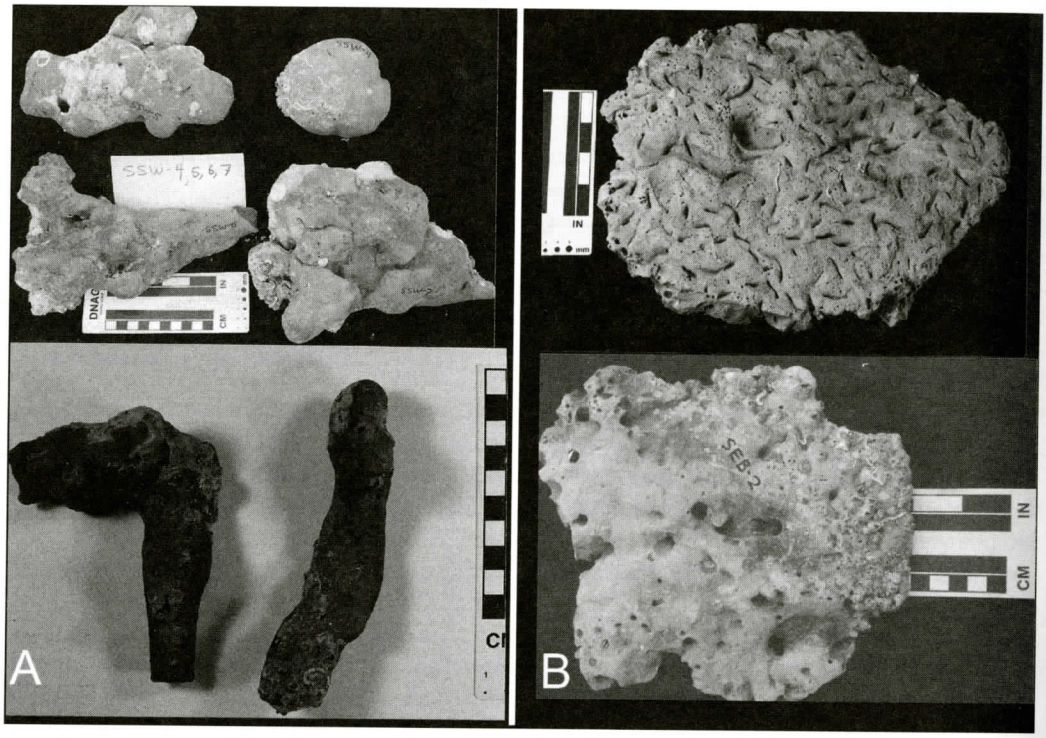

Figure 3. — A. Nodular and elongate morphologies of inner shelf hardbottom samples. Lower photo scale in cm. B. Tabular, slab-like morphologies of inner shelf hardbottom samples.

study include aragonite, high-Mg calcite (HMC), very-high-Mg calcite (VHMC), and siderite. Traces of low Mg calcite (LMC) were identified in a few samples by XRD, but are inferred to represent bioclastic material and are not discussed in detail. Table 3 presents sample mineralogy and isotopic composition. A crossplot of ^{13}C and ^{18}O isotope data (Figure 4) highlights the less-^{13}C-depleted range exhibited by siderites in comparison to the calcareous samples. Unless otherwise noted, carbonate minerals are authigenic.

Aragonite

Aragonite was identified by XRD in approximately half of all samples. In most cases, presence of trace aragonite in whole-rock XRD analysis can be attributed to skeletal grains rather than to authigenic aragonite. Petrographically, authigenic aragonite displays characteristic acicular morphology and dull brown cathodoluminescence.

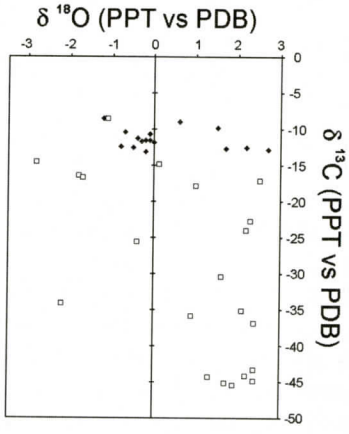

Figure 4. Crossplot of oxygen and carbon isotope data, representing samples with calcareous cements (open squares) and siderite cement (solid diamonds). Units in parts per thousand (PPT).

Authigenic aragonite occurs as needles, as large as 3 x 0.02 mm but typically about 50 x 5

Table 3. Mineralogy and isotopic composition

Sample	Site	Lithology	Carbonate Composition				% Mg	$\delta^{13}C_{PDB}$	$\delta^{18}O_{PDB}$
			Aragonite	HMC	VHMC	Siderite			
25	1	Calcareous ss	20	30	50	- -	36	-36.9	+2.4
25A	1	Calcareous ss	20	30	50	- -	35	-35.2	+2.1
26	1	Calcareous ss	70	30	0	- -	38	-44.3	+1.3
24	1	Calcareous ss	10	30	60	- -	44	-22.7	+2.3
16	1	Calcareous ss	10	30	60	- -	39	-24.0	+2.2
11	1	Calcareous ss	30	30	40		33	-30.4	+1.6
28	2	Calcareous ss	5	35	60	- -	36	-45.2	+1.7
28A	2	Calcareous ss	0	40	60	- -	38	-45.4	+1.9
17	2	Calcareous ss	0	20	80	- -	35	-44.1	+2.2
10	2	Calcareous ss	0	100	0	- -	5	-34.2	-2.2
32	2	Calcareous ms		100		- -	7	-16.4	-1.8
33	3	Calcareous ms	20	60	20	- -	35	-14.9	+0.1
34	2	Sideritic ss	- -	- -	- -	100	- -	-12.5	-0.5
34A	2	Sideritic ss	- -	- -	- -	100	- -	-11.5	-0.1
35	2	Sideritic ss	- -	- -	- -	100	- -	-10.4	-0.7
35A	2	Sideritic ss	- -	- -	- -	100	- -	-11.5	-0.2
36	2	Sideritic ss	- -	- -	- -	100	- -	-13.1	-0.2
36A	2	Sideritic ss	- -	- -	- -	100	- -	-10.7	-0.1
37	2	Sideritic ss	- -	- -	- -	100	- -	-11.8	0.0
38	2	Sideritic ss	- -	- -	- -	100	- -	-11.3	-0.4
39	4	Sideritic ss	- -	- -	- -	100	- -	-11.7	-0.3
40	4	Sideritic ss	- -	- -	- -	100	- -	-8.5	-1.2
41	5	Sideritic ss	- -	- -	- -	100	- -	-12.4	-0.8

Carbonate compositions are estimates.
Designation "A" indicates a subsample of same specimen.

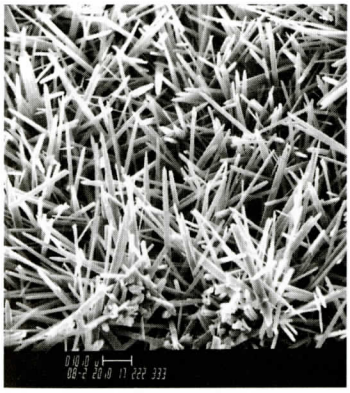

Figure 5. Aragonite, displaying characteristic acicular form. Scale bar = 10 microns.

μm (Figure 5). In contrast to calcite crystals with rhombohedral or scalenohedral faces, aragonite needles tend to be elongate-prismatic, with blunt terminations. Aragonite most frequently occurs together with HMC and VHMC in calcareous sandstones. In such samples, aragonite is generally the earliest authigenic mineral and is surrounded or covered by HMC and VHMC without evidence of replacement.

Minor-element composition of aragonite is distinguished by the presence of strontium in quantities as great as 2% by weight. Mn, Fe, and Mg are generally below detection levels. Carbon isotope ratios (Table 3) indicate substantial depletion in ^{13}C. In samples with significant aragonite, $\delta^{13}C$ ranges from -30.4 to -44.3‰, and $\delta^{18}O$ from 1.3 to 2.4‰.

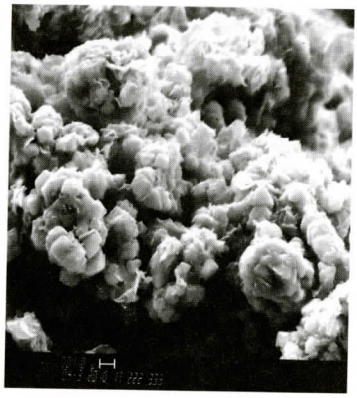

Figure 6. SEM image of cryptocrystalline mud matrix. Scale bar = 1 micron.

High Mg Calcite (HMC)

High Mg calcite occurs in almost all samples of calcareous sandstone and mudstone. Identification is based on XRD and EMP analysis. Most HMC could be stained with Alizarin red.

HMC occurs as cryptocrystalline mud (Figure 6) and as authigenic pore-lining crystals. Cryptocrystalline mud particles of HMC are anhedral to subhedral, equant to bladed, with bright to dull red cathodoluminescence. In thin section, the mud is brown and turbid, with dark flecks of organic matter and pyrite. Distinct pore-lining crystals of HMC are generally small (<20 μm) and occur as dentate rims and as loose, equant to elongate particles. In most samples, HMC is associated with VHMC (Figure 7A).

Estimates of $MgCO_3$ content from XRD range from 5 to 7 mol%. EMP analysis confirms the presence of individual grains within this compositional range. Stable isotope ratios from samples that contain HMC in addition to aragonite and VHMC are comparable to those without HMC. However, HMC-dominated samples with little or no aragonite or VHMC tend to show less ^{13}C depletion (-14.9, -16.4‰; Table 3).

Very High Mg Calcite (VHMC)

The material identified here as very high Mg calcite closely resembles HMC as described above. VHMC is usually present in cryptocrystalline mud, alone or in association with HMC, in calcareous sandstones and mudstones. Some samples contain pore-lining crystals of VHMC up to 20 μm in size. Pyrite and organic matter are also associated. Identification of VHMC is based on XRD and EMP analysis. Staining by Alizarin red is equivocal, but most VHMC does not stain. Dull red cathodoluminescence was noted.

Composition based on XRD peak positions ranges from 35 to 44 mol% $MgCO_3$ based on whole-rock analyses of 7 samples comprised of ≥ 50% VHMC (Table 3). Peaks for (105) "order" spacing were present in about one-third of these samples, but 105/006 intensity ratios averaged 0.2 and in no instances exceeded 0.4.

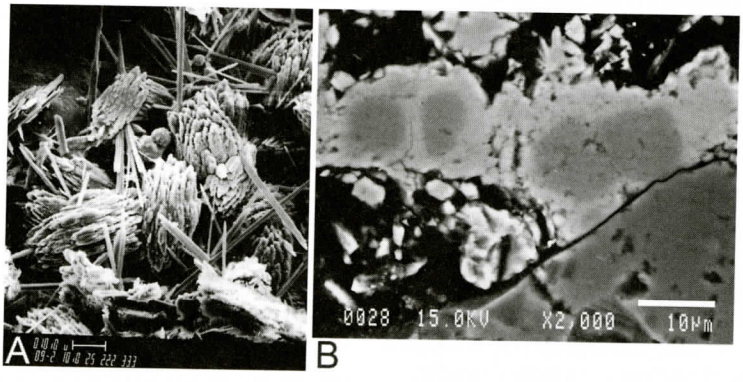

Figure 7. — A. SEM image of microcrystalline HMC (large irregular forms) and VHMC (smaller spheroids), with aragonite. Scale bar = 10 microns. B. Equant HMC crystals, showing VHMC interior (dark) and HMC exterior (light) in backscattered electron image of polished thin section. 2000X, scale bar = 10 microns.

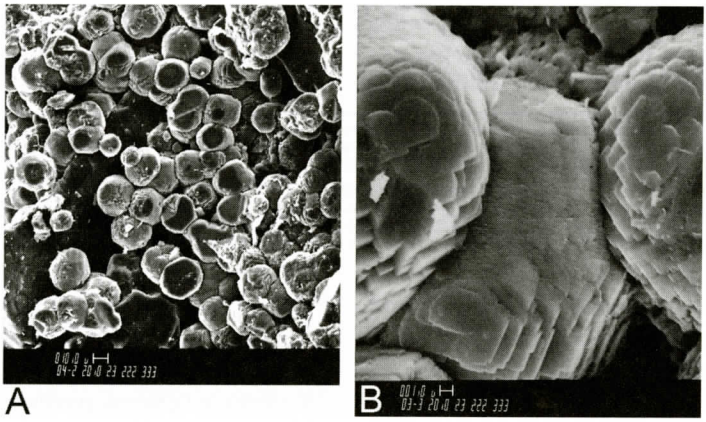

Figure 8. — A. SEM image of siderite in sideritic sandstone. Scale bar = 10 microns. B. SEM image of siderite with rounded and stepped crystal faces. Scale bar = 1 micron.

Microprobe analyses of individual grains in 3 samples give average compositions of 36 to 45 mol% $MgCO_3$; Sr, Mn, and Fe are at or below detection limits. Crystals are generally equant, subhedral, and typically 1 to 3 μm in size.

Larger crystals (5 to 20 μm) in samples 7 and 24 are zoned, with cores of VHMC and rinds of HMC (Figure 7B). Surfaces of these particles are notched or grooved, suggesting leaching. The boundary between HMC and VHMC regions is curved and is more rounded than the particle's external surface, suggesting an origin related to a diffusion-controlled surface-alteration phenomenon rather than accretionary zonation during crystal growth.

Zoning was not initially detected in optical petrographic or SEM-EDX studies. However, compositions originally estimated by SEM-EDX analyses of these zoned crystals in rock chips had Ca/Mg ratios that were too high to be reconciled with bulk XRD compositional data. Subsequent EMP analyses, from polished sections which exposed the interiors of crystals, gave results that were more consistent with XRD. Apparently, EDX data indicated only the composition of HMC surface rinds, and not the VHMC cores.

Stable-isotope ratios (Table 3) in VHMC-dominated samples are similar to those in aragonite-bearing samples ($\delta^{13}C$ from -22.7 to -45.4‰; $\delta^{18}O$ from 1.6 to 2.4‰).

Siderite

Siderite occurs exclusively in ferruginous sandstones and mudstones, where it is the dominant intergranular mineral. Some rocks of similar appearance were found by XRD to contain goethite but not siderite. In thin section, goethite is nearly opaque whereas siderite is yellowish and highly birefringent, but in a few samples siderite was masked by goethite.

Siderite occurs as distinct equant particles 5 to 30 μm in diameter, varying in shape from euhedral or anhedral rhombohedra to spheroids (Figure 8A, 8B). No cathodoluminescence or UV fluorescence was seen. Pyrite and organic matter are both associated with siderite. In some mudstones, siderite appears to have partially replaced mica, and mud-support textures indicate that siderite replaced clay in mudstones. Siderite-filled shell molds were seen in one sandstone.

EDX and EMP data for siderite indicate the presence of Ca, Mg, and Mn, with Ca generally the most abundant by weight. Diffraction peak positions are consistent with minor cation substitution; average CuKα 2θ for (104) is 31.87° (d = 2.808 Å) as opposed to 32.07° (d = 2.791Å) in the pure mineral. These values equate to an average composition of 93%mol $FeCO_3$, 7%mol $CaCO_3$. Siderite samples show moderate depletion in ^{13}C, with $\delta^{13}C$ ranging from -8.5‰ to -13.1‰ (Table 3; Figure 4). For oxy-

gen, $\delta^{18}O$ values were between -1.2‰ and 0.2‰. Comparisons of interior and exterior portions of two nodular rocks failed to reveal any systematic trend in zonation in mineralogy or isotopic composition.

CONDITIONS OF CARBONATE PRECIPITATION

Evidence from mineralogy, thin-section petrography and isotope geochemistry indicates that authigenic Ca-Mg carbonates described here precipitated from marine pore waters near the sediment-water interface. Acicular aragonite and microcrystalline void-filling magnesian calcite are typical cements of the shallow marine phreatic zone (Longman, 1980). The presence of framboidal pyrite indicates an origin in sulfidic, anoxic conditions.

Oxygen isotope ratios are consistent with normal marine salinities and temperatures not too different from those at present. However, oxygen isotopic analyses are subject to mineralogical fractionation effects, and should be interpreted with some caution. Fractionation factors for calcite, dolomite, and Holocene "protodolomite" are known to differ (Land, 1980); and the actual fractionation involved in VHMC precipitation is unknown. Calcite fractionation factors were used in computing $\delta^{18}O$ values for aragonite, HMC, and VHMC; consequently, errors of 1 or 2‰ are possible. However, isotopic signatures of high-temperature or meteoric waters are expected to be expressed as shifts of larger magnitude, so that their presence would not have been masked by this uncertainty.

The oxygen isotopic compositions, together with the presence of pyrite and its indication of reducing, sulfidic conditions, rule out intertidal littoral cementation (beachrock formation), as well as any meteoric water influence. Although cryptocrystalline HMC cements have been described from beachrock (Meyers, 1987), they are also known from other settings (Allen and others, 1969; Fischer and Garrison, 1967).

Primary evidence for methane-induced cementation is the consistent depletion in ^{13}C. A characteristic and strong vital effect of microbial methanogenesis is the exclusion of ^{13}C, resulting in depletion in ^{13}C relative to ^{12}C by as much as -75‰ in biogenic methane (Rosenfeld and Silverman, 1959). As sedimentary organic matter in Gulf of Mexico coastal sediments typically has a $\delta^{13}C$ value of -21 to -26‰ (Sackett and Thompson, 1963), significantly lower values are most likely due to methane. The lightest isotopic composition of carbonate samples analyzed here ($\delta^{13}C$ = -45‰) is comparable to other examples of inferred methane-induced cementation (Roberts and Whelan, 1975; Jorgensen; 1976; Hovland and others, 1987).

Carbonate cements produced from methane oxidation are typically less depleted in ^{13}C than is methane. This relative enrichment in ^{13}C requires either additional fractionation during methane oxidation, or else an admixture of carbon from other sources. Actually, depletion in $\delta^{13}C$ rather than enrichment during methane oxidation has been reported although its effects are not likely to be great unless oxidation is stopped in its early stages (Whiticar and Faber, 1986). Thus, the addition of isotopically heavy carbon from the oxidation of organic matter or dissolution of shell debris appears most likely. In the present samples, shell material is abundant and undissolved; oxidized organic matter is therefore the most likely contributor.

In sideritic samples, carbon isotope values are consistent with precipitation in zones of methanogenesis or mixed methanogenesis/sulfate reduction. The range of ^{18}O values (-1.2 to 0.2‰ PDB) offers no clear evidence of meteoric waters. However, the small amount of Ca substitution is more typical of siderite from low-salinity environments (Mozley, 1989). Origin in organic, muddy sediment of a brackish bay or marsh would seem most likely.

Given these geochemical constraints, a general depth relationship among the carbonate phases can be postulated (Table 4). Within the uppermost oxic and marginally oxic layers of sediment, a zone probably only a few centimeters in thickness, aragonite precipitates in response to methane oxidation. Dissolved sulfate in these pore waters interferes with precipitation of any other carbonate phases (Walter, 1986). A highly ^{13}C-depleted isotope signature reflects little or no contribution of heavier car-

Table 4. Cementation processes versus depth, Northern Gulf hardbottom specimens. (Depth data modified from Martens and Klump, 1984)

DEPTH (in sediment column)	PROCESSES	CEMENTS
0 - 10 cm	Methane Oxidation	Aragonite
10 - 25 cm	Sulfate Reduction / Methane Oxidation	VHMC, HMC
10 / 25 cm to (?) 1-3 m	Methanogenesis	Siderite

bon from other sources (i.e. marine bicarbonate or bicarbonate generated from sulfate reduction). Below this, microbial sulfate reduction is coupled with oxidation of organic matter, producing bicarbonate whose ^{13}C signature (-20 to -25‰) exhibits less depletion (Gautier and Claypool, 1984).

At or near the base of active sulfate reduction, in the presence of methane, coupled anaerobic methane oxidation/sulfate reduction generates supersaturation with bicarbonate, causing HMC and VHMC cements to precipitate. These cements display ^{13}C values reflecting a mixture of carbon derived from both methane oxidation (methane $\delta^{13}C$ approximately -70 ‰; Claypool and Kaplan 1974) and from sulfate reduction (bicarbonate $\delta^{13}C$ approximately -25 to -30 ‰; Reeburgh 1980, Rice and Claypool 1981). Water-chemistry depth profiles from a similar modern site in North Carolina suggest that the sulfate reduction zone extends to only 10 to 30 cm below the sediment/water interface (Martens and Klump, 1984).

Below the level of sulfate depletion, reduction ceases, and microbial methanogenesis by CO_2 reduction proceeds in this sulfide-free environment. Siderite cements described here exhibit ^{13}C depletion that is representative of the methanogenic zone (Gautier 1985).

Radiocarbon age determinations suggest differences among the hardbottom rocks according to lithology and location (Table 5). Sideritic rocks and a few calcareous rocks from Site 2 yield radiocarbon apparent ages in excess of 15,000 years BP. These rocks are associated with oyster shells of probable Pleistocene age in a lag veneer that is interpreted as the result of erosion of possibly as much as a few meters of paleoestuarine sediment (Schroeder and others, 1995). In contrast, calcareous rocks from other sites have radiocarbon apparent ages generally less than 10,000 years BP and are associated with shells that are dated as mostly Holocene. These rocks have apparently experienced a lesser history of erosion and reworking than the Pleistocene lag materials, and are more likely to represent in-situ transgressive deposits. We recognize that these radiocarbon apparent ages should not be taken as actual absolute ages, as they are based on radiocarbon content that is complicated by the likelihood of mixing of carbonate from older, contemporaneous, and subsequent sources. Respectively, these potential sources could include Pleistocene or older organic matter and methane derived anaerobically from it; marine bicarbonate and products of methane biodegradation contemporaneous with carbonate authigenesis; and replacement by younger or modern marine carbonate. Nonetheless, the relative age relationships are difficult to discount entirely.

DISCUSSION

Seabed escape of methane, a greenhouse gas, has been recognized in recent years as a globally significant and widespread process, occurring in every ocean and almost all oceanographic settings (Judd, 2003). This suggests that while there are other known mechanisms giving rise to Recent authigenic cementation in marine sediments, occurrences of methane-sourced carbonate cements could be much more common than is reflected in the literature.

Methane-derived early cements reported previously include aragonite and dolomite as well as HMC and VHMC (Allen and others, 1969; Hathaway and Degens, 1969; Roberts and Whelan, 1975; Jorgensen, 1976, 1979; Nelson

Table 5. Sample radiocarbon ages

Sample	Site	Lithology	Age (yrs BP)	+/-	δ13C	$\delta 18O_{PDB}$
42	1	calcareous	8,450	140	-35.9	0.9
43	2	sideritic ss	19,940	360	-12.8	2.7
39A	5	sideritic ss	22,730	200	-9.8	1.5
44	2	calcareous ss	29,550	410	-14.5	-2.8
45	2	calcareous ss	29,320	510	-16.7	-1.7
46	4	sideritic ss	21,300	170	-9.0	0.6
47	2	calcareous ss	16,090	120	-25.6	-0.4
48	1	calcareous ss	8,880	60	-17.8	1.0
36B	2	sideritic ss	17,210	90	-12.5	2.2
49	2	calcareous ss	14,830	90	-44.8	2.4
17A	2	calcareous ss	12,810	70	-43.3	2.4
50	1	calcareous ss	8,780	70	-17.2	2.5
51	2	sideritic ss	21,410	190	-12.7	1.7
52	2	calcareous ss	25,060	200	-8.5	-1.1

Ages are uncorrected.
Designations "A," "B," indicate subsamples of same specimen.

and Lawrence, 1984; Kocurko, 1986; Roberts and others, 1987). Previous reports of rhombohedral Ca-Mg carbonates similar to those described here as VHMC have been described as HMC and dolomite with little apparent difference.

Comparison of these samples with those from other studies reveals a number of similarities, particularly with regard to cement crystal morphology. Generally similar clastic lithologies, as well as similar "fluted" Mg-calcite cement textures, have been observed in samples from the North Sea (Jorgensen 1976; Hovland and others, 1987), the Chandeleur Islands (northern Gulf of Mexico; Roberts and Whelan, 1975), and the Louisiana Gulf coast (Kocurko, 1986). These studies also described strongly ^{13}C-depleted cements of inferred methanogenic origin.

However, the environments of formation appear significantly different. Cement precipitation in microenvironments of varying porewater salinity (Roberts and Whelan 1975) is not indicated by our ^{18}O ratios, nor is a meteoric-water influence on cementation (Jorgensen 1976). Our samples differ from the "rip-up clasts" of Kocurko (1986), in lacking evidence of significant dissolution and reprecipitation, and of truly ordered dolomite, in any samples.

Mg-depleted rims on HMC cement crystals, generally similar to the HMC-rimmed VHMC crystals seen in these samples, have also been described in lithified sediment samples from the North Sea (Jorgensen, 1979). Mg content was found by EDX to vary from less than 5% in crystal cores to approximately 11% away from the crystal cores, but some crystals had thin (<2 micrometer) rims with abruptly lower Mg content. This zonation was attributed to rapid pore fluid enrichment in Mg, followed by an abrupt cutoff of methane and a return to a normal marine composition. Rims are inferred to have become depleted in Mg by leaching. By contrast, we believe that alteration of VHMC to HMC in our samples involved leaching from an initial VHMC phase that had a much higher Mg content (Figure 7B).

Designation of VHMC as a separate phase

distinct from dolomite and HMC is indicated both mineralogically and genetically. The presence of order reflections in some samples originally led us to refer to these materials as dolomite. Upon further analysis, order reflections were found to be absent from most samples and weak when present. Furthermore, the lack of correlation of ordering with crystal size, habit, composition (as mol% $MgCO_3$), or distribution suggests that the ordered and disordered varieties are merely members of a continuum. Finally, evidence for instability of VHMC and its alteration to HMC suggests a closer kinship to HMC than to dolomite. This relationship supports statements such as those by Land (1980) that "protodolomite" is perhaps not related genetically to dolomite at all. We differ from Kocurco (1986) in preferring the designation of VHMC over simply HMC for materials with >25 mol%$MgCO_3$.

While calcareous carbonate cements are subject to significant dissolution and reprecipitation during diagenesis, there are no known examples of such modification of siderite (Mozley, 1992). Thus siderite has been recognized as a useful indicator of initial pore fluid composition, as reflected in siderite ^{13}C ratios (Gautier, 1982, 1985; Curtis and Coleman, 1986), ^{18}O ratios (Mozley 1992), and elemental geochemistry (Mozley, 1989). The siderite cements described in this study are an example of such an early cement for comparison to the record. The cement is an impure $FeCO_3$ with considerable cation substitution. No compositional zonation was observed in the offshore Alabama samples.

Early diagenetic cements with methane-derived origins have been described from a number fossil methane-seep sites worldwide, including the Canadian Arctic (Beauchamp and others, 1989; Beauchamp and Savard, 1992), northern Italy (Clari and others, 1988), southeastern France (Gaillard and others, 1992), and Colorado USA (Kaufmann and others, 1996). These studies describe outcrops representing methane "cold seeps," rather than "hot seeps" of seafloor hydrothermal-vent origin. The latter are characterized by massive mounds or chimneys of sulfide deposits, the environmental predominance of hydrogen sulfide, and the abundance of fossil worm tubes. Cold seeps, by contrast, are methane-dominated and often occur as "pseudobioherms," carbonate mounds of generally low relief found in fine-grained clastic rocks which have characteristic distributions of infaunal, non-building biota (Gaillard and others, 1992).

Known fossil cold seeps range in age from Jurassic through Neogene. Cements at these sites include micritic calcite generally similar to that described here. Other calcite cements occur as botryoids, crusts, or equant, rhombohedrally-terminated crystals, dissimilar in most respects to cements in the present rocks. However, splays and isopachous coats of fine, acicular aragonite very similar to cements in the present samples, both morphologically and isotopically, were found in the Canadian Arctic methane-seep mounds (Beauchamp and Savard, 1992; Savard and others, 1996). Generally, carbon and oxygen isotopic signatures of this aragonite, and of other fossil-seep cements from the other sites, are close to the range of the calcareous samples described in this study. However, the cementation processes that formed the offshore Alabama hardbottom rocks, together with the present-day shallow shelf conditions, do not seem likely to favor preservation of any seafloor structures such as mounds, pipes, or cemented zones containing diagnostic fauna, which have been observed in the outcrops of fossil methane seeps. Most of the fossil seeps are believed to have resulted from long-term escape of methane from deeper sources, often transported along extensional joints (e.g. Aiello and others, 2001), faults, diapirs, or other structural features. In an example from France, methane seepage is believed to have been active for hundreds of thousands of years (Gaillard and others, 1992). The methanogenesis responsible for cementation of our samples, in contrast, seems more locally-sourced, acting (vertically) over a smaller range of only meters to tens of meters, and relatively short-lived.

Other studies of early diagenetic concretions provide insights about some of the physical and chemical processes likely to control diagenesis of the offshore Alabama samples and similar occurrences, and thus their appearance in the

stratigraphic record. In studying calcite concretions from the Lower Jurassic of England, Raiswell (1987) identified the primary controls on concretion distribution and morphology as a) changes in sedimentation rates, b) time, and c) the shape of the carbonate saturation index versus depth profile. In this scheme, long periods of little or no deposition would favor spatial "fixing" of the sulfate reduction and methanogenic zones (and thus the concretions) to a thin band having little vertical extent, and favor horizontal coalescence of adjacent concretions. Vertically-narrow HCO_3 saturation profiles would also favor cementation within thin bands. By contrast, rapid sedimentation would favor a wider depth range for the occurrence of cemented materials.

Pirrie and Marshall (1991) described large-scale, tabular "sheet concretions" of calcite within Cretaceous-Tertiary silty sandstones at James Island, Antarctica. The authors concluded that, as proposed by Raiswell (1987), a depositional hiatus furthered lateral amalgamation of individual concretions, creating flat, concretionary horizons more than one kilometer in size. The tops of these cemented horizons, but not their full thickness, are extensively reworked and bioturbated. Likewise, Klein and others (1999) describe large-scale cemented horizons accompanying early diagenetic carbonate concretions within a sandstone-siltstone interval of the Prairie Canyon Member of the Mancos Shale (Cretaceous) in western Colorado. The tops of coarsening-upward sequences are believed to represent periods of reduced sedimentation or perhaps even non-deposition, and most of the stratabound concretions and cemented layers are located just below these tops. The concretions are interpreted to have grown laterally into cemented horizons, under varying pore water compositions caused by progressive burial. Early cementation occurred within the zone of methanogenesis, while later growth of the laterally-cemented zones incorporated ^{13}C-depleted carbon from thermocatalytic decarboxylation processes. Measured thicknesses of cemented layers ranged from 0.3m to more than 1.1 meters.

Recent studies suggest that Late Pleistocene and Holocene sea-level history may have involved multiple rises, falls, and stillstands (Chappell and Shackleton 1986, Siringan 1993; Schroeder and others 1995). Within such a framework, in our study area, seismic and other studies of the Late Quaternary in the northern Gulf have established the presence of multiple deltas underlying the Alabama-Mississippi shelf (Coleman and Roberts, 1988; Kindinger, 1988; Sager and others, 1999). Additional work explored the depositional history and approximate paleogeography of the Lagniappe Delta (Kindinger 1989a, 1989b; Sydow and others, 1992) and two other distinct shelf-edge deltas located east of the Lagniappe Delta (Sager and others, 1999). In addition to the deltas, seismic data have also revealed the locations of the associated ancestral Mobile and Pascagoula River systems (Kindinger and others 1994). All five of the hardbottom sites appear to be located close to former incised valleys within these river systems (Figure 9). Brackish, estuarine environments associated with the former river channels and delta system are the likely cementation environments of the siderite samples. Holocene transgression and reworking would then uncover and re-bury the rocks within shoal sands or other transgressive deposits, accompanied by contemporaneous cementation of the calcareous sandstones and mudstones (Figure 10).

A pattern of transgression, regression, and changing sea level would be expected, through time and varying sedimentation rate, to greatly influence hardbottom morphology and distribution. For example, after transgression and burial of highly-organic lagoonal sediments, and the consequent hardbottom cementation as described by the processes above, preservation might follow two general directions. In areas that were more protected and less susceptible to storms, stillstands could further the formation of horizontal cementation horizons through lateral growth, in the general manner described by Raiswell (1987). The physical description of Site 2, a tabular outcrop about 7 to 9 meters in diameter (Schroeder and others, 1988), suggests that it could represent a zone of lateral growth, and that other such flat, cemented tabu-

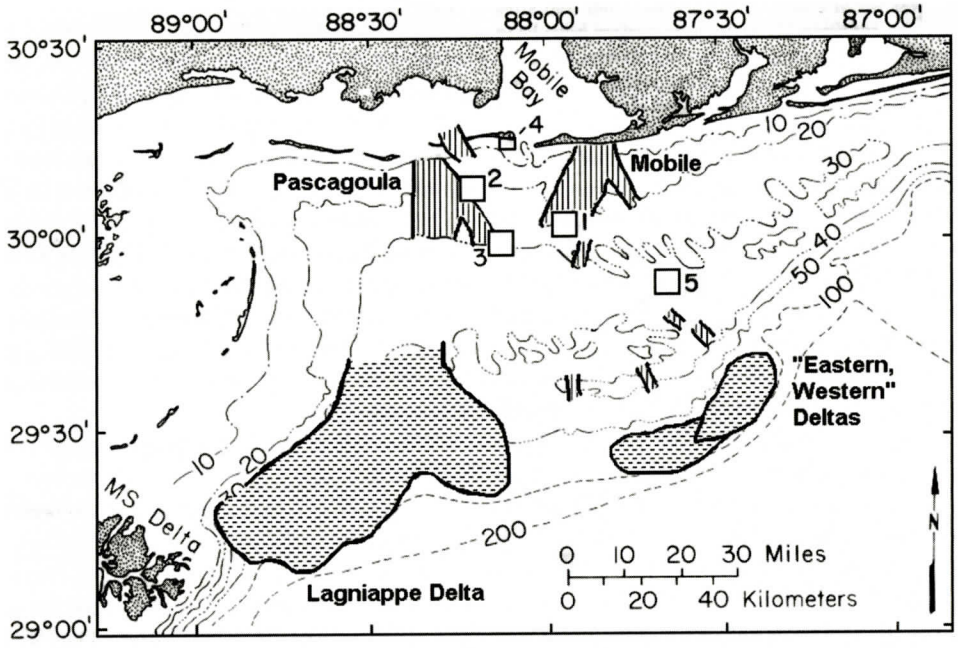

Figure 9. Location of hardbottom sites in relation to ancestral Mobile and Pascagoula river valleys, the Lagniappe Delta, and two other shelf-edge deltas. (Modified from Kindinger and others, 1994; Sager and others, 1999.)

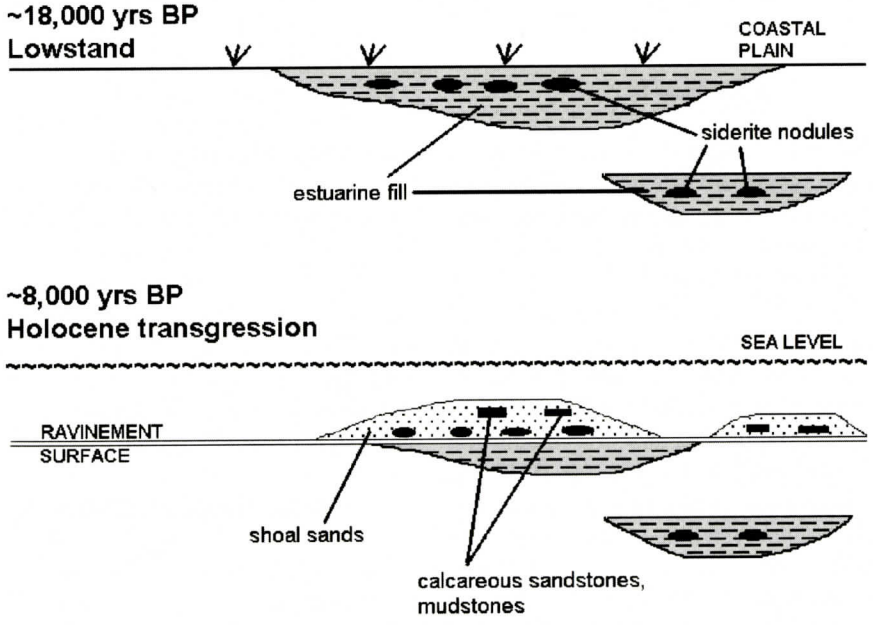

Figure 10. Schematic illustration of Pleistocene-Recent hardbottom formation in the northern Gulf of Mexico.

lar outcrops may be encountered in the future. In locations of rapid burial, a vertically expanded sequence of cemented slabs or zones could be produced, at the expense of lateral growth.

In less-protected offshore areas, the uppermost (shallowest) cemented materials are ex-

humed and reworked by storms and wave erosion. The prevalence of rubble-covered areas at our sites suggests that frequent storm erosion and reworking may have effectively broken up some laterally-extensive cemented areas, had they been present.

The various hardbottom morphologies and cement minerals likely reflect not only site-specific differences in the original chemical environments of formation (e.g. methanogenic and sulfate reduction zones), but also differences in sedimentation and burial rates, and in the degree of subsequent erosion (i.e. original depth, wave regime). For example, our previous studies have shown that the sideritic samples are not always present at locations of the calcareous rocks (Schroeder and others, 1988; Howard 1990). The shell-and burrow-cast shapes of many nodules suggest an origin in lower-energy estuarine or lagoonal environments containing both abundant organic matter and iron-rich clays. Occurrences of such siderite nodules may thus prove useful in recognizing and locating those types of paleoenvironments in stratigraphic studies.

SUMMARY

Carbonate-cemented slabs and nodules of sandstone, siltstone and mudstone have been recovered from five sites on the Alabama continental shelf of the northern Gulf of Mexico. Cements include aragonite, siderite, high-magnesium calcite (HMC), and a very high magnesium calcite phase (VHMC) containing up to 45 mol% magnesium. Aragonite displays a characteristic acicular morphology, while siderite cements typically appear as anhedral to euhedral rhombohedra from 5 to 30 μm in size. HMC and VHMC occur as generally equant, anhedral to subhedral, cryptocrystalline to microcrystalline pore-filling cements, along with larger (15-20 μm) crystals lining pore spaces. Some of the high-magnesium calcite crystals were found to have cores of VHMC and rims of HMC, suggesting alteration of early VHMC to HMC. Petrographic features and stable isotopic evidence indicate that aragonite formed as a result of microbial methane oxidation just below the sediment-water interface, while HMC authigenesis occurred deeper, in the (anoxic) sulfate reduction zone. At the base of the sulfate reduction zone, HMC and VHMC cements precipitated due to coupled sulfate reduction/methane oxidation. Below this, siderite formed as a result of CO_2 reduction within the region of methanogenesis. Radiocarbon analysis of a limited suite of hardbottom samples suggests late Pleistocene ages for the siderites and a few calcareous rocks from one of the five sites, while calcareous rocks from several other sites give Holocene ages.

The offshore Alabama samples are generally similar to a few of the Holocene methane-derived marine cements described in the literature in terms of morphology and stable isotope signatures, particularly to examples from the North Sea (Jorgensen 1976; Hovland and others, 1987). Some VHMC cements appear to have undergone leaching and alteration to HMC. Fossil-bearing outcrops of methanic cold seeps display cements with similar isotopic compositions, but the Alabama samples do not incorporate or preserve biota indicative of methanic influence. Comparison with studies of early diagenetic concretions, however, would suggest that the processes active in the cementation of these samples, as well as subsequent diagenesis, could generate laterally-cemented zones of significant size, as long as a methane source (resulting from, for example, abiotic degradation of underlying organic-rich sediments) is present. Finally, the siderite hardbottom rocks could be useful in recognizing transgressive surfaces of erosion associated with shallow estuary or lagoon paleoenvironments in the geologic record.

ACKNOWLEDGMENTS

This work represents a portion of the ongoing coastal research sponsored in part by the NOAA Office of Sea Grant, U.S. Department of Commerce, through the Mississippi-Alabama Marine Sciences Consortium (Sea Grant Program), under Grant No. NA85AA-D-SG005 (Projects R/ER-19-PD and R/ER-19. Sea Grant cruises recovered all samples described in this

paper. The University of Alabama provided the main analytical instruments for petrographic study. We are indebted to Dr. E. M. Ripley of Indiana University for providing stable isotope data on a large subgroup of samples. Constructive comments were provided by Southeastern Geology reviewers. Finally, we thank our colleagues Steven J. Parker and Carl R. Froede, Jr. for their reviews and suggestions. This investigation was conducted outside of the duties associated with the lead author's work for the U.S. Environmental Protection Agency.

REFERENCES CITED

Aiello, I.W., Garrison, R.E., Moore, J.C., Kastner, M., and Stakes, D.S., Anatomy and origin of carbonate structures in a Miocene cold-seep field: Geology, v. 29, p. 1111-1114.

Allen, R.C., Gavish, E., Friedman, G.M., and Sanders, J.E., 1969, Aragonite-cemented sandstone from outer continental shelf off Delaware Bay: submarine lithification mechanism yields product resembling beachrock: Journal of Sedimentary Petrology, v. 39, p. 136-149.

Beauchamp, B., and Savard, M., 1992, Cretaceous chemosynthetic carbonate mounds in the Canadian Arctic: Palaios, v. 7, p. 434-450.

Beauchamp, B., Krouse, H.R., Harrison, J.C., Nassichuk, W.W., and Eliuk, L.S., 1989, Cretaceous cold-seep communities and methane-derived carbonates in the Canadian Arctic: Science, v. 244, p. 53-56.

Chappell, J. and Shackleton, N.J., 1986, Oxygen isotopes and sea level: Nature, v. 324, p. 137-140.

Clari, P., Gagliardi, C., Governa, M.E., Ricci, B., and Zuppi, G.M., 1988, I Calcari di Marmorito: Una testimonianza de processi diagenetici in presenza di metano: Bolletino del Museo regionale di Scienze naturali, Torino, v. 6, p. 197-216.

Claypool, G.E., and Kaplan, I.R., 1974, The origin and distribution of methane in marine sediments, in Kaplan, I.R., ed., Natural Gases in Marine Sediments: Plenum, New York, p. 99-139.

Coleman, J.M., and Roberts, H.H., 1988, Sedimentary development of the Louisiana continental shelf related to sea level cycles: Geo-Marine Letters, v. 8, p. 1-119.

Curtis, C.D., and Coleman, M.L., 1986, Controls on the precipitation of early diagenetic calcite, dolomite, and siderite in complex depositional sequences: *in* Gautier, D.L., ed., Roles of organic matter in sediment diagenesis: Society of Economic Paleontologists and Mineralogists Special Pub. 38, p. 23-33.

Doyle, L.J., and Sparks, T.N., 1980, Sediments of the Mississippi, Alabama and Florida continental shelf: Journal of Sedimentary Petrology, v. 50, p. 905-915.

Fischer, A.G., and Garrison, R.E., 1967, Carbonate lithification on the sea floor: Journal of Geology, v. 75, p. 488-496.

Folk, R.L., 1974, The natural history of crystalline calcium carbonate: effect of magnesium content and salinity: Journal of Sedimentary Petrology, v. 44, p. 40-53.

Gaillard, C., Rio, M., Rolin, Y., and Roux, M., 1992, Fossil chemosynthetic communities related to vents and seeps in sedimentary basins: The pseudobioherms of southeastern France compared to other world examples: Palaios, v. 7, p. 451-465.

Gautier, D.L., 1982, Siderite concretions: indicators of early diagenesis in the Gammon Shale (Cretaceous): Journal of Sedimentary Petrology, v. 52, p. 859-871.

Gautier, D.L., 1985, Interpretation of early diagenesis in ancient marine sediments, *in* Relationship of Organic Matter and Mineral Diagenesis: Society of Economic Paleontologists and Mineralogists, Short Course, v. 17, p. 6-78.

Gautier, D.L., and Claypool, G.E., 1984, Interpretation of methanic diagenesis in ancient sediments by analogy with processes in modern diagenetic environments, *in* McDonald, D.A. and Surdham, R.C., eds., Clastic Diagenesis: Am. Soc. Petroleum Geologists Memoir 37, 434 p.

Ginsburg, R.N., 1953, Beachrock in South Florida: Journal of Sedimentary Petrology, v. 23, p. 89-92.

Hanor, J.S., 1978, Precipitation of beachrock cements: Mixing of marine and meteoric waters vs. CO_2 degassing: Journal of Sedimentary Petrology, v. 48, p. 489-501.

Hathaway, J.C., and Degens, E.T., 1969, Methane-derived marine carbonates of Pleistocene age: Science, v. 165, p. 690-692.

Hovland, M., Talbot, M., Qvale, H., Olausson, S., and Aasberg, L., 1987, Methane-related carbonate cements in pockmarks of the North Sea: Journal of Sedimentary Petrology, v. 57, p. 881-892.

Howard, R.O. Jr., 1990, Petrology of Hardbottom Rocks, Mississippi-Alabama-Florida Continental Shelf: Unpublished Masters Thesis, Department of Geology, University of Alabama, Tuscaloosa, Alabama, 121 p.

Jorgensen, N.O., 1976, Recent high-magnesian calcite/aragonite cementation of beach and submarine sediments from Denmark: Journal of Sedimentary Petrology, v. 46, p. 940-951.

Jorgensen, N.O., 1979, Magnesium incorporation in recent marine calcite cement from Denmark: Journal of Sedimentary Petrology, v. 49, p. 945-949.

Judd, A.G., 2003, The global importance and context of methane escape from the seabed: Geo-Marine Letters, v. 23, p 147-154.

Kauffman, E.G., Arthur, M.A., Howe, B., and Scholle, P.A., 1996, Widespread venting of methane-rich fluids in Late Cretaceous (Campanian) submarine springs (Tepee Buttes), Western Interior seaway, U.S.A.: Geology, v. 24, p. 799-802.

Kindinger, J.L., 1988, Seismic stratigraphy of the Mississippi-Alabama shelf and upper continental slope: Marine Geology, v. 83, p. 79-94.

Kindinger, J.L., 1989a, Upper Pleistocene to Recent shelf

and upper slope deposits of offshore Mississippi-Alabama, *in* Seventh Annual Research Conference Proceedings, Society of Economic. Paleontologists and Mineralogists, Gulf Coast Section, p. 163-174.

Kindinger, J.L., 1989b, Depositional history of the Lagniappe Delta, northern Gulf of Mexico: Geo-Marine Letters, v. 9, p. 59-66.

Kindinger, J.L., Balson, P.S., and Flocks, J.G., 1994, Startigraphy of the Mississippi-Alabama shelf and the Mobile River Incised-Valley System: *in* Dalrymple, R.W., Boyd, R., and Zaitlin, B.A., eds., Incised-Valley Systems: Origin and Sedimentary Sequences: Society of Economic Paleontologists and Mineralogists Special Publication No. 51, p. 83-95.

Klein, J.S., Mozley, P., Campbell, A., and Cole, R., 1999, Spatial distribution of carbon and oxygen isotopes in laterally extensive carbonate-cemented layers: implications for mode of growth and subsurface identification: Journal of Sedimentary Research, v. 69, p. 184-191.

Kocurko, M.J., 1986, Interaction of organic matter and crystallization of high magnesium calcite, south Louisiana: *in* Gautier, D.L., ed., Roles of Organic Matter in Diagenesis: Society of Economic Paleontologists and Mineralogists Special Publication No. 38, p. 13-21.

Land, L.S., 1980, The isotopic and trace element geochemistry of dolomite: the state of the art: *in* Concepts and Models of Dolomitization: Society of Economic Paleontologists and Mineralogists Special Publication No. 28, p. 87-110.

Longman, M.W., 1980, Carbonate diagenetic textures from nearsurface diagenetic environments: Bulletin of American Association of Petroleum Geologists, v. 64, p. 461-487.

Ludwick, J.C., 1964, Sediments in the northeastern Gulf of Mexico, *in* Miller, R.L. (ed), Papers in Marine Geology: New York, Macmillan, p. 204-238.

Martens, C.S., and Klump, J.V., 1984, Biogeochemical cycling in an organic-rich coastal marine basin 4, An organic carbon budget for sediments dominated by sulfate reduction and methanogenesis: Geochemica et Cosmochimica Acta, v. 48, p. 1987-2004.

Meyers, J.H., 1987, Marine vadose beachrock cementation by cryptocrystalline magnesian calcite in Maui, Hawaii: Journal of Sedimentary Petrology, v. 57, p. 558-570.

Morgan, J.P., and Treadwell, R.C., 1954, Cemented sandstone slabs of the Chandeleur Islands, Louisiana: Journal of Sedimentary Petrology, v. 24, p. 71-75.

Mozley, P.S., 1989, Relation between depositional environment and the elemental composition of early diagenetic siderite: Geology, v. 17, p.704-706.

Mozley, P.S., 1992, Isotopic composition of siderite as an indicator of depositional environment: Geology, v. 20, p. 817-820.

Nelson, C.S., and Lawrence, M.F., 1984, Methane-derived high-Mg cement in Holocene nodules from the Fraser Delta, British Columbia, Canada: Sedimentology, v. 31, p. 645-654.

Parker, S.J., Shultz, A.W., and Schroeder, W.W., 1992, Sediment characteristics and seafloor topography of a palimpsest shelf, Mississippi-Alabama continental shelf: in Quaternary Coasts of the United States: Marine and Lacustrine Systems, Society of Economic Paleontologists and Mineralogists Special Publication No. 48, p. 243-251.

Pirrie, D., and Marshall, J.D., 1991, Field relationships and stable isotope geochemistry of concretions from James Ross Island, Antarctica: Sedimentary Geology, v. 71, p. 137-150.

Raiswell, R., 1987, Non-steady state microbiological diagenesis and the origin of concretions and nodular limestones: *in* Marshall, J.D. (ed), Diagenesis of Sedimentary Sequences: Geological Society Special Publication No. 36, London, p. 41-54.

Reeburgh, W.S., 1980, Anaerobic methane oxidation rate depth distribution in Skan Bay sediments: Earth and Planetary Science Letters, v. 47, p. 345-352.

Rice, D.D., and Claypool, G.E., 1981, Generation, accumulation, and resource potential of biogenic gas: Bulletin of American Association of Petroleum Geologists, v. 67, p. 5-25.

Ritger, S., Carson, B., and Suess, E., 1987, Methane-derived authigenic carbonates formed by subduction-induced pore-water expulsion along the Oregon/Washington margin: Geol. Soc. Am. Bull., v.98, p. 147-156.

Roberts, H.H., and Whelan, T., 1975, Methane-derived carbonate cements in barrier and beach sands of a subtropical delta complex: Geochemica et Cosmochimica Acta, v. 39, p. 1085-1089.

Roberts, H.H., Sassen, R., and Aharon, P., 1987, Carbonates of the Louisiana slope: 19th Annual Offshore Technology Conference, Houston, Texas, p. 373-381.

Rosenfeld, W.D., and Silverman, S.R., 1959, Carbon isotope fractionation in bacterial production of methane: Science, v. 130, p. 1658.

Sackett, W.M., and Thompson, R.R., 1963, Isotopic organic carbon composition of recent continental derived clastic sediments of eastern gulf coast, Gulf of Mexico: Bulletin of American Association of Petroleum Geologists, v. 47, p. 525-531.

Sager, W.W., Schroeder, W.W., Davis, K.S., and Rezak, R., 1999, A tale of two deltas: seismic mapping of near surface sediments on the Mississippi-Alabama outer shelf and implications for recent sea-level fluctuations: Marine Geology, v. 160, p. 119-136.

Savard, M.M., Beauchamp, B., and Veizer, J., 1996, Significance of aragonite cements around Cretaceous marine methane seeps: Journal of Sedimentary Research, v. 66, p. 430-438.

Schroeder, W.W., Shultz, A.W., and Dindo, J.J., 1988, Inner-shelf hardbottom areas, northern Gulf of Mexico: Transactions, Gulf Coast Association of Geological Societies, v. 38, p. 535-541.

Schroeder, W.W., Gittings, S.R., Dardeau, M.R., Fleischer, P., Sager, W.W., Shultz, A.W., and Rezak, D., 1989, Topographic features of the L'MAFLA continental

shelf, northern Gulf of Mexico: Oceans '89 Proceedings, IEEE Publication No. 89CH2780-5, New York, pp. 54-58.

Schroeder, W.W., Shultz, A.W., and Pilkey, O.H., 1995, Late Quaternary oyster shells and sea level history, inner shelf, northeast Gulf of Mexico: Journal of Coastal Research, v. 11, p. 664-674.

Shultz, A.W., Schroeder, W.W., and Abston, J.R., 1990, Along-shore and offshore variations in Alabama inner-shelf sediments, in Tanner, W.F. (ed.), Coastal Sediments and Processes: Proceedings, Ninth Symposium on Coastal Sedimentology, Florida State University, Tallahassee, p. 141-152.

Siringan, F.P., 1993, Coastal Lithosome Evolution and Preservation During an Overall Rising Sea Level: East Texas Gulf Coast and Continental Shelf: Unpublished Ph.D. Thesis, Department of Geology and Geophysics, Rice University, Houston, Texas, 226p.

Sydow, J.C., Roberts, H.H., Bouma, A.H., and Winn., R., 1992, Constructional subcomponents of a shelf-edge delta, northeast Gulf of Mexico: Transactions, Gulf Coast Association of Geological Societies, v. 42, p. 717-426.

Walter, L.M., 1986, Relative efficiency of carbonate dissolution and precipitation during diagenesis: a progress report on the role of solution chemistry: *in* Gautier, D.L., ed., Roles of Organic Matter in Diagenesis: Society of Economic Paleontologists and Mineralogists Special Publication No. 38, p. 1-11.

Weiss, C.P., and Wilkinson, B.H., 1988, Holocene cementation along the central Texas coast: Journal of Sedimentary Petrology, v. 58, p. 468-478.

Whiticar, M.J., and Faber, E., 1986, Methane oxidation in sediment and water column environments--Isotope evidence: Organic Geochemistry, v. 10, p. 759-768.

SOUTHEASTERN GEOLOGY
V. 43, No. 3, February 2005, p. 157-172

A NEW GENUS AND SPECIES OF ARCHAEOCETE WHALE FROM MISSISSIPPI

MARK D. UHEN

Cranbrook Institute of Science
39221 Woodward Avenue
P.O. Box 801
Bloomfield Hills, Michigan 48303-0801
muhen@cranbrook.edu

ABSTRACT

A new genus and species (*Cynthiacetus maxwelli*) of basilosaurid archaeocete is described here based on a specimen that includes: a skull; jaws; teeth; cervical, thoracic, and lumbar vertebrae; ribs and sternum; and forelimb elements. This specimen was recovered from the late Eocene Yazoo Clay of the Cynthia Clay Pit, Hinds County, Mississippi. Taxonomy of this and other species is clarified and their phylogenetic position within the Basilosauridae are identified. This new specimen is compared to other basilosaurids, particularly *Basilosaurus cetoides* and *Pontogeneus priscus* (*brachyspondylus*). Additional less complete specimens of *C. maxwelli* are also identified from Alabama, Georgia, Florida, North Carolina, and Egypt.

INTRODUCTION

Joseph Leidy named a new species of archaeocete whale, *Pontogeneus priscus,* in 1852 in a presentation to the Academy of Natural Sciences of Philadelphia, as reported in the Proceedings of the ANSP (Leidy, 1852). The only remains in his possession was the body of a single cervical vertebra from the Ouachita River of northeastern Louisiana (Leidy, 1952). Kellogg (1936) considered this vertebra to belong to the same species as some vertebrae that had been included in Koch's (1846) chimera *Hydrarchos harlani*. (Koch had assembled a skeleton for display from at least four individual specimens from at least three different species of archaeocetes [Müller, 1849]). This species had normally proportioned vertebrae similar to those of smaller dorudontines and unlike the elongate posterior thoracic, lumbar, and anterior caudal vertebrae of *Basilosaurus*, even though they were otherwise similar in size to those of *Basilosaurus*. At the time, so few specimens of this species were known that Kellogg did not attribute this species to any family, but simply included it in Archaeoceti *incertae sedis*. Since then, similar specimens have been found that have large trunk vertebrae that are not elongate, including a relatively complete skull and skeleton from the Yazoo Clay Formation of Hinds County, Mississippi (MMNS VP 445), discovered by Britt Maxwell and excavated by Elanor Daly in May of 1988. These specimens were compared to the type specimen of *Pontogeneus priscus*, and to specimens of *Basilosaurus cetoides*. Based on these comparisons, *Pontogeneus priscus* has been determined to be a *nomen nudum*, and a new genus and species, *Cynthiacetus maxwelli* is characterized and placed in phylogenetic context with other archaeocetes.

Abbreviations used in the text and figure captions are as follows: ANSP, Academy of Natural Sciences of Philadelphia, Philadelphia; CGM, Cairo Geological Museum, Cairo; MMNS, Mississippi Museum of Natural Science, Jackson; SMNS, Staatliches Museum für Naturkunde, Stuttgart; UF, University of Florida, Florida Museum of Natural History, Gainesville; UF FGS, University of Florida, Florida Geological Survey collection, Florida Museum of Natural History, Gainesville; UISPM, Universitäts-Institut und Staatssammlung für Paläontologie und Historische Geologie, Munich; UM, University of Michigan Museum of Paleontology, Ann Arbor; USNM, United States National Museum of Natural History, Washington DC.

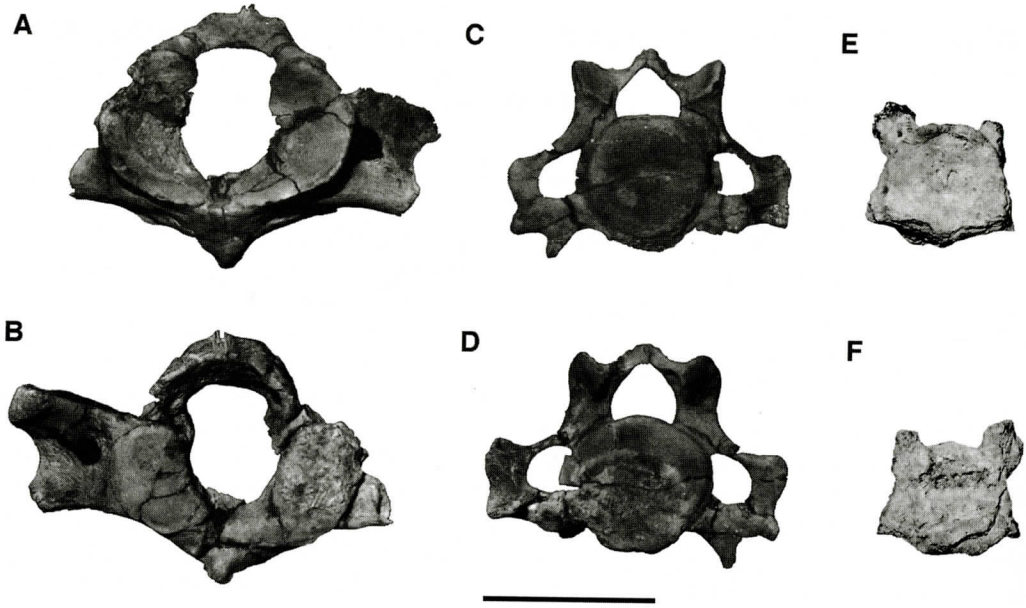

Figure 1: Cervical vertebrae of *Cynthiacetus maxwelli*, MMNS VP 445 compared to *Pontogeneus priscus*. A and B are the atlas (C1) of MMNS VP 445 in A, anterior and B, posterior views. The right transverse process was located and reattached after this photo was taken. C and D are C3 of MMNS VP 445 in C, anterior and D, posterior views. Type specimen of *Pontogeneus priscus* ANSP 13668, third or fourth cervical vertebra in E, anterior, and F, posterior views. Scale bar is 10 centimeters.

SYSTEMATICS

Mirorder Cete Linné, 1758 *sensu* McKenna and Bell, 1997

Order Cetacea Brisson, 1762

Suborder Archaeoceti Flower, 1883

Family Basilosauridae Cope, 1868 *sensu* Barnes and Mitchell, 1978

Subfamily Dorudontinae Miller, 1923 *sensu* Barnes & Mitchell, 1978

Genus *Pontogeneus* Leidy, 1852, *nomen nudum*

Species *Pontogeneus priscus* Leidy, 1852, *nomen nudum*

Hydrarchos harlani* Koch, 1846, p. 1 (in part), *nomen nudum.

Zeuglodon brachyspondylus* Müller, 1849, p. 26, *nomen nudum.

Pontogeneus priscus* Leidy, 1852, p. 52, *nomen nudum.

Zeuglodon brachyspondylum* Abel, 1914, p. 203, *nomen nudum.

Pontogeneus brachyspondylus* Kellogg, 1936, p. 248, *nomen nudum.

TYPE SPECIMEN

ANSP 13668, a single third or fourth cervical vertebral body (Figure 1 E, F).

AGE AND DISTRIBUTION

Late Eocene of Louisiana.

DIAGNOSIS

Leidy (1852) named *Pontogeneus priscus* in a brief note based on a centrum of a single cervical vertebra, later designated as ANSP 13668 (Figure 1 E, F). Leidy (1852) noted the "rela-

tively deep concavity of its surfaces before and behind", but this feature does not distinguish *Pontogeneus* from other archaeocetes. The vertebral body of the type specimen is larger than those of *Zygorhiza*, and it is smaller than most cervical vertebral bodies from *Basilosaurus*, but it its difficult to be certain that the type specimen of *P. priscus* is not a small individual of *Basilosaurus cetoides*. Based on the limited nature of the type specimen and the similarity of the type specimen to cervical vertebral centra of *Basilosaurus*, *Pontogeneus priscus* is here designated a *nomen nudum*.

TYPE LOCALITY

Leidy (1852) notes that the type specimen of *Pontogeneus priscus* is "from the Eocene formation of Ouachita, Louisiana." Kellogg (1936) suggested that the specimen came from the Jackson Formation (now known as the Jackson Group). Jackson Group sediments do not crop out in Ouachita Parish, Louisiana, but the Ouachita River flows through Caldwell Parish to the south, where the Jackson Group is exposed (Huner, 1939; Snead *et al.*, 1984).

DISCUSSION

Müller (1849) stated that many of the vertebrae in Koch's *Hydrarchos harlani* belong in the species *Zeuglodon brachyspondylus*, lacking elongate vertebral centra, but he failed to designate any set of vertebrae as the type specimen for the species. Kellogg (1936) stated that these vertebrae probably came from Alabama, from "the vicinity of Washington Old Court House." In 1851, Müller separated out some of the *Zeuglodon brachyspondylus* vertebrae as belonging to *Zeuglodon brachyspondylus minor* (= *Zygorhiza kochii*). Kellogg (1936) indicated that the vertebrae Müller left in *Zeuglodon brachyspondylus* belonged with Leidy's *Pontogeneus priscus* in a new combination he called *Pontogeneus brachyspondylus*, but he also failed to designate a type specimen. Because the generic name *Zeuglodon* is a junior subjective synonym of *Basilosaurus* (Kellogg, 1936; Uhen, 1998), and the species referred to as *Zeuglodon brachyspondylus* never had a type specimen designated, the combination *Zeuglodon brachyspondylus* should be considered a *nomen nudum*. Since Kellogg never designated a type specimen for *Pontogeneus brachyspondylus*, it too should be considered a *nomen nudum*.

Genus *Cynthiacetus*, new genus

TYPE SPECIES

Cynthiacetus maxwelli, new species, described below.

INCLUDED SPECIES

Cynthiacetus currently includes only the type species.

ETYMOLOGY

The name *Cynthiacetus* is derived from the name of the quarry in which the type specimen was discoverer, the Cynthia Clay Pit, and the Greek *ketos* (masc.), meaning whale.

AGE AND DISTRIBUTION

Same as for the species.

DIAGNOSIS

Same as for the species.

DISCUSSION

Previously, Uhen (1998) followed Kellogg (1936) in combining Müller's *Zeuglodon brachyspondylus* with Leidy's *Pontogeneus priscus* in the combination *Pontogeneus brachyspondylus*. Given the difficulty in distinguishing *Pontogeneus priscus* from other basilosaurids, the new genus *Cynthiacetus* is named here for those specimens that had previously been assigned to *Pontogeneus brachyspondylus*.

Species *Cynthiacetus maxwelli*, new species

TYPE SPECIMEN

MMNS VP 445 (Figures 1-7), skull, mandibles, teeth, auditory bullae, cervical, thoracic, and lumbar vertebrae, humerus, radius, ulna. Yazoo Clay Formation, Priabonian, near Cynthia, Hinds County, Mississippi.

TYPE LOCALITY

Yazoo Clay Formation, Cynthia Clay Pit, Hinds County, Mississippi. See Dockery (1992) and Dockery and Slesser (1984) for descriptions of the Cynthia Clay Pit.

ETYMOLOGY

The specific epithet *maxwelli* honors the discoverer of the type specimen, Britt Maxwell.

REFERRED SPECIMENS

SMNS 11413, skull fragments (*Zeuglodon brachyspondylus*, specimen St. 8 of Stromer, 1908). Gehannam Formation?, Bartonian, Fayum, Egypt.

SMNS 11414, discontinuous series of atlas, axis, 3 thoracic, 12 lumbar vertebrae and 1 caudal vertebrae from the same individual as SMNS 11413. Gehannam Formation?, Bartonian, Fayum, Egypt.

UF 3572, vertebral centrum. Alachua County, Florida, formation unknown.

UF 40048, lumbar vertebra. Columbia County, Florida, formation unknown, age listed as Late Pleistocene in the UF catalog, which is almost certainly in error.

UF 137602, posterior thoracic vertebra.

UF FGS V2184, lumbar vertebra. Alachua County, Florida, formation unknown, listed as Pliocene? in the UF catalog, which is almost certainly in error.

UF FGS V2603, lumbar vertebra. Alachua County, Florida, formation unknown, listed as Pliocene? in the UF catalog, which is almost certainly in error.

UF FGS V3233, lumbar vertebra. Alachua County, Florida, formation unknown.

UF FGS V4556, one lumbar and one caudal vertebra, Florida, locality unknown, formation unknown.

UF FGS V4894, lumbar vertebra. Alachua County, Florida, formation unknown.

UF FGS V7235, three thoracic, two lumbar vertebrae, and four undetermined vertebrae and 4 partial ribs. Crystal River Formation, Priabonian, Lafayette County, Florida.

UISPM 1904 XII 135, posterior thoracic vertebra. Gehannam Formation?, Bartonian, Fayum, Egypt. This vertebra was figured by Stromer, 1908, p. 136, Plate II.

USNM 776, anterior lumbar vertebra. Kellogg (1936) notes that this specimen is from the upper Jackson Formation, locality unknown. The USNM catalog lists the locality as Patuxent River, Maryland, which is almost certainly in error.

USNM 2211, five lumbar and one caudal vertebrae. Yazoo Clay Formation? (listed as upper Jackson Formation in the USNM catalog), Priabonian, Choctaw County, Alabama.

USNM 4678 (in part), one thoracic vertebra. Yazoo Clay Formation? (listed as Jackson Formation in the USNM catalog), Priabonian, Clarke County, Alabama.

USNM 11401, six lumbar vertebrae. Ocala Formation, Priabonian, Crisp County, Georgia.

USNM 13883, one lumbar vertebra. Probably from the Clinchfield Sand Formation (Domning *et al.*, 1982), Houston County, Georgia.

USNM 310637, right parietal, one thoracic vertebra, and three lumbar vertebrae. Castle Hayne Formation, Comfort Quarry, Jones County, North Carolina.

UM 97535, lumbar vertebra. Birket Qarun Formation, Priabonian, Fayum, Egypt.

UM 101222, lumbar vertebra. Birket Qarun Formation, Priabonian, Fayum, Egypt.

AGE AND DISTRIBUTION

Bartonian and Priabonian (middle to late Eocene) deposits of the southeastern United States and Fayum, Egypt.

Table 1: Dental measurements of *Cynthiacetus maxwelli*, MMNS VP 445. All measurements are in millimeters and to the nearest tenth of a millimeter unless otherwise noted. ~ indicates an approximate measurement.

Tooth	Length		Width		Height		Mesial denticles		Distal denticles	
	left	right	left	right	left	right	left	right	left	right
I^1	18.8	-	13.5	-	23.3	-	0	-	0	-
I^1	31.7	-	16.8	-	37.7	-	0	-	0	-
I^3	-	28.4	-	17.2	-	~31	-	-	-	-
C^1	36.4	41.8	22.2	23.6	~55	~52	0	0	0	0
P^3	~75	-	-	-	~37	-	5	-	5+?	
P^4	~68	-	-	-	-	-	4+?	-	-	-
M^1	31.7	-	103.	-	12.7	-	2	2	33	-
M^2	-	~29	-	11.3	-	13.8	-	?	-	3
I_1	-	17.2	-	11.7	-	20.8	-	0	-	0
I_2	29.8	31.2	18.3	19.9	~45	41.6	0	0	0	0
I_3	-	34.2	-	18.3	-	-	-	0	-	0
C_1	-	37.1	-	21.6	-	56.2	-	0	-	0
P_1	-	45.0	17.4	18.5	32.1	33.4	0	0	?	1
P_2	-	67.5	-	17.5	-	33.3	-	2	-	3
P_4	86.8	-	17.8	-	37.5	-	5	-	6	-
M_1	-	34.8	-	-	-	-	-	0	-	4
M_3	-	34.8	-	10.2	-	22.8	-	0	-	4

DIAGNOSIS

Large body size distinguishes *Cynthiacetus* from other dorudontines. Skull, cervical vertebrae, and anterior thoracic vertebrae are similar in morphology to those of *Basilosaurus*. The posterior thoracic vertebrae, lumbar vertebrae, and anterior caudal vertebrae are not elongate, but have proportions similar to other dorudontines, distinguishing *Cynthiacetus* from *Basilosaurus*.

DISCUSSION

The newly prepared specimen MMNS VP 445 has cervical vertebrae which are slightly smaller than those typically assigned to *Basilosaurus*. In addition, the posterior thoracic and lumbar vertebrae of MMNS VP 445 indicate that this specimen is not *Basilosaurus cetoides*. The posterior thoracic vertebrae in *Basilosaurus*, are markedly elongate, and elongation is fully developed in the lumbar region (see Kellogg, 1936, Plate 1A). None of the vertebrae of MMNS VP 445 show elongation of the vertebral bodies relative to their height and width. For these reasons, it is placed in a new genus and species and designated as the holotype specimen.

DESCRIPTION

The description that follows is based on MMNS VP 445. Other specimens conform to this description unless otherwise noted. Much of MMNS VP 445 has been prepared, but portions of the skeleton, including some vertebrae and ribs remain unprepared in blocks.

Teeth—*Cynthiacetus maxwelli* appears to have had the typical compliment of teeth for basilosaurids: three upper and lower incisors (I), one upper and one lower canine (C), four upper and

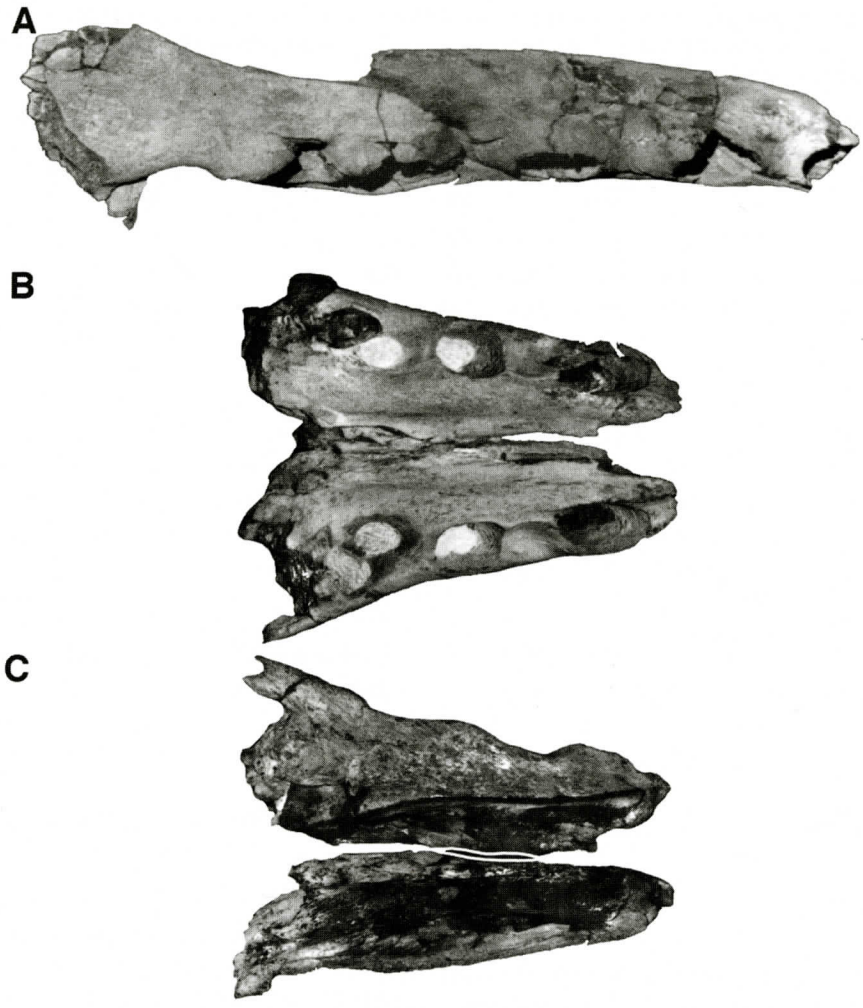

Figure 2: Anterior cranial elements of *Cynthiacetus maxwelli*, MMNS VP 445. A, right premaxilla and maxilla in right lateral view. The posterior portion of the premaxilla is missing dorsal to the maxilla. B, anterior maxillae in ventral view. Alveoli from anterior to posterior are: C^1, P^1, and the anterior root of P^2. Depressions between alveoli are embrasure pits. C, anterior maxillae in dorsal view. Scale bar is ten centimeters.

lower premolars (P), three lower and two upper molars (M). Some teeth are preserved in place in the skull or jaw (P_1, P_2, P^3, P^4, M^2), while others were identified by comparison with each other and to other basilosaurids. The teeth that are preserved out of the jaw are hollow, indicating that dentin deposition was still in progress at the time of death of MMNS VP 445. This, along with the almost complete lack of wear on the teeth, indicates that this individual was an adolescent or young adult, as dental eruption was complete, but the teeth were not finished developing.

Incisors and canines are single rooted, conical teeth. They show strong vertical ridges, and have well-developed mesial and distal midline carinae. Lower P1 appears to be single rooted, but there is an obvious division in the root near the base of the crown. More posterior premolars and molars are double rooted. P^1 and P^2 are preserved only as alveoli (Figure 2B). Upper and lower premolars have well-developed mesial

and distal accessory denticles, with the exception of P_1, which lacks mesial denticles, and has only weakly developed distal denticles. Dental measurements are listed in Table 1. Lower molars lack mesial denticles and have a mesial reentrant groove, as in other basilosaurids. Upper molars are small with long roots.

Table 2: Cranial measurements of *Cynthiacetus maxwelli*, MMNS VP 445. All measurements are in millimeters and to the nearest millimeter. ~ indicates an approximate measurement.

Measurement	Value
Condylobasal length	~1300
Rostrum breadth at I1	~70
Rostrum breadth at C1	~130
Frontal shield breadth	~426
Auditory bulla length	86.7 (l) 85.7 (r)
Nuchal crest breadth	172
Nuchal crest height	198
Condylar breadth	~142
Occipital breadth	421
Zygomatic skull breadth	~532

Skull—The skull of *Cynthiacetus maxwelli* is large, rivaling the size of *Basilosaurus cetoides*. Cranial measurements are listed in Table 2, see Kellogg (1936, Table 62) for measurements of *Basilosaurus cetoides* and other archaeocetes. The maxilla articulates anteriorly with the premaxilla (Figure 2), and the posterior premaxilla lies dorsal to the anterior maxilla, but there is no fusion between the premaxilla and maxilla, nor the left and right premaxillae. The medial edge of the posterior premaxilla articulates with the nasal. The premaxilla bears alveoli for the incisors and embrasure pits (see Figure 2 B) along its lateral face between the alveoli. These embrasure pits accept the tips of the lower incisors when the jaw is closed.

The maxilla bears alveoli for the upper canine, premolars, and molars on its palatal surface separated by embrasure pits. These pits are placed more medially toward the posterior end of the maxilla. Laterally, the maxilla bears multiple infraorbital foramina. Dorsomedially, the maxilla articulates with the premaxilla while posteriorly the maxilla articulates with the frontal. The nasals are long and thin. The medial borders of the nasals are not separated by a projection of the frontal as they are in *Dorudon*.

The frontal flares laterally and along with the maxilla, lacrimal, and jugal form the orbit. The jugal projects posteriorly from its dorsal articulation with the lacrimal and ventral articulation with the maxilla. The dorsal surface of the pos-

Table 3: Vertebral measurements of *Cynthiacetus maxwelli*, MMNS VP 445. All measurements are in millimeters and to the nearest millimeter. * missing both epiphyses. † missing one epiphysis.

Vertebra	Anterior width	Anterior height	Ventral length	Posterior width	Posterior height	Dorsal length
C1	151.6		58.5			
C2						
C3	71.2	71.3	36.7	87	78.8	
C4	77.9	74.5	37.0	80.1	76.8	
C5						
C6						
C7*						35
Ta*	85	67				
Tb*		69	52.0	101.4	68.8	52.3
Tc†	111.6	90.8	85.3	114.7	97.5	
Td*			73			
Te*	116	91	76.0	117.1	101.7	83
Tf*		97	75.9	114.3	98.2	82
La*	118.4		82	116.3		86.5

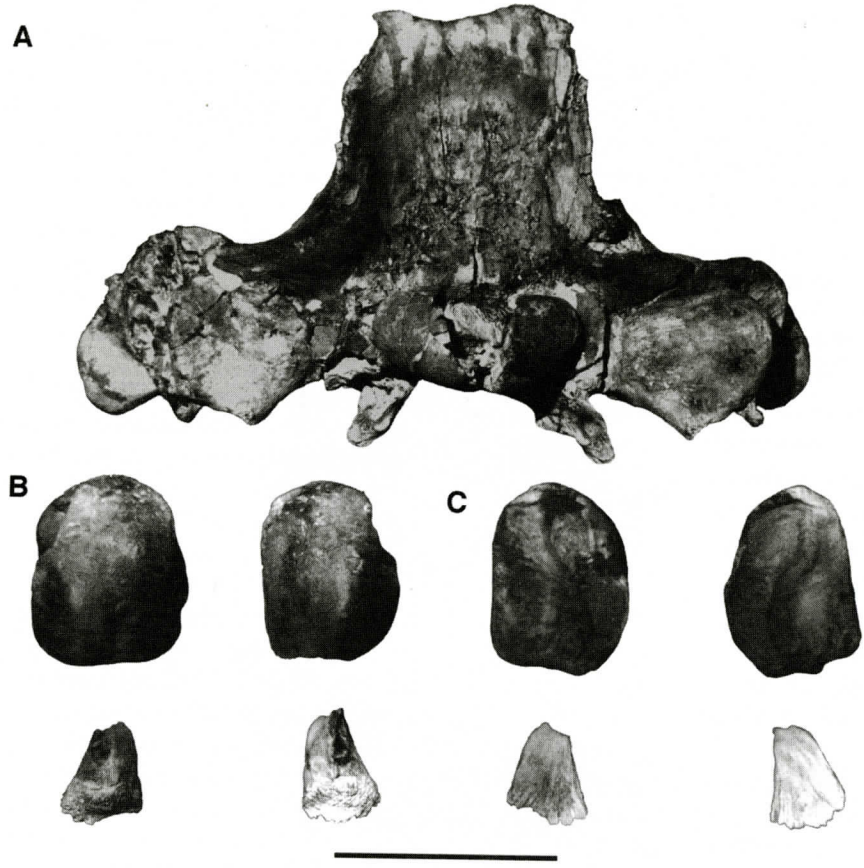

Figure 3: A, Posterior view of the skull of *Cynthiacetus maxwelli*, MMNS VP 445. Note the high, vertical nuchal crest. Auditory bullae of *Cynthiacetus maxwelli*, MMNS VP 445 in B, ventral and C, dorsal views. Posterior processes of the bullae are broken off and shown separately. Scale bar is 10 centimeters.

terior end of the jugal contacts the ventral surface of the zygomatic processes of the squamosal. Posteriorly, the frontal articulates with the parietal. The parietal forms the medial wall of the temporal fossa, and articulates posteriorly with the supraoccipital and posterolaterally with the squamosal. The parietal, squamosal, and supraoccipital together form a high, vertical nuchal crest.

The supraoccipital is fused ventrally with the exoccipitals (Figure 3). There is no trace of a suture between the supraoccipital and exoccipital. The exoccipital flares laterally and articulates anteriorly with the squamosal. The exoccipital also includes the occipital condyles and have ventral projections that form the posterior portion of the falcate process. The exoccipital articulates with the basioccipital at this point, which forms the remainder of the falcate process and the posterior portion of the basicranium.

Much of the basicranium is damaged, but many features can still be made out. The medial and lateral laminae of the pterygoids form the pterygoid sinus anterior to the periotic. The left stapes was found in articulation with the left periotic. Both auditory bullae were recovered, but both were damaged (Figure 3B, C). The posterior processes of the bullae were broken off, but both were recovered.

Mandible—The anterior portion of the left dentary (Figure 4 A) was recovered and includes the alveoli for the incisors, along with embrasure pits between the I_2 and I_3 alveoli and

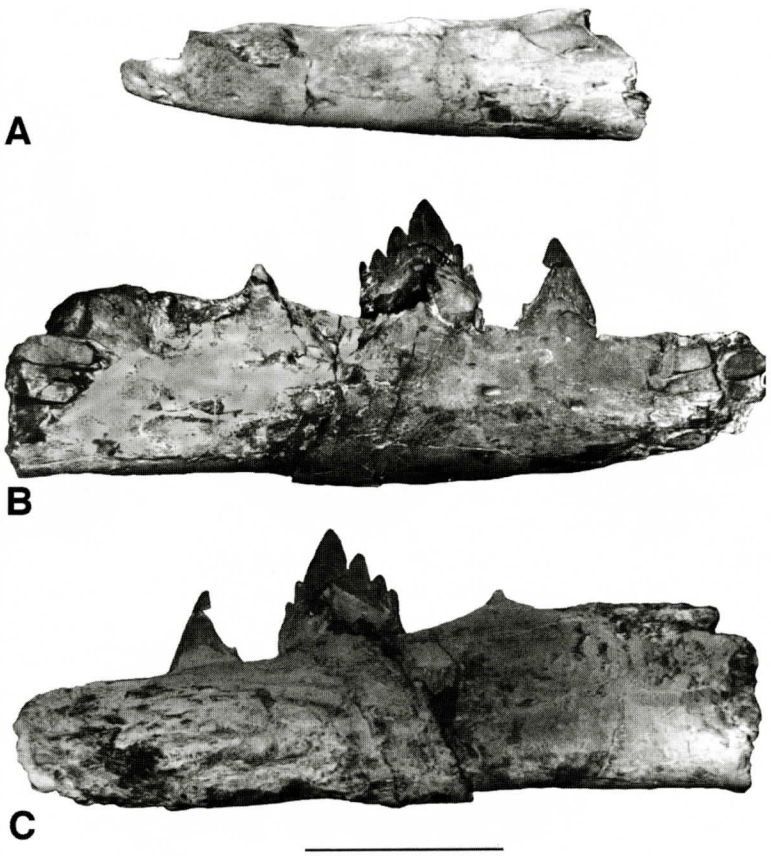

Figure 4: Mandible fragments of *Cynthiacetus maxwelli*, MMNS VP 445. A, anterior potion of the left dentary in left lateral view. B, middle portion of the right dentary in lateral view showing P_1 and P_2 in place in lateral view. C, middle portion of the right dentary in medial view showing P_1 and P_2 in place in medial view. Note the termination of the mandibular symphysis posterior to P_2. Scale bar is 10 centimeters.

posterior to the I_3 alveolus. I_1 and I_2 alveoli are close together, while those of I_2 and I_3 are farther apart. A portion of the right dentary was recovered that includes the crushed canine alveolus, P_1, P_2, and the P_3 alveolus (Figure 4 B, C). The medial side of the right dentary shows the mandibular symphysis extended back to P_2. No more posterior portions of the mandible were recovered.

Cervical vertebrae—Five of seven cervical vertebrae were recovered with MMNS VP 445. The atlas (C1) is virtually complete (Figure 1A, B), while the axis (C2) is heavily damaged. C3 and C4 are also virtually complete (Figure 1C, D), C5 and C6 are missing, and C7 is heavily damaged. The dorsal arch of the atlas still has a visible suture line between the left and right pedicles. Vascular foramina are present in the dorsal arch, as well as the transverse processes. The dorsal surface of the transverse process forms a flat shelf where in most specimens of *Basilosaurus* it is a ridge.

The third and fourth cervical vertebrae are similar to each other and to those of other basilosaurids. The fourth cervical is slightly larger than the third. Vertebral measurements are listed in Table 3. The anterior and posterior epiphyses are adherent to the bodies of C3 and C4, but there is a prominent suture line visible.

Thoracic vertebrae—Six thoracic vertebrae have been prepared from MMNS VP 445. They have been identified with lower case letters to

Figure 5: Thoracic vertebrae of *Cynthiacetus maxwelli*, MMNS VP 445. A to C are Tc in A, anterior, B, posterior, and C, left lateral views. D shows the bodies of Td, Te, and Tf in right lateral view. Scale bar is 10 centimeters.

indicate their relative positions in the thoracic series. Ta and Tb come from the anterior part of the thoracic series as indicated by the presence of two costal fovea on each vertebral body. Tc through Tf represent a contiguous series of vertebrae (Figure 5). Tc is the most anterior vertebra with a single costal fovea on each side. In fact, on the left side of the vertebra the costal fovea is partially divided. This vertebra is comparable to T12 in *Dorudon atrox* (Uhen, 1996), T11 in *Zygorhiza kochii*, and T10 in *Basilosaurus cetoides* (Kellogg, 1936). In Tc through Tf, the costal fovea is present on a transverse process that becomes longer and more ventrally placed on the vertebral body from Tc to Tf.

Lumbar vertebrae—The single lumbar vertebra that has been prepared is similar in size and shape to the posterior thoracic vertebrae. It differs in that it has the transverse processes placed more ventrally on the vertebral body and lacks costal fovea.

Sternum and Ribs—Four elements of the sternum of MMNS VP 445 have been recovered including the manubrium, two mesosternal elements, and the xiphisternum. Basilosaurids usually have five sternal elements: a manubrium, three mesosternal elements, and a xiphisternum. The manubrium of *Cynthiacetus* (Figure 6A, B, C) is similar to those of other basilosaurids. It is longer than it is wide, and the posterior end is U-shaped, with an anterior end that is caudally indented along the midline. The articular margins of the sternal elements bear a rough, spongy texture indicative of a cartilaginous articulation. The mesosternal elements are hexagonal in shape (Figure 6D, E), and the xi-

Table 4: Character states for *Cynthiacetus maxwelli*. See Uhen (2003) and references therein for additional taxa and characters.

	Character	*Cynthiacetus*
1	frontal shield size rel to CB	>2.5
2	posterior frontal border	straight
3	rostrum breadth	moderate
4	skull length relative to CB	>8
5	emprassure pits	present
6	orbit height rel to CB	?
7	orbit position	?
8	palate narrows at	?
9	palate shape	flat
10	falcate process of BO	large
11	vomer covers BO/BS suture	?
12	pachyosteosclerotic bulla	present
13	medial bulla articulation	absent
14	pt sinus depth	present
15	lateral wall of pt sinus	present
16	sigmoid process	large
17	hypoglossal foramen in jugular	yes
18	anterior palatine foramen	?
19	nuchal crest orientation	vertical
20	exoccipital shape	squared
21	position of posterior nares	?
22	posterior nasal breadth	?
23	posterior medial max contacts	premaxilla
24	mandibular foramen	large
25	mandibular symphisis position	P2
26	mandibular symphisis fused	no
27	incisors in tooth row	yes
28	cheek teeth with many denticles	yes
29	number P1/ roots	one
30	number of upper molars	two
31	#M1/ roots	two
32	#M2/ roots	two
33	#M3/ roots	?
34	tooth replacement	?
35	number of P/1 roots	two
36	reentrant groove on lower molar	present
37	cervical vertebrae compressed	a lot
38	number of thoracics	?
39	number of lumbars	?
40	lumbars elongated	no
41	lumbar zygapophyses	flat
42	# sacrals solidly ankylosed	?
43	# sacrals loosely joined	?
44	# sacrals articulate with pelvi	?
45	posterior caudals d-v com-presse	?
46	anterior caudals elongate	no
47	posterior caudals elongate	?
48	infraspinous fossa on scapula	?
49	coracoid process oriented anter	?
50	acromion process oriented anter	?
51	humeral shaft a/p thick	yes
52	deltopectoral crest position	distal
53	distal humeral articulation div	yes
54	radius and ulna flat	yes
55	broad olecranon process	yes
56	distal ulna	broad
57	saddle-shaped carpal arts	?
58	trapezoid and magnum	?
59	carpals in alternating rows	?
60	pisiform	?
61	hyperphalangy	?
62	pelvis	?
63	pelvis rotation	?
64	femur	?
65	tarsals	?
66	tibia/fibula	?
67	sternum form	big and heavy
68	body size	very large
69	stratigraphic position	late Bartonian & early Priabonian

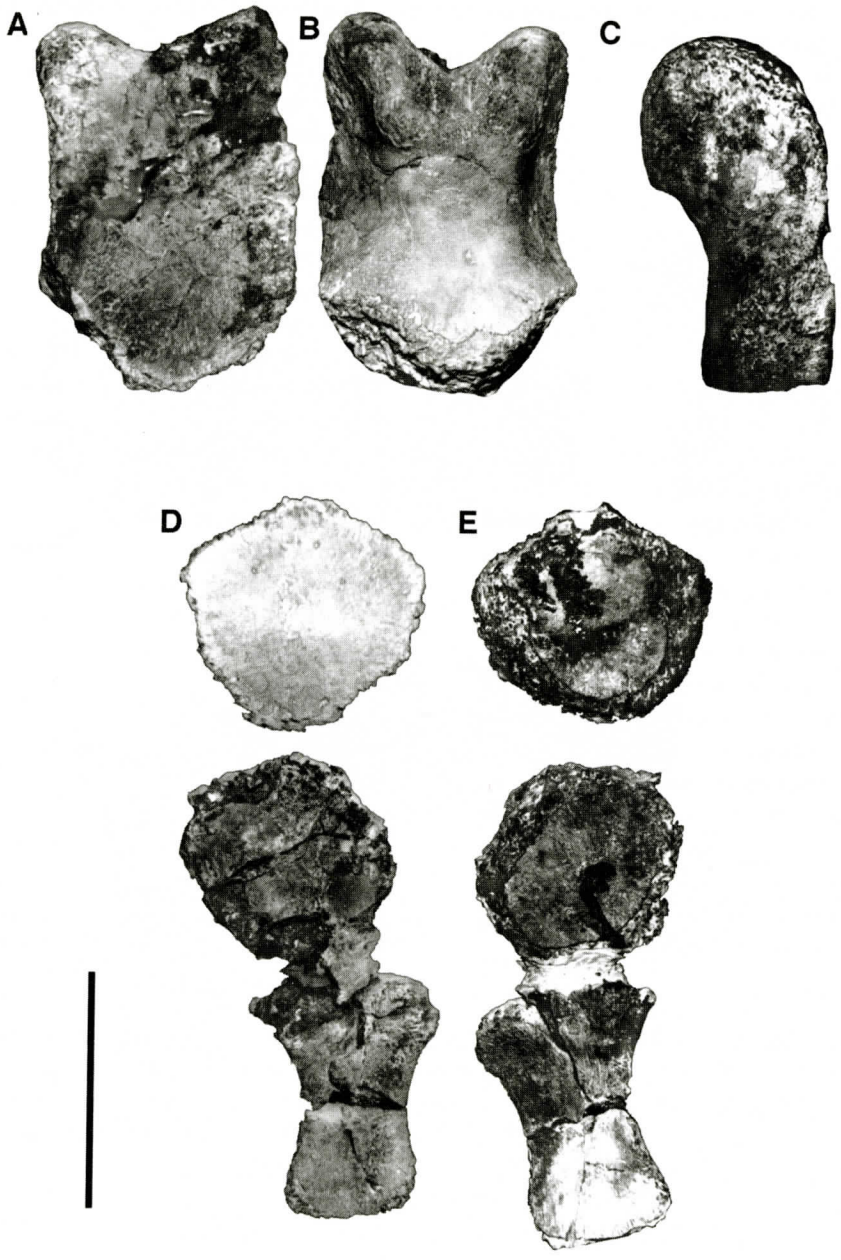

Figure 6: Sternal elements of *Cynthiacetus maxwelli*, MMNS VP 445. Manubrium in A, ventral, B, dorsal, and C, right lateral views. Two mesosternal elements and xiphisternum in D, ventral and E, dorsal views. Scale bar is 10 centimeters.

phisternum articulates with the posteriormost mesosternal element (Figure 6D, E). The xiphisternum dorsoventrally thins toward its posterior end. The ribs of *Cynthiacetus* are similar to those of other basilosaurids. Anterior ribs have both a capitulum and tuberculum while posterior ribs lack the tuberculum.

Humerus—The right humerus of MMNS VP 445 is present, but its proximal end is crushed, preventing any description of the head or proximal tubercles (Figure 7A, B). The deltopectoral crest is prominent and terminates more

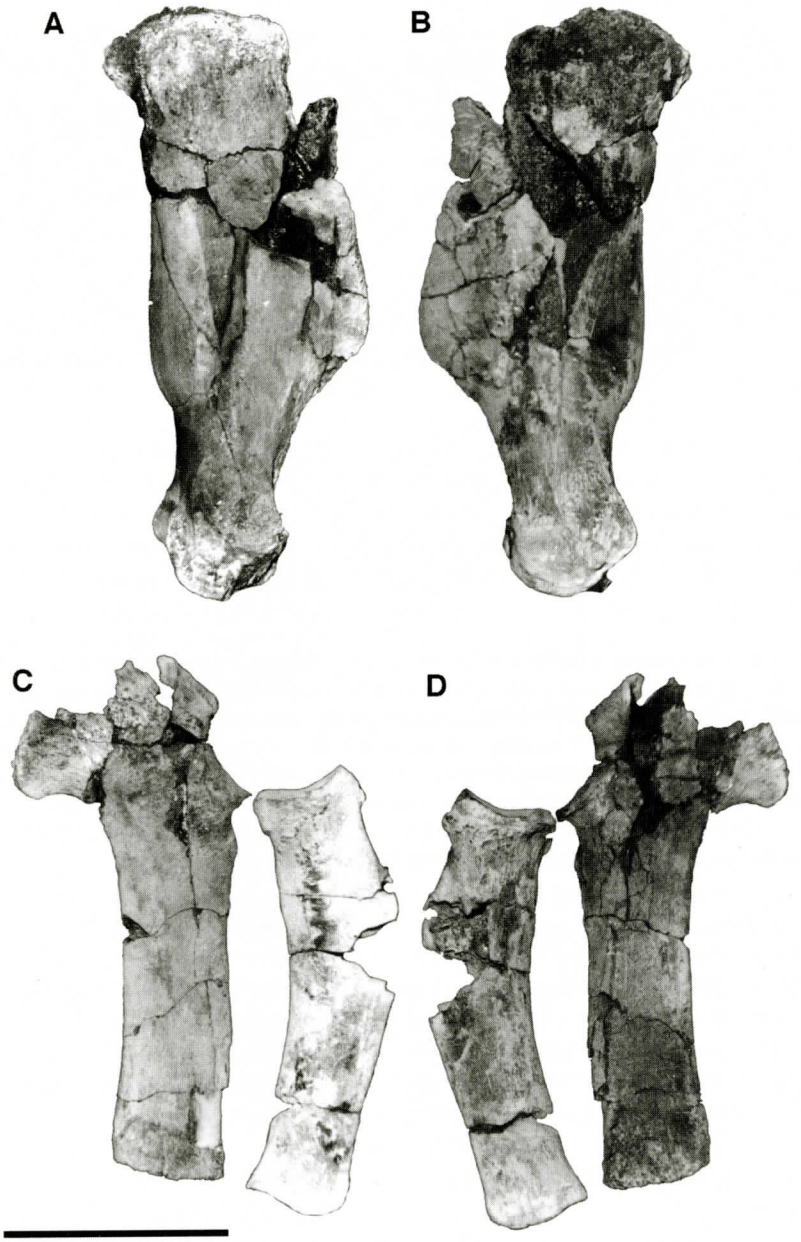

Figure 7: Forelimb elements of *Cynthiacetus maxwelli*, MMNS VP 445. A and B, right humerus in A, lateral, and B medial views. C and D, right ulna and radius in C, lateral and D, medial views. Scale bar is 10 centimeters.

proximally than the deltopectoral crest of *Dorudon atrox* (Uhen, 1998). The distal end of the humerus bears a single trochlea for the articulation of the ulna and radius.

Ulna—The ulna of MMNS VP 445 bears a large olecranon process which is damaged on its proximal end (Figure 7C, D). The trochlear notch is confluent with the proximal articular surface of the radius when the two bones are brought into articulation with one another. The shaft of the ulna is long and straight, slightly flattened in the plane of the flipper. It is missing

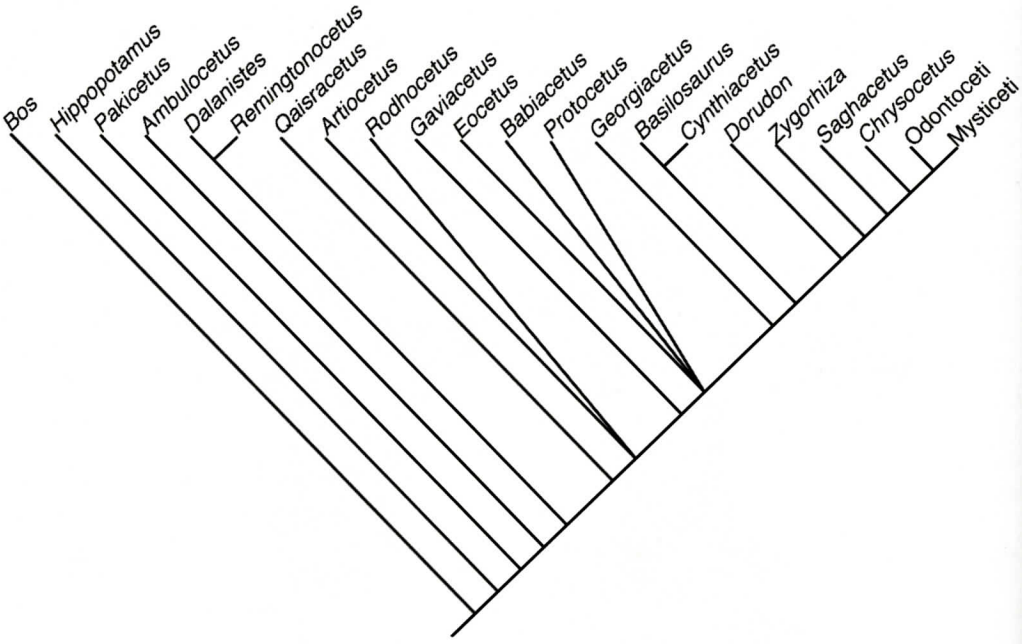

Figure 8: Strict consensus cladogram of six equally overall most parsimonious cladograms resulting from the procedure outlined in the text. The stratigraphic character was not included in the morphological cladistic analysis. Basilosaurinae is represented by *Basilosaurus*. Basilosaurines have elongate posterior thoracic, lumbar and anterior caudal vertebrae. Dorudontinae are a paraphyletic assemblage including *Cynthiacetus* that give rise to Neoceti and Basilosaurinae. Note that *Cynthiacetus* is the sister taxon to Basilosaurinae (*Basilosaurus*). Neoceti (Odontoceti + Mysticeti) arise from within the Dorudontinae. Early Neoceti share a number of derived features with basilosaurids and lack the autapomorphic features of basilosaurines.

its distal epiphysis.

Radius—The radius of MMNS VP 445 is similar in shape to that of *Zygorhiza kochii*, but somewhat larger (Figure 7C, D). The proximal articular surface is roughly circular in outline and cup-shaped. At about one third of the way along the shaft of the radius is a prominent bend towards the ulna, and is slightly flattened in the plane of the flipper. The radius is missing its distal epiphysis.

PHYLOGENETIC RELATIONSHIPS

A phylogenetic analysis was performed on *Cynthiacetus maxwelli*, other basilosaurids, selected non-basilosaurid archaeocetes, and hypothetical ancestral mysticetes and odontocetes. The analysis follows that discussed by Uhen (2004). The analysis was performed using stratocladistics, a phylogenetic analysis method that includes morphologic character data like a conventional cladistic analysis, as well as information on the relative stratigraphic relationships of fossils. See Uhen and Gingerich (2001) and Uhen (2004) for a more in-depth discussion of stratocladistics and other applications of it to archaeocete cetaceans.

Stratocladistic analyses must be performed in multiple steps since no phylogenetic analysis program includes both optimal tree finding algorithms and the stratigraphic character type. First, a preliminary phylogenetic analysis was performed on 22 taxa using the morphologic characters (Uhen, 2004, Appendix. VIII and references therein) using PAUP 4.0b3 (Swofford, 2000). Character states for *Cynthiacetus* are listed in Table 4. Two artiodactyl genera (*Bos* and *Hippopotamus*) were considered outgroup taxa, while the rest (20) were ingroup

taxa. Characters were equally weighted, and multistate characters were ordered. Characters were chosen that vary in state among taxa in the analysis. A branch and bound search was performed, which guarantees to find the optimal tree. 229 morphologically most parsimonious trees of length 176 were found. The matrix and these trees were then taken into MacClade 4.0 (Maddison and Maddison, 2000), where the stratigraphic character (character 69) was added. The trees with the stratigraphic character added ranged in length from 217 to 222. These trees were further explored by in MacClade and by swapping branches by hand. Six overall most parsimonious topologies of length 217 were found, although others may exist. These six trees were taken back into PAUP, where a strict consensus was computed, which is shown in Figure 8. The trees differ in the relative positions of *Eocetus*, *Protocetus*, and *Babiacetus*, as well as *Artiocetus* and *Rhodocetus*.

The result shows that *Cynthiacetus* is the sister taxon to *Basilosaurus*. These genera are grouped together based on body size independent of trunk vertebrae length. Basilosaurids *Basilosaurus drazindai* and *Basiloterus hussaini* were not included in this analysis because they are based on a pair and a single lumbar vertebra, respectively (Gingerich *et al.*, 1997). While these type specimens do not contain enough morphological information for their inclusion in a phylogenetic analysis, the lumbar vertebrae of both species are elongate, suggesting that they might be more closely related to *Basilosaurus isis* and *Basilosaurus cetoides* than either is to *Cynthiacetus*. At this time, *Cynthiacetus* is retained in the subfamily Dorudontinae because it lacks the distinguishing feature of Basilosaurinae, elongate trunk vertebrae. These and previous results (Fordyce and Barnes, 1994; Uhen, 1998; Uhen and Gingerich, 2001; Uhen, 2004) show that Archaeoceti, Protocetidae, Basilosauridae, and Dorudontidae are all paraphyletic taxa.

SUMMARY AND CONCLUSIONS

Poor specimens of a large species of basilosaurid archaeocete lacking elongate vertebral centra have been collected for over 100 years in both North America and Egypt. Kellogg attributed some of these specimens to the same species as Leidy's *Pontogeneus priscus*, a species described based on a single cervical vertebra, here considered a *nomen nudum*. A new specimen including a relatively complete skull and skeleton from the Yazoo Clay Formation of Hinds County, Mississippi (MMNS VP 445) is here placed in a new genus and species, *Cynthiacetus maxwelli*, and other specimens are referred to this new species. These specimens show that *C. maxwelli* is similar to other basilosaurids and phylogenetic analysis shows that *C. maxwelli* is the sister taxon to *Basilosaurus* because they share large body size independent of vertebral body length. Other basilosaurids with large, non-elongate vertebral bodies, even larger than those of *C. maxwelli* (UF FGS V3888 for example) may represent another as yet undescribed species.

ACKNOWLEDGMENTS

I would like to thank Eleanor Daly and Libby Hartfield of the Mississippi Museum of Natural Science, Jackson, who loaned specimen MMNS VP 445 to me for study. I would also like to thank the many volunteers in the preparation laboratory at the Cranbrook Institute of Science for their work on preparing the specimen. Without their hard work this study would not have been possible. Thanks also goes to David Bohaska (United States National Museum, Washington DC), Philip D. Gingerich (University of Michigan Museum of Paleontology, Ann Arbor), Elmar P. J. Heizmann (Staatliches Museum für Naturkunde, Stuttgart), and P. David Webb (University of Florida, Florida Museum of Natural History, Gainesville) who provided access to additional specimens used in this study. I would also like to thank Elanor Daly and Earl Manning who reviewed an earlier version of this paper.

LITERATURE CITED

Abel, O., 1914, Die vorfahren der bartenwale: Denkschriften der Kaiserlichen Akademie der Wissenschaften Mathematisch-Naturwissenschaftliche

Klasse, v. 90, p. 155-224.

Barnes, L. G. and Mitchell, E. D., 1978, Cetacea, *in* Maglio, V. J. and Cooke, H. B. S., eds., The Evolution of African Mammals: Harvard University Press, p. 582-602.

Brisson, A. D., 1762, Regnum Animale in Classes IX distributum sive synopsis methodica. Edito altero auctior.: Theodorum Haak, p. 294.

Cope, E. D., 1867, An addition to the vertebrate fauna of the Miocene period, with a synopsis of the extinct Cetacea of the United States: Proceedings of the Academy of Natural Sciences of Philadelphia, v. 19, p. 138-156.

Dockery, D. T. III, 1992, Jackson ready mix Miss-Lite plant and clay pit to close after 34 years of operation: Mississippi Geology, v. 13, p. 22.

Dockery, D. T. III and Slesser, W. G., 1984, Age of the Upper Yazoo Formation in Central Mississippi: Mississippi Geology, v. 5, p. 1-10.

Domning, D. P., Morgan, G. S., and Ray, C. E., 1982, North American Eocene sea cows (Mammalia, Sirenia): Smithsonian Contributions to Paleobiology, v. 52, p. 1-69.

Fisher, D. C., 1992, Stratigraphic Parsimony, *in* Maddison, W. P. and Maddison, D. R., MacClade 3.0 Manual: Sinauer Associates, p. 124-129.

Fisher, D. C., 1994, Stratocladistics: morphological and temporal patterns and their relation to phylogenetic process, *in* Grande, L. and Rieppel, O., eds., Interpreting the Hierarchy of Nature: Academic Press, p. 133-171.

Flower, W. H., 1883, On the characters and divisions of the Family Delphinidae: Proceedings of the Zoological Society London, v. 1883, p. 466-513.

Fordyce, R. E. and Barnes, L. G., 1994, The evolutionary history of whales and dolphins: Annual Review of Earth and Planetary Sciences, v. 22, p. 419-455.

Gingerich, P. D., Arif, M., Bhatti, M. A., Anwar, M., and Sanders, W. J., 1997, *Basilosaurus drazindai* and *Basiloterus hussaini*, new Archaeoceti (Mammalia, Cetacea) from the middle Eocene Drazinda Formation, with a revised interpretation of ages of whale-bearing strata in the Kirthar Group of the Sulaiman Range, Punjab (Pakistan): Contributions from the Museum of Paleontology, University of Michigan, v. 30, p. 55-81.

Huner, J. Jr., 1939, Geology of Caldwell and Winn Parishes: State of Louisiana Department of Conservation Geological Bulletin, v. 15, p. 1-356.

Kellogg, R., 1936, A Review of the Archaeoceti: Carnegie Institute of Washington Special Publication, v. 482, p. 1-366.

Koch, A. C., 1846, Kurze Beschreibung des *Hydrarchos harlani* (Koch) eines reisenmässigen Meerungeheuers und dessen Entdeckung in Alabama in Nordamerika im Frühjahr 1845.: Druck der Königl. Hofbuchdruckerei von C. C. Meinhold and Söhnen, p. 20.

Leidy, J., 1852, [Description of *Pontogeneus priscus*]: Proceedings of the Academy of Natural Sciences of Philadelphia, v. 6, p. 52.

Maddison, W. P. and Maddison, D. R., 2000, MacClade: Analysis of Phylogeny and Character Evolution Version 4.0: Sinauer Associates, Inc., p. 398.

McKenna, M. C. and Bell, S. K., 1997, Classification of Mammals Above the Species Level: Columbia University Press, p. 631.

Miller, G. S. Jr., 1923, The telescoping of the cetacean skull: Smithsonian Miscellaneous Collections, v. 76, p. 1-71.

Müller, J., 1849, Über die fossilen Reste der Zeuglodonten von Nordamerica: Verlag von G. Reimer, p. 1-38.

Snead, John I. and McCulloh, Richard P., 1984, Geologic Map of Louisiana: Louisiana Geological Survey, Baton Rouge, Louisiana.

Stromer, E., 1908, Die Urwale (Archaeoceti): Anatomischer Anzeiger, v. 33, p. 81-88.

Swofford, D. L., 2002, PAUP* Phylogenetic Analysis Using parsimony (* and Other Methods): Sinauer Associates, p. Version 4.0b10.

Uhen, M. D.1996, *Dorudon atrox* (Mammalia, Cetacea): Form, Function, and Phylogenetic Relationships of an Archaeocete from the Late Middle Eocene of Egypt

Uhen, M. D., 1997, What is *Pontogeneus brachyspondylus*?: Journal of Vertebrate Paleontology, v. 17, p. 82A.

Uhen, M. D., 1998, Middle to Late Eocene Basilosaurines and Dorudontines, *in* Thewissen, J. G. M., ed., The Emergence of Whales: Plenum Press, p. 29-61.

Uhen, M. D., 2004, Form, Function, and Anatomy of *Dorudon atrox* (Mammalia, Cetacea): An Archaeocete from the Middle to Late Eocene of Egypt: University of Michigan Museum of Paleontology Papers on Paleontology, v. 34, p.

Uhen, M. D. and Gingerich, P. D., 2001, New genus of dorudontine archaeocete (Cetacea) from the middle-to-late Eocene of South Carolina: Marine Mammal Science, v. 17, p. 1-34.